FIRST-PRINCIPLES MECHANISTIC STUDIES OF AMMONIA-RELATED INDUSTRIAL PROCESSES

Jaime Gómez Díaz

ISBN: 978-84-694-1247-3
Dipòsit Legal: T-317-2011

UNIVERSITAT ROVIRA I VIRGILI
FIRST-PRINCIPLES MECHANISTIC STUDIES OF AMMONIA-RELATED INDUSTRIAL PROCESSES
Jaime Gómez Díaz
ISBN:978-84-694-1247-3/T-317-2011

UNIVERSITAT ROVIRA I VIRGILI
FIRST-PRINCIPLES MECHANISTIC STUDIES OF AMMONIA-RELATED INDUSTRIAL PROCESSES
Jaime Gómez Díaz
ISBN:978-84-694-1247-3/T-317-2011

UNIVERSITAT ROVIRA I VIRGILI
FIRST-PRINCIPLES MECHANISTIC STUDIES OF AMMONIA-RELATED INDUSTRIAL PROCESSES
Jaime Gómez Díaz
ISBN:978-84-694-1247-3/T-317-2011

First-principles mechanistic studies of ammonia-related industrial processes

Jaime Gómez Díaz

Doctoral Thesis supervised by:

Dra. Núria López Alonso

Departament de Química Física i Inorgànica

UNIVERSITAT ROVIRA I VIRGILI

Tarragona

2010

UNIVERSITAT ROVIRA I VIRGILI
FIRST-PRINCIPLES MECHANISTIC STUDIES OF AMMONIA-RELATED INDUSTRIAL PROCESSES
Jaime Gómez Díaz
ISBN:978-84-694-1247-3/T-317-2011

UNIVERSITAT ROVIRA I VIRGILI
FIRST-PRINCIPLES MECHANISTIC STUDIES OF AMMONIA-RELATED INDUSTRIAL PROCESSES
Jaime Gómez Díaz
ISBN:978-84-694-1247-3/T-317-2011

Institute of Chemical Research of Catalonia
Avgda. Països Catalans 16
43007 Tarragona (Spain)

I STATE that the present work entitled "First-principles mechanistic studies of ammonia-related processes" presented by Jaime Gómez Díaz to opt to the title of European Doctor, has been carried out under my supervision at the Institute of Chemical Research of Catalonia (ICIQ) and that it fulfils all the necessary requirements.

Tarragona, November 2010

Dr. Núria López

UNIVERSITAT ROVIRA I VIRGILI
FIRST-PRINCIPLES MECHANISTIC STUDIES OF AMMONIA-RELATED INDUSTRIAL PROCESSES
Jaime Gómez Díaz
ISBN:978-84-694-1247-3/T-317-2011

UNIVERSITAT ROVIRA I VIRGILI
FIRST-PRINCIPLES MECHANISTIC STUDIES OF AMMONIA-RELATED INDUSTRIAL PROCESSES
Jaime Gómez Díaz
ISBN:978-84-694-1247-3/T-317-2011

Acknowledgments

Esta tesis no hubiera sido posible sin su directora, Núria López, y sin la beca que me concedió para trabajar en un centro con recursos tan extraordinarios como los del ICIQ. Haluan kiittää tällä erityisellä tavalla FT Karoliina Honkalaa hänen vieraanvaraisuudestaan, mutta ennen kaikkea hänen ystävällisestä omistautumisestaan ohjaamiselleni. Una altra persona que em va ajudar força a acabar aquesta tesi va ser la Núria Vendrell i la seva, sempre impecable, feina. Me gustaría también agradecer a todas las instituciones que han financiado/apoyado mi trabajo de investigación: ante todo el ICIQ, pero también otras como BSC, CSC, HPC-Europa2 program, etc.

Ahora bien, si he llegado a esta etapa del camino en casi aceptables condiciones de salud mental y con pelo por encima de las cejas, es también *culpa* de mucha otra gente. No me gustaría imaginarme como hubieran sido estos más de 4 años sin ella en el despacho... ¡Hecho, Mónica! Mucho, muchísimo han contribuido también a esta tesis el resto de "los teóricos". Gracias, Ata, Gerard, Pere, Torstein, Maria, Eva, Crisa, Martín, Joan y tod@s los demás (así no me dejaré a nadie y no llenaré 8 páginas...), con un saludo especial para Carles y Feliu. He de agradecer a *mi cocina* el regalarme una hora diaria (y alguna *extra* los fines de semana) de buen humor, conversaciones y sobre todo desconexión: ¡muchas gracias, chic@s!

Thanks also to Ville, Sergio, Jenni, Riita-Liisa, Vesa, Kaisa, Olga and Lauri; for making me feel as in my own (cold) home at Jyväskylä and Helsinki. Gracias también al resto de gente del ICIQ, de la URV, de Tarragona-*city* y de la UAM (¡con vosotros empezó todo esto!) que no formaba parte de ninguno de los subconjuntos anteriores, pero, especial-

UNIVERSITAT ROVIRA I VIRGILI
FIRST-PRINCIPLES MECHANISTIC STUDIES OF AMMONIA-RELATED INDUSTRIAL PROCESSES
Jaime Gómez Díaz
ISBN:978-84-694-1247-3/T-317-2011

mente, a mis increíbles compañeros de los cursos de doctorado y del *master*: ¡cómo nos lo pasamos!

Muchas gracias también a toda la gente que rodea "mi otra vida". Especialmente a María, Ricardo, Chus y tod@s (nunca olvidados, os lo prometo) los demás: Luis, Willy, Kaka, Nuria, Sergio, el Kalvo, Marcos, Robles, Zahara, Berta, Belén, Dani, Yolanda, Ana, Alla, Nacho, Desi, la gente del GRM... y muchos, muchos otros.

Tengo mucho que agradecer a mi familia: mis padres (¡todavía me acuerdo de lo de la gasolinera!), mi hermana, Nena y Diana; y por último, a Laura. Espero que el dejarla en último lugar represente de alguna manera todas las cosas que le tengo que agradecer y que no creo que se pudieran expresar en papel (ni en formato electrónico).

UNIVERSITAT ROVIRA I VIRGILI
FIRST-PRINCIPLES MECHANISTIC STUDIES OF AMMONIA-RELATED INDUSTRIAL PROCESSES
Jaime Gómez Díaz
ISBN:978-84-694-1247-3/T-317-2011

Nada habría podido suceder
si alguien no lo hubiera imaginado primero,

Reinhold Messner

UNIVERSITAT ROVIRA I VIRGILI
FIRST-PRINCIPLES MECHANISTIC STUDIES OF AMMONIA-RELATED INDUSTRIAL PROCESSES
Jaime Gómez Díaz
ISBN:978-84-694-1247-3/T-317-2011

UNIVERSITAT ROVIRA I VIRGILI
FIRST-PRINCIPLES MECHANISTIC STUDIES OF AMMONIA-RELATED INDUSTRIAL PROCESSES
Jaime Gómez Díaz
ISBN:978-84-694-1247-3/T-317-2011

Contents

UNIVERSITAT ROVIRA I VIRGILI
FIRST-PRINCIPLES MECHANISTIC STUDIES OF AMMONIA-RELATED INDUSTRIAL PROCESSES
Jaime Gómez Díaz
ISBN:978-84-694-1247-3/T-317-2011

UNIVERSITAT ROVIRA I VIRGILI
FIRST-PRINCIPLES MECHANISTIC STUDIES OF AMMONIA-RELATED INDUSTRIAL PROCESSES
Jaime Gómez Díaz
ISBN:978-84-694-1247-3/T-317-2011

UNIVERSITAT ROVIRA I VIRGILI
FIRST-PRINCIPLES MECHANISTIC STUDIES OF AMMONIA-RELATED INDUSTRIAL PROCESSES
Jaime Gómez Díaz
ISBN:978-84-694-1247-3/T-317-2011

UNIVERSITAT ROVIRA I VIRGILI
FIRST-PRINCIPLES MECHANISTIC STUDIES OF AMMONIA-RELATED INDUSTRIAL PROCESSES
Jaime Gómez Díaz
ISBN:978-84-694-1247-3/T-317-2011

Part I

Introduction

UNIVERSITAT ROVIRA I VIRGILI
FIRST-PRINCIPLES MECHANISTIC STUDIES OF AMMONIA-RELATED INDUSTRIAL PROCESSES
Jaime Gómez Díaz
ISBN:978-84-694-1247-3/T-317-2011

UNIVERSITAT ROVIRA I VIRGILI
FIRST-PRINCIPLES MECHANISTIC STUDIES OF AMMONIA-RELATED INDUSTRIAL PROCESSES
Jaime Gómez Díaz
ISBN:978-84-694-1247-3/T-317-2011

Chapter 1

Introduction

1.1 Catalysis

The term catalyst was first coined by Berzelius in 1836. His definition, *"substances apparently not consumed in chemical reactions that awaken affinities by their mere presence"* severely differs from the present one. A catalyst is basically a substance that changes the rate of a chemical reaction without being consumed by the reaction itself. If the rate is increased, the catalyst is call "positive" or just catalyst and if the rate is decreased, it is call "negative" or inhibitor.

Catalysts are fundamental in processing all kind of materials and compounds. In living cells, the catalytic function is made by natural compounds called enzymes, which show a very large specificity towards reactants and products. However, not only natural systems can act as catalyst. Man-made catalysts are the workhorses for chemical transformations in industry [1]. Approximately 85-90% of the chemical products are made through catalytic processes. Catalyst are indispensable in fuel production, bulk and fine chemicals synthesis and to prevent and/or reduce pollution.

The search for new catalysts has been traditionally performed by means of trial-and-error procedures. This method is ineffective and time and money consuming. In recent times, the combination of surface science techniques, catalysts characterization and testing, and the use of theoretical simulations (see Fig. 1.1), have started to produce new catalysts based on rational design. In fact, theoretical simulations have proved to be able

UNIVERSITAT ROVIRA I VIRGILI
FIRST-PRINCIPLES MECHANISTIC STUDIES OF AMMONIA-RELATED INDUSTRIAL PROCESSES
Jaime Gómez Díaz
ISBN:978-84-694-1247-3/T-317-2011

to both, reproduce experimental results on a heterogeneous catalyst under working conditions [2], and also to predict the activity of new compounds [3].

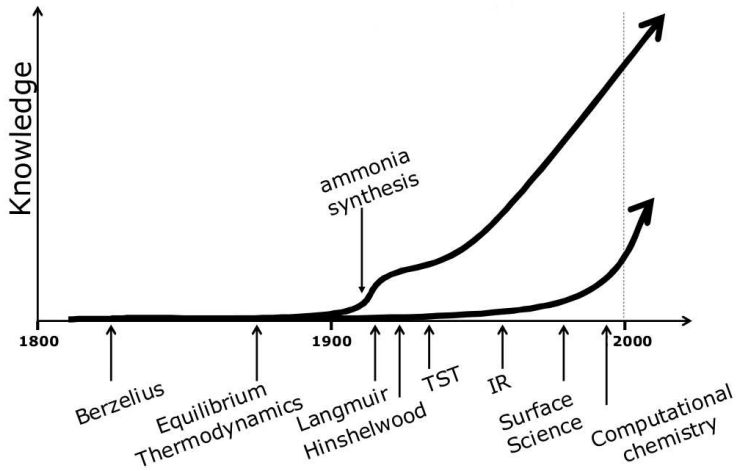

Figure 1.1: Knowledge of heterogeneous catalysis during the last centuries. Adapted from Ref. [1].

1.1.1 Heterogeneous catalysis

Among synthetic catalysts, those based in solid phases are the most commonly used in bulk chemical processes, and are known as heterogeneous catalysts. The word heterogeneous comes from the fact that these catalysts are in a separate (solid) phase from the gas-phase or solution reactants and products. In solid catalysts, reactions mainly occurs at the surface. Due to the frequent use of expensive materials (e.g. Pt, Pd, Rh...), catalysis are frequently nanometer-sized particles, supported on a generally inert, porous support (e.g. alumina, ceramic materials...). This increases the active surface area of the catalyst. The main advantages of heterogeneous catalysis with respect to homogeneous ones are: i) the easy separation of the catalyst from the products and ii) the wide range of pressure and temperature available. On the other hand, heterogeneous catalysts are not generally as selective as homogeneous ones.

UNIVERSITAT ROVIRA I VIRGILI
FIRST-PRINCIPLES MECHANISTIC STUDIES OF AMMONIA-RELATED INDUSTRIAL PROCESSES
Jaime Gómez Díaz
ISBN:978-84-694-1247-3/T-317-2011

Among the most important industrial processes using catalysts are the cracking and reforming of crude oil (using zeolites, Co-Mo and Pt as catalyst), ammonia synthesis (Fe-based), ammonia oxidation to NO and HNO_3 (Pt-Rh) and the sulfuric acid synthesis (V-based).

1.2 Ostwald process: HNO_3 production

1.2.1 HNO_3: properties and uses

Nitric acid (*aka aqua fortis*, azotic acid and hydrogen nitrate) is a chemical of major industrial importance. It is a very strong acid and oxidizing agent, and it easily nitrates organic compounds. The acid is a clear and colorless liquid completely miscible in water. Its most important physical properties are shown in Table 1.1.

Table 1.1: Physical properties of Nitric Acid [4].

Property	Value
molecular weight	63.012
acidity (pK_a)	-1.4
melting point, °C	-41.59
boiling point, °C	83.40
density, g/mL 20 °C	1.5129
vapor pressure, kPa 20.0 °C	6.20
liquid viscosity at 20.0 °C, mPa·s (=cP)	0.9

The first reports date from the Arab alchemist of the eight century. In the Middle Ages it was referred as *aqua fortis* and was produced from saltpeter (potassium nitrate) and sulphuric acid. Chilean saltpeter (sodium nitrate) replaced largely potassium nitrate in the nineteenth century. In 1908, Wilhelm Ostwald (Nobel prize in 1909 for his work on catalysis, chemical equilibria and reaction velocities) created a pilot plant that produced 3 ton per day of nitric acid based on the catalytic oxidation of ammonia with air. After the development of the Haber-Bosch process (1913), where ammonia is synthesized from coal, air and water; ammonia oxidation firmly established as the industrial route to nitric acid manufacture. Those processes were widely used during the First and Second

UNIVERSITAT ROVIRA I VIRGILI
FIRST-PRINCIPLES MECHANISTIC STUDIES OF AMMONIA-RELATED INDUSTRIAL PROCESSES
Jaime Gómez Díaz
ISBN:978-84-694-1247-3/T-317-2011

World Wars to produce ammonium-nitrate explosives. In the 90's, its production decreased as result of the popularization of urea as fertilizer, but the increasing production of polyurethanes, fibers and explosives has enlarged the demand.

HNO_3 is essential in the synthesis of many chemicals, in a wide variety of fields (pharmaceuticals, dyes, synthetic fibers, insecticides, fungicides, treatment of metals, as a rocket propellant and for nuclear fuel processing). Nevertheless, its principal use is the production of ammonium nitrate for the fertilizer industry.

1.2.2 Production

The Ostwald process is the set of chemical reactions devoted to produce nitric acid from ammonia and oxygen. This synthetic route was patented in 1902 [5]. It is a mainstay of the modern chemical industry. As previously mentioned, historically and practically it is closely associated with the Haber process, which provides the principal required raw material, ammonia. The global production of nitric acid was $46{\cdot}10^6$ tons/year in 2002, being one of the ten most important inorganic chemicals.

Description of the Process:

Ammonia is converted to nitric acid in two stages. First, it is oxidized by heating with oxygen to form nitric oxide, NO, and water.

$$4NH_3(g) + 5O_2(g) \longrightarrow 4NO(g) + 6H_2O(g);\ \Delta H = -950\ kJ \qquad (1.1)$$

This step is strongly exothermic, making it a useful heat source once initiated. The catalyst for this step contains platinum with an approximately 10% of rhodium. The reasons to add rhodium are supposed to be for increased strength and improved reaction yield. It is used as multiple (10-50) layers of a fine wire mesh or gauze several milimeters thick and up to several meters in diameter. During the life of the catalyst, its surface changes until activity loss, see Figure 1.2. It is believed that the surface loses Pt (as volatile PtO_2) and forms rhodium oxides.

Linear velocity of the gases in the process is high, giving a total contact time of about 10^{-3}-10^{-4} s with a negligible pressure drop. Several metal

UNIVERSITAT ROVIRA I VIRGILI
FIRST-PRINCIPLES MECHANISTIC STUDIES OF AMMONIA-RELATED INDUSTRIAL PROCESSES
Jaime Gómez Díaz
ISBN:978-84-694-1247-3/T-317-2011

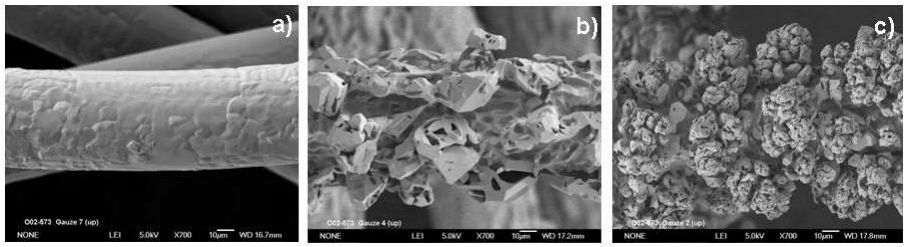

Figure 1.2: $Pt_{90}Rh_{10}$ catalyst used in the Ostwald process: a) fresh catalyst, b) faceted catalyst and c) cauliflowers formed after use. Taken from Ref. [6].

oxides can and have been used as catalysts for this reaction, but none have found wide use in industry and the Pt-Rh alloy remains the catalyst of choice. Obviously, interest in finding a less expensive material than platinum continues.

Using such platinum-based catalysts, the conversion of ammonia to nitric oxide is high, between 93-98%. The optimum reaction temperature for conversion efficiency increases with operating pressure. Although, the combination of higher operation pressure and temperature results in decreased conversion efficiency.

At typical gauze temperatures of 975-1125 K, nitric oxide is thermodynamically unstable and slowly decomposes into nitrogen and oxygen. Decomposition losses are minimized by avoiding excessive catalyst contact time and rapidly cooling the gases as they exit the converter. Fortunately, the conversion of ammonia to NO is very rapid. Small amounts of nitrous oxide N_2O are also formed but much lower reaction temperatures of around 750 K are required to become a significant yield loss.

The typical reaction conditions are:

- pressure between 4 and 10 atmospheres (approx. 400-1010 kPa)
- temperatures between 975 and 1125 K (approx. 700-900 °C)

The second stage combines two reaction steps, and it is carried out in the presence of water in an absorption apparatus. Initially, nitric oxide is oxidized again to yield nitrogen dioxide, NO_2:

$$2NO(g) + O_2(g) \longrightarrow 2NO_2(g) \tag{1.2}$$

UNIVERSITAT ROVIRA I VIRGILI
FIRST-PRINCIPLES MECHANISTIC STUDIES OF AMMONIA-RELATED INDUSTRIAL PROCESSES
Jaime Gómez Díaz
ISBN:978-84-694-1247-3/T-317-2011

This gas is then readily absorbed by water, yielding the desired product (nitric acid, albeit in a dilute form), while reducing a portion of it back to nitric oxide:

$$3NO_2(g) + H_2O(l) \longrightarrow 2HNO_3(aq) + NO(g) \tag{1.3}$$

The NO is recycled, while the acid is concentrated to the required strength by distillation. Alternatively, if the last step is carried out in air the reaction can be written as:

$$4NO_2(g) + O_2(g) + 2H_2O(l) \longrightarrow 4HNO_3(aq) \tag{1.4}$$

A schematic representation of a whole production plant is shown in Fig. 1.3.

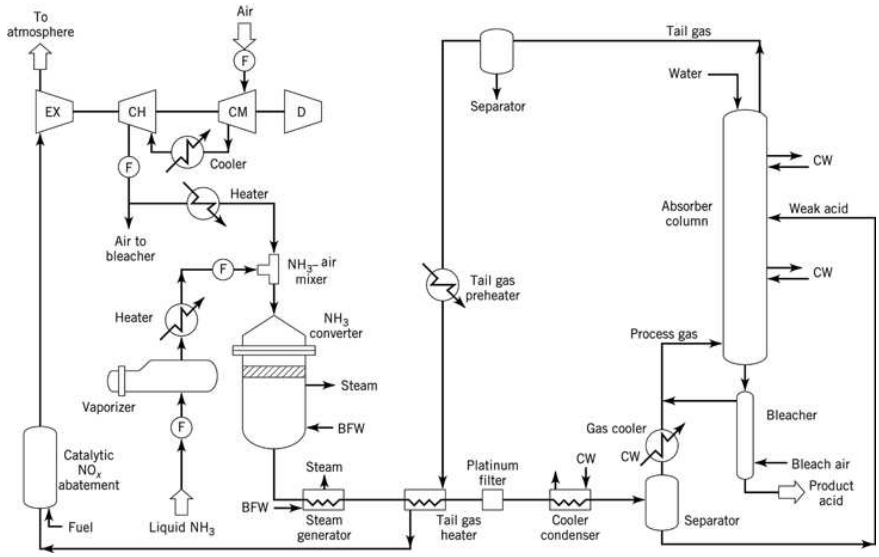

Figure 1.3: Schematic representation of a HNO_3 production plant through Ostwald process. Taken from Ref. [4].

UNIVERSITAT ROVIRA I VIRGILI
FIRST-PRINCIPLES MECHANISTIC STUDIES OF AMMONIA-RELATED INDUSTRIAL PROCESSES
Jaime Gómez Díaz
ISBN:978-84-694-1247-3/T-317-2011

1.3 Degussa and Andrussow processes: HCN production

1.3.1 HCN: properties and uses

Hydrogen cyanide (*aka* hydrocyanic acid, Prussic acid or formonitrile) is a colorless liquid or gas (boiling point at 1 atm, 25.70°C), although usually appears as a blue gas due to iron contamination. Its most important physical properties are shown in Table 1.2.

Table 1.2: Physical properties of Hydrogen Cyanide [7].

Property	Value
molecular weight	27.03
melting point, °C	-13.24
triple point, °C	-13.32
boiling point, °C	25.70
density, g/mL 20 °C	0.6884
vapor pressure, kPa 27.2 °C	107.6
liquid viscosity at 20.2 °C, mPa· s (=cP)	0.2014

The first known isolation of HCN was made from a well known blue dye (Prussian blue) which structure was unknown. In 1752, the French chemist Pierre Macquer transformed this dye into iron oxide plus a volatile compound and he reversed the reaction to reconstitute the dye. This new component was hydrogen cyanide. Around 1783, the Swedish chemist Carl Wilhelm Scheele isolated in pure form and characterized the hydrogen cyanide, and was eventually given the German name Blausäure (literally "Blue acid"), as it was acid in water and derived from Prussic blue.

Cyanides are very toxic, although they are non-cumulative, that is, they are eliminated readily from body. Cyanide combines with the enzyme *cytochrome c oxidase* that regulate oxygen transfer to the cellular tissues [8]. Unless the cyanide is removed, death results through insufficient oxygen in the cells, asphyxia. People can generally detect hydrogen cyanide by odor or taste at concentrations around 1-5 ppm. Exposure to 300 ppm in air can be rapidly fatal. Despite its toxicity, small concentrations of cyanide (around 0.02-0.04 mg/l) are always present in human

UNIVERSITAT ROVIRA I VIRGILI
FIRST-PRINCIPLES MECHANISTIC STUDIES OF AMMONIA-RELATED INDUSTRIAL PROCESSES
Jaime Gómez Díaz
ISBN:978-84-694-1247-3/T-317-2011

bodies.

Some of the principal uses for HCN are:

- Adiponitrile synthesis: is an important precursor of the polymer Nylon 66. It is mainly produced by this reaction

$$H_2C = (CH)_2 = CH_2 + 2HCN \rightarrow NC - (CH_2)_4 - CN \quad (1.5)$$

  that is catalysed by nickel.

- Acetone cyanohydrin: is the monomer of the transparent plastic polymethyl methacrylate, formed by treating hydrogen cyanide with sodium hydroxide.

- Sodium Cyanide: it is used mainly in gold mining (see section 1.4), but several commercially significant chemical compounds are derived from cyanide, including cyanogen chloride, and many nitriles.

- Methionine: methionine is an essential amino acid. It was estimated a production of $268{\cdot}10^3$ tons in 2009 [9]. It is used as additive in animal feed, food and beverage complements and pharmaceuticals.

- Cyanuric chloride: it is synthesized by these reactions

$$HCN + Cl_2 \rightarrow ClCN + HCl \quad (1.6)$$
$$3ClCN \rightarrow (ClCN)_3 \quad (1.7)$$

  and is estimated that 70% of cyanuric chloride is used in the preparation of the triazine-class pesticides, especially atrazine. Cyanuric chloride is also used as a precursor to dyes and crosslinking agents.

- Cyanides are also used as chelating agents.

1.3.2 Production

Currently, hydrogen cyanide is produced in high quantities, around 1 million tons per year [10]. Although there are several processes that can be used, the majority of the HCN produced around the world is manufactured through the Andrussow process. An alternative to that process is given by the BMA-Degussa.

UNIVERSITAT ROVIRA I VIRGILI
FIRST-PRINCIPLES MECHANISTIC STUDIES OF AMMONIA-RELATED INDUSTRIAL PROCESSES
Jaime Gómez Díaz
ISBN:978-84-694-1247-3/T-317-2011

Andrussow process

Andrussow process was patented by Leonid Andrussow in 1933 [11] at IG Farben. It has many similarities to the oxidation of ammonia in the production of Nitric Acid. The production of HCN is achieved by passing ammonia, methane and air over a Pt-Rh catalyst at 1400-1500 K. The global reaction can be summarized as follows

$$2CH_4 + 2NH_3 + 3O_2 \rightarrow 2HCN + 6H_2O;\ \Delta H = -962.8\ kJ \qquad (1.8)$$

To obtain an optimum yield, a very short contact time (on the order of milliseconds) is required and consequently that high operating temperature is required to reach equilibrium. Typical conversion efficiencies are of the order of 60-70% [7].

The standard catalyst used in this process is PtRh-based. It is used as a wire with a diameter of less than 0.1 mm. Until the introduction of knitted catalyst, this was traditionally a woven gauze at around 1000 mesh/cm^2. Due to the high operating temperature, $Pt_{90}Rh_{10}$ alloy is the one used, although alternatives have been tried with limited success (essentially, platinum alloyed with one or more metals selected from the group consisting of nickel, cobalt, palladium, ruthenium, iridium, gold, silver and copper) [12]. A schematic representation of the whole process is shown in Fig. 1.4.

Degussa process

An alternative way to produce HCN is the Degussa or Blaüsure-Methan-Ammoniak (BMA) process. It is performed by feeding a mixture of methane and ammonia through an array of ceramic tubes coated internally with a platinum-based catalyst layer without air presence. The tubes are heated externally to 1473-1573 K. The reaction is highly endothermic, but very high yields (around 90%) and the useful hydrogen gas are obtained. It has high investment and maintenance costs [13].

The typical catalyst consist in an alumina tube lined with platinum, and they are directly fired with natural gas. The life of the catalyst is around 10^4 hours, and the global reaction can be summarized as follows

UNIVERSITAT ROVIRA I VIRGILI
FIRST-PRINCIPLES MECHANISTIC STUDIES OF AMMONIA-RELATED INDUSTRIAL PROCESSES
Jaime Gómez Díaz
ISBN:978-84-694-1247-3/T-317-2011

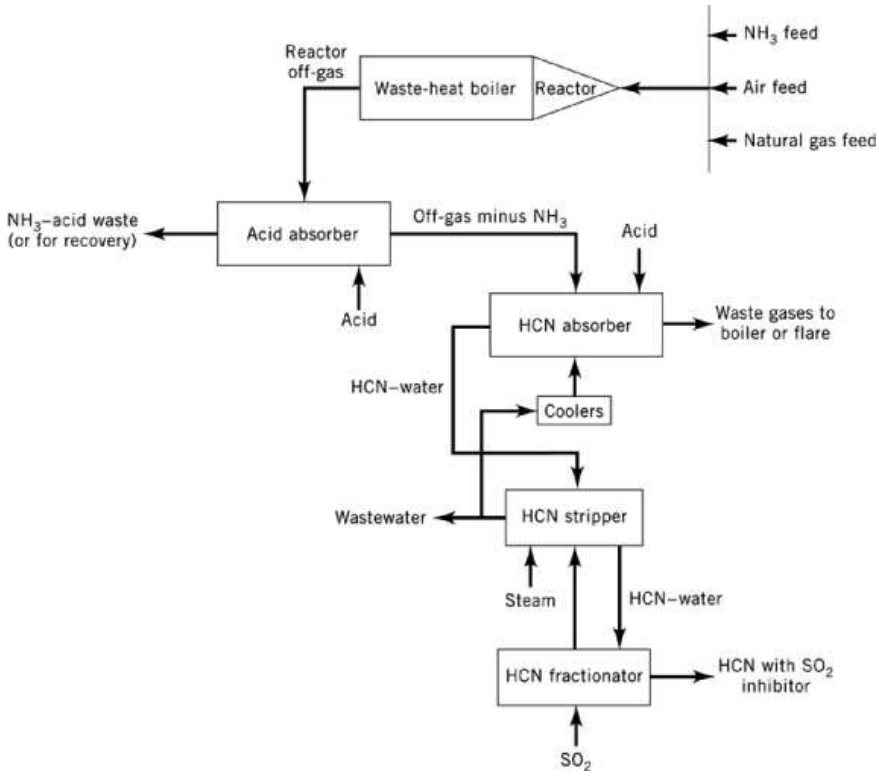

Figure 1.4: Schematic representation of a HCN production plant through Andrussow process (without ammonia removal). Taken from Ref. [7].

UNIVERSITAT ROVIRA I VIRGILI
FIRST-PRINCIPLES MECHANISTIC STUDIES OF AMMONIA-RELATED INDUSTRIAL PROCESSES
Jaime Gómez Díaz
ISBN:978-84-694-1247-3/T-317-2011

$$CH_4 + NH_3 \rightarrow HCN + 3H_2;\ \Delta H = +256\ kJ \tag{1.9}$$

Linear velocity of the gases is high, giving a total contact time of about 10^{-3}-10^{-4}s with a negligible pressure drop. Several metal oxides have been tested as catalysts for this reaction, but none have found wide use in industry and the Pt-Rh alloy remains the catalyst of choice. Obviously, interest in finding a less expensive material than platinum continues.

1.4 MacArthur-Forrest process: gold ore extraction

1.4.1 Gold: properties and uses

Gold has been valuable since the beginning of history. This noble metal has been used as a measurement of resources and material possessions throughout the world during centuries (*The Gold standard*). During this time, only around 130,000 tons of gold have been mined [14], barely enough to fill a cube with an edge length of 19 m.

Figure 1.5: Gold price in USD/oz from 1973 to 2010. Taken from Ref. [15].

UNIVERSITAT ROVIRA I VIRGILI
FIRST-PRINCIPLES MECHANISTIC STUDIES OF AMMONIA-RELATED INDUSTRIAL PROCESSES
Jaime Gómez Díaz
ISBN:978-84-694-1247-3/T-317-2011

Gold is extremely ductile and malleable, and an excellent thermal and electrical conductor; it does not oxidize in air or water, and remains soft and bright. Its principal uses include jewelery (its is easy to work, as it is not hard, has a considered attractive bright brilliance, remains soft and bright, but mainly, due to its high value), dentistry and other medical implants (inertness, not allergenic) and electronics (excellent thermal and electrical conductivity, corrosion resistance) [16]. Lately, a new gold rush has appeared due to unexpected rich and complex chemistry [17, 18, 19, 20, 21]. Many of the properties of gold (its color or reactivity, just to name two) are due to relativistic effects [22].

Gold is found in ores (as veins and different size grains and particles) most often as a metal solid solution with silver (usually 8-10% of Ag). Other metals like K, Na, Ba, Cu,... can also be present in the mineral in different amounts. These ores are mined, and Au is extracted and purified. Extraction is typically performed via the MacArthur-Forrest process [23], which uses cyanides to form the $[Au(CN)_2]^-$ soluble species. This process has been used during a century because of its high gold recoveries, robustness and relatively low costs.

However, cyanides are very toxic, and uncontrolled spills have produced serious damages to ecosystems [24]. Therefore, modifications to the present extraction procedure are called for to develop a more environmentally friendly process.

1.4.2 Extraction

The whole process of the extraction of gold is shown in Fig. 1.6 and can be summarized as follows:

1. Mining: samples are taken and assayed to define the ore from the waste rock. Assay results are used to mark out areas of ore and waste rock, which are mined separately.

2. Crushing: the primary crushers receive ore and waste. They break the larger rocks down to a size suitable for transport.

3. Transport: the rubber belted conveyor transports the ore and waste rock to the mill and waste disposal area.

UNIVERSITAT ROVIRA I VIRGILI
FIRST-PRINCIPLES MECHANISTIC STUDIES OF AMMONIA-RELATED INDUSTRIAL PROCESSES
Jaime Gómez Díaz
ISBN:978-84-694-1247-3/T-317-2011

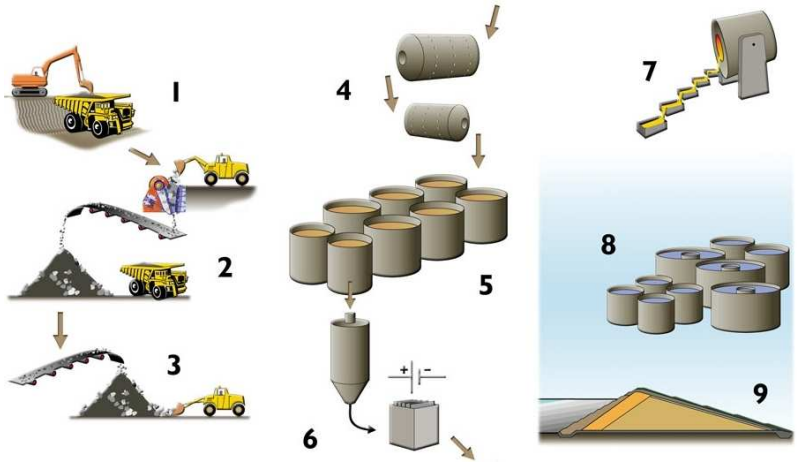

Figure 1.6: Gold extraction steps. 1, mining; 2, crushing; 3, transport; 4, grinding and sizing; 5, leaching and adsorption; 6, elution and electrowinning; 7, bullion production; 8, water treatment; 9 tailings disposal. Taken from Ref. [25].

4. Grinding and sizing: ore is stockpiled before being fed into a mill with limestone, water and steel balls. The larger particles from this mill are recirculated into the mill for more grinding. The finer particles receive more grinding in a ball mill, and are size classified to give a final product of 80% <70 μm.

5. Leaching and adsorption: a slurry of ground ore, water and a weak cyanide solution is fed into large steel leach tanks where the gold and silver are dissolved. CN^- anion forms the soluble molecule $[Au(CN)_2]^-$ as part of a redox process. Following this leaching process, the slurry passes through several adsorption tanks containing carbon granules which adsorb the gold and silver. This process removes around 93% of the gold and 70% of the silver.

6. Elution and electrowinning: the loaded carbon is fed into an elution column where the precious metals are washed off. The barren carbon is recycled and the wash solution is passed through electrowinning cells where gold and silver are won onto stainless steel cathodes in a process inverse to the dissolution.

UNIVERSITAT ROVIRA I VIRGILI
FIRST-PRINCIPLES MECHANISTIC STUDIES OF AMMONIA-RELATED INDUSTRIAL PROCESSES
Jaime Gómez Díaz
ISBN:978-84-694-1247-3/T-317-2011

7. Bullion production: the loaded cathodes are rinsed to yield a gold and silver bearing sludge which is dried, mixed with fluxes and put into the furnace. After several hours the molten material is poured into a cascade of moulds producing bars.

8. Water treatment: some water from dewatering the mine, from the embankment underdrains and decantation from the tailings pond is recycled to use in the grinding circuit. Excess water is pumped to a water treatment plant to achieve the required standards before discharge it.

9. Tailings disposal: waste rock from the mine is used to build the embankment structure. The embankment retains the tailings slurry in a pond where solids settle and compact. Water is decanted off and used in the process plant or treated before it is discharged.

1.5 Thesis outline

The structure of the thesis is as follows:

In Chapter 2 a brief review in the most important theories and computational tools used throughout the thesis is presented.

In Chapter 3 a detailed theoretical study on the mechanism of the first step of the Ostwald process is stated, as well as a thermodynamic study in the thermodynamic stability of the different possible structures of the PtRh catalyst. The reaction mechanism on Pt and PtRh is extended to Au, Cu, Ir, Pd and Rh.

Chapter 4 states a theoretical work on the Degussa and Andrussow processes. The reactions that govern the mechanism are studied on Au, Cu, Ir, Pd, Pt and Rh.

In Chapter 5 the extraction of gold from ore through MacArthur-Forrest process is studied by means of Density Functional Theory.

After that, the main conclusions of the thesis are stated, and in Appendix A the methods used to calculate bulk cells parameters and gas phase molecules are shown.

UNIVERSITAT ROVIRA I VIRGILI
FIRST-PRINCIPLES MECHANISTIC STUDIES OF AMMONIA-RELATED INDUSTRIAL PROCESSES
Jaime Gómez Díaz
ISBN:978-84-694-1247-3/T-317-2011

Chapter 2

Theoretical background

In this chapter, I will revise the most important theories and tools in the field of first principles atomistic heterogeneous catalysis calculations. First, Density Functional Theory is briefly discussed. Second, basic aspects of the implementation are described. After that, some analysis tools (Bader charges and Electron Localization Function) are described. Finally, transition states searching, *ab-initio* thermodynamics and linear relationships are concisely discussed.

2.1 Introduction

In 1926, Erwin Schrödinger proposed the equation that takes his name

$$\widehat{H}\Psi = E\Psi \tag{2.1}$$

opening the way to accurate atomic and molecular accurate calculations. The development and subsequent spread of computers stablished the use of the calculations in the framework of quantum theory. Due to its complexity, the complete Schrödinger equation can be analitically resolved only for two body systems, as hydrogenoid atom. For more complex calculations, approximations are needed. All the calculations carried out in this thesis make use of Density Functional Theory (DFT) to solve the stationary Schrödinger equation.

UNIVERSITAT ROVIRA I VIRGILI
FIRST-PRINCIPLES MECHANISTIC STUDIES OF AMMONIA-RELATED INDUSTRIAL PROCESSES
Jaime Gómez Díaz
ISBN:978-84-694-1247-3/T-317-2011

2.2 Density Functional Theory

The electronic wavefunction of an N-electron system depends on 3N space coordinates and N spin coordinates. The hamiltonian operator includes one and two electrons space terms, then the system energy can be written in terms of integrals that imply six space coordinates. Moreover, the wavefunction of a polielectronic system has an excess of information, and it lacks a direct physical meaning. In 1964, inspired in the Thomas-Fermi model (1927) and Dirac additions (1928), Pierre Hohenberg and Walter Kohn proved that [26], for non-degenerated ground state systems, the energy, the wave function and the electronic properties, are univocally determined by the electronic probability density of the ground state, $n_0(x, y, z)$, a function of only three variables. Density Functional Theory attempts to calculate E_0 (the ground state energy) and other properties from the electronic density. This theorem was proved for degenerate ground states by Levy [27].

2.3 Formalism

In many-body electronic structure calculations, the nuclei of the molecules or clusters are seen as fixed (Born-Oppenheimer or adiabatic approximation), generating a static external potential, V, in which the electrons are moving. A stationary electronic state is then described by a wave function, $\Psi(\vec{r_1}, \ldots, \vec{r_N})$, fulfilling the many-electron Schrödinger equation:

$$\begin{aligned} \widehat{H}\Psi = \left[\widehat{T} + \widehat{V} + \widehat{U}\right]\Psi &= \\ = \left[\sum_i^N -\frac{\hbar^2}{2m}\nabla_i^2 + \sum_i^N V(\vec{r_i}) + \sum_{i<j} U(\vec{r_i}, \vec{r_j})\right]\Psi &= E\Psi \end{aligned} \tag{2.2}$$

Where $\widehat{T}$ is the kinetic energy operator of the electrons, $\widehat{V}$ the external potential and $\widehat{U}$ the electron-electron interaction. DFT provides an appealing alternative to this equation, being much more versatile as it provides a way to systematically map the many-body problem onto a single-body problem. In DFT, the key variable is the particle density $n(\vec{r})$, which is given by

UNIVERSITAT ROVIRA I VIRGILI
FIRST-PRINCIPLES MECHANISTIC STUDIES OF AMMONIA-RELATED INDUSTRIAL PROCESSES
Jaime Gómez Díaz
ISBN:978-84-694-1247-3/T-317-2011

$$n(\vec{r}) = N \int \mathrm{d}^3\, r_2 \int \mathrm{d}^3\, r_3 \cdots \int \mathrm{d}^3\, r_N \Psi^*(\vec{r}, \vec{r}_2, \ldots, \vec{r}_N)\Psi(\vec{r}, \vec{r}_2, \ldots, \vec{r}_N) \tag{2.3}$$

Hohenberg and Kohn proved in 1964 [26] that the relation expressed above can be reversed, i.e. to a given ground state density $n_0(\vec{r})$, it is, in principle, possible to calculate the corresponding ground state wavefunction $\Psi_0(\vec{r}_1, \ldots, \vec{r}_N)$. In other words, Ψ_0 is a unique functional of n_0

$$\Psi_0 = \Psi_0[n_0] \tag{2.4}$$

and consequently, all other ground state observables O are also functionals of n_0

$$\langle O \rangle [n_0] = \left\langle \Psi_0[n_0] \left| \widehat{O} \right| \Psi_0[n_0] \right\rangle \tag{2.5}$$

This is called the first Hohenberg and Kohn theorem, that can be easily demonstrated. From this follows, in particular, that also the ground state energy is a functional of n_0

$$E_0 = E[n_0] = \left\langle \Psi_0[n_0] \left| \widehat{T} + \widehat{V} + \widehat{U} \right| \Psi_0[n_0] \right\rangle \tag{2.6}$$

where the contribution of the external potential $\left\langle \Psi_0[n_0] \left| \widehat{V} \right| \Psi_0[n_0] \right\rangle$ can be written explicitly in terms of the density

$$V[n] = \int V(\vec{r}) n(\vec{r}) \mathrm{d}^3 r \tag{2.7}$$

The functionals $T[n]$ and $U[n]$ are called universal functionals while $V[n]$ is obviously non-universal, as it depends on the system under study. Given a specified system, *i.e.* V is known, the functional has to be minimised

$$E[n] = T[n] + U[n] + \int V(\vec{r}) n(\vec{r}) \mathrm{d}^3 r \tag{2.8}$$

with respect to $n(\vec{r})$, assuming that reliable expressions for $T[n]$ and $U[n]$ exist. In order to transform this formal equation in an affordable problem, a second Hohenberg and Kohn theorem and the Kohn-Sham method are needed. This second theorem states that the electronic density

UNIVERSITAT ROVIRA I VIRGILI
FIRST-PRINCIPLES MECHANISTIC STUDIES OF AMMONIA-RELATED INDUSTRIAL PROCESSES
Jaime Gómez Díaz
ISBN:978-84-694-1247-3/T-317-2011

for a non-degenerated ground state system is that which minimise the energy of the system. The implications of this theorem, as well easily demonstrable, are that for a test density $n_v(\vec{r})$

$$E_0 \leq E_v[n_v(\vec{r})] \tag{2.9}$$

Thus, a successful minimisation of the energy functional will yield the ground state density n_0 (second theorem) and thus all other ground state observables (first theorem). The variational problem of minimising the energy functional $E[n]$ can be solved by applying the Lagrangian method of undetermined multipliers, which was done by Kohn and Sham in 1965 (Kohn-Sham method [28]). Hereby, one uses the fact that the functional in the equation above can be written as a fictitious density functional of a non-interacting system

$$E_s[n] = \left\langle \Psi_s[n] \left| \widehat{T}_s + \widehat{V}_s \right| \Psi_s[n] \right\rangle \tag{2.10}$$

where T_s denotes the non-interacting kinetic energy and V_s is an external effective potential in which the particles are moving. Obviously, $n_s(\vec{r}) \equiv n(\vec{r})$ if V_s is chosen to be

$$V_s = V + U + (T - T_s) \tag{2.11}$$

Thus, one can solve the so-called Kohn-Sham equations of this auxiliary non-interacting system

$$\left[-\frac{\hbar^2}{2m}\nabla^2 + \widehat{V}_s(\vec{r}) \right] \phi_i(\vec{r}) = \epsilon_i \phi_i(\vec{r}) \tag{2.12}$$

which yields the orbitals ϕ_i that reproduce the density $n(\vec{r})$ of the original many-body system

$$n(\vec{r}) \equiv n_s(\vec{r}) = \sum_i^N |\phi_i(\vec{r})|^2 \tag{2.13}$$

The effective single-particle potential V_s can be written in more detail as

$$V_s = V + \int \frac{e^2 n_s(\vec{r}\,')}{|\vec{r} - \vec{r}\,'|} \mathrm{d}^3 r' + V_{\mathrm{XC}}[n_s(\vec{r})] \tag{2.14}$$

UNIVERSITAT ROVIRA I VIRGILI
FIRST-PRINCIPLES MECHANISTIC STUDIES OF AMMONIA-RELATED INDUSTRIAL PROCESSES
Jaime Gómez Díaz
ISBN:978-84-694-1247-3/T-317-2011

where the second term denotes the so-called Hartree term describing the electron-electron Coulomb repulsion, while the last term V_{XC} is called the exchange-correlation potential. Here, V_{XC} includes all the many-particle interactions. Since the Hartree term and V_{XC} depend on $n(\vec{r})$, which depends on the ϕ_i, which in turn depend on V_s, the problem of solving the Kohn-Sham equation has to be made in a self-consistent (*i.e.* iterative) way.

The general procedure starts with an initial guess for $n(\vec{r})$, then calculates the corresponding V_s and solves the Kohn-Sham equations for the ϕ_i. From these one calculates a new density and starts again. This procedure is then repeated until convergence is reached.

2.4 Approximations

The major problem of DFT is that the exact exchange-correlation functional, $\mathrm{V_{XC}}$, is not known, except for the free electron gas. However, approximations exist which allow calculating certain physical quantities quite accurately. In physics, the most widely used approximation is the Local-Density Approximation (LDA), where the functional depends only on the density at each point in space where the functional is evaluated and they are based on the Homogeneous Electron Gas (HEG) model. For non-spin polarized systems is written as

$$E_{\mathrm{XC}}[n] = \int \epsilon_{\mathrm{XC}}(n) n(\vec{r}) \mathrm{d}^3 r \tag{2.15}$$

where ϵ_{XC} is the exchange-correlation energy density. The functional can be generalized to Local Spin-Density Approximation (LSDA) to include electron spin

$$E_{\mathrm{XC}}[n_\uparrow, n_\downarrow] = \int \epsilon_{\mathrm{XC}}(n_\uparrow, n_\downarrow) \mathrm{d}^3 r \tag{2.16}$$

The exchange-correlation energy and can be linearly decomposed in exchange and correlation terms $E_{\mathrm{XC}} = E_X + E_C$. The exchange-energy density of a HEG is known analytically. For not spin polarized systems takes this form

UNIVERSITAT ROVIRA I VIRGILI
FIRST-PRINCIPLES MECHANISTIC STUDIES OF AMMONIA-RELATED INDUSTRIAL PROCESSES
Jaime Gómez Díaz
ISBN:978-84-694-1247-3/T-317-2011

$$E_x^{\mathrm{LDA}}[n] = -\frac{3}{4}\left(\frac{3}{\pi}\right)^{1/3} \int n(\vec{r})^{4/3}\ \mathrm{d}\vec{r} \tag{2.17}$$

LDA functionals employ this expression for exchange, under the approximation that the exchange-energy in a system where the density is not homogeneous, is obtained by applying the HEG results. There is no analytic expression for the whole correlation functional, not even for the HEG, but it is known for the upper and lower density limits (infinitely-strong and infinitely-weak correlation). For spin-polarized systems the expression has to be expanded.

Accurate quantum Monte Carlo simulations for the energy of the HEG have been performed for several intermediate values of the density. The most popular LDA functionals interpolate these accurate values obtained from simulation while reproducing the exactly known limiting behavior. Several approaches, that use different analytic forms for ϵ_C, have generated several LDA functionals. Among them, the most widely used in solid state physics is probably "Perdew-Zunger" (PZ81) [29].

A further approximation is the Generalized Gradient Approximation (GGA), that although it is still local, takes into account the gradient of the density at the same point, and for spin-polarized systems is

$$E_{\mathrm{XC}}[n_\uparrow, n_\downarrow] = \int \epsilon_{\mathrm{XC}}(n_\uparrow, n_\downarrow, \vec{\nabla} n_\uparrow, \vec{\nabla} n_\downarrow)\mathrm{d}^3 r \tag{2.18}$$

This approach is better for systems where the density oscilate not smoothly than those based in the homogeneous electron gas. Good results for molecular geometries and ground state energies are achieved using this GGA functionals. In solid state physics, "Perdew-Wang 1991" (PW91) [30, 31],"Perdew-Burke-Ernzerhof" (PBE) [32], and the revision of the last (RPBE) [33] functionals are profusely used as they provide good results in terms of the calculation time/accuracy balance.

2.5 Implementation

2.5.1 Pseudopotentials

The wavefunction in the proximities of the nuclei oscillate severely due to the strong interaction with the ionic core. As a consequence, the basis

UNIVERSITAT ROVIRA I VIRGILI
FIRST-PRINCIPLES MECHANISTIC STUDIES OF AMMONIA-RELATED INDUSTRIAL PROCESSES
Jaime Gómez Díaz
ISBN:978-84-694-1247-3/T-317-2011

cut-off energy (mentioned in the following section) has to be very large to describe the inner electrons. This makes computationally very demanding to solve the Kohn-Sham equations in this region. To reduce the computational cost, pseudopotentials are used. These pseudopotentials can be viewed as the potential that the valence electrons "feel" around the nucleus and the core electrons. This approximation is based on the assumption that *only* the valence electrons are chemically active.

The pseudopotentials are constructed by replacing the true potential in regions near to the nucleus by a smoother function, see Fig. 2.1. Further away, the new potential has the same form as the ionic potential. The smoothness of the potential decreases the number of basis functions needed to describe the wave functions and diminishes the computational time required.

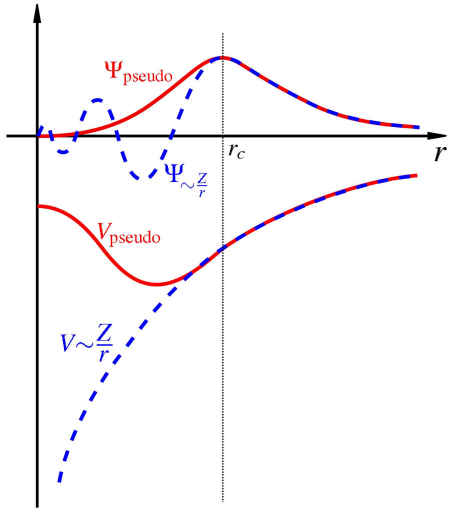

Figure 2.1: Schematic representation of the real wave function Ψ and the pseudopotentials equivalent around the nuclei. r_c stands for the core radius. Taken from Ref. [34].

Two types of pseudopotentials used in solid state physics are the Vanderbilt UltraSoft (US-PP) [35] and the so called Projector Augmented Wave (PAW) [36] pseudopotentials. In this work we use the PAW pseudopotentials. This method for describing electron density will be revised

UNIVERSITAT ROVIRA I VIRGILI
FIRST-PRINCIPLES MECHANISTIC STUDIES OF AMMONIA-RELATED INDUSTRIAL PROCESSES
Jaime Gómez Díaz
ISBN:978-84-694-1247-3/T-317-2011

in more detail in Section 2.5.3.

Generally, pseudopotentials generated by PAW method are more accurate than the UltraSoft ones. This is due to two reasons. First, the core radii (the cut-off distance or the extension in space of the pseudopotential) are smaller in PAW than in US pseudopotentials. Second, the PAW pseudopotentials reconstruct the real wave function with all the nodes of it in the core region and US-PP do not. On the other hand, the required energy cut-offs for PAW pseudopotentials and the basis sets are somewhat larger.

2.5.2 Plane waves as basis sets

For a numerical description of the Kohn-Sham wave functions, a basis set has to be chosen. Two types of basis sets are commonly used in DFT calculations, local basis functions and plane wave basis sets. The former include sets such as the Gaussian and Slater basis sets, and are mainly used for finite systems [37]. In DFT calculations for periodic systems, a plane wave basis set is often chosen as it follows the periodicity of the system. The expansion of the wave function is based on Blöch's theorem [38], and allows the use of Fast Fourier Transform (FFT), increasing the calculation speed for medium size systems. According to this theorem it is possible to expand the wave functions as follows:

$$\Psi_{[i,k]}(\vec{r}) = \sum_{\vec{G}} c_{i,\vec{k}+\vec{G}} e^{i(\vec{k}+\vec{G})\vec{r}} \tag{2.19}$$

where $\vec{G}$ is the reciprocal lattice vector and $\vec{k}$ is the wave vector limited to the first Brillouin zone. An infinite number of plane waves is needed to expand the wave functions in each point in the Brillouin zone, that makes the problem numerically unsolvable. This difficulty is resolved by expanding the wave function only in the plane waves with the lowest kinetic energy.

2.5.3 Real space methods

The results presented in Chapter 5 were performed using Grid-based Projector Augmented Wave method (GPAW) [39, 40]. The use of uniform three-dimensional real space grids for representing wave functions allows

UNIVERSITAT ROVIRA I VIRGILI
FIRST-PRINCIPLES MECHANISTIC STUDIES OF AMMONIA-RELATED INDUSTRIAL PROCESSES
Jaime Gómez Díaz
ISBN:978-84-694-1247-3/T-317-2011

for flexible boundary conditions, efficient multigrid algorithms for solving Poisson and Kohn-Sham equations and efficient parallelization using simple real-space domain decomposition. Now, a short description of the method is shown.

- The Projector Augmented Wave method.

  The PAW method [36] is based on a transformation between smooth pseudo-wavefunctions $\widetilde{\psi}_n$, and the true all-electron Kohn-Sham wave function ψ_n. The core states of the atoms are considered frozen. Given a smooth pseudo-wave function, the corresponding all electron wave function (that is orthogonal to the set of core orbitals) can be obtained through a linear transformation

  $$\psi_n(\vec{r}) = \widehat{\tau}\widetilde{\psi}_n(\vec{r}) \tag{2.20}$$

  The transformation operator $\widehat{\tau}$ is given in terms of atomic-centered all-electron wave function $\phi_i^a(\vec{r})$, the corresponding smooth partial waves $\widetilde{\phi}_i^a(\vec{r})$ and projector functions $\widetilde{p}_i^a(\vec{r})$. The atom-centered all-electron wave functions from a calculation of a single atom with spherical symmetry

  $$\phi_i^a(\vec{r}) = \phi_{nl}^a(\vec{r})Y_{l,m}(\hat{\vec{r}}) \tag{2.21}$$

  where $Y_{l,m}$ are the real-valued spherical harmonics. A radial cut-off distance, r_a^c, that defines the atomic augmentation sphere is chosen, similarly to a cut-off radius for a pseudopotential. The larger is the augmentation sphere, the smoother the pseudo-wavefunctions, but overlap with neighboring augmentation spheres must be avoided.

  For all the all-electron valence states, smooth partial waves are constructed, and one smooth projector must also be defined for each partial wave. These partial waves must match the corresponding all-electron waves for $r{>}r_c^a$. A smooth projector function must also be defined for each partial wave, $\widetilde{p}_i^a(\vec{r}) = \widetilde{p}_{nl}^a(\vec{r})Y_L(\widehat{\vec{r}})$. In principle, an infinite number of projectors and partial waves are required for the PAW method to be exact. For practical (real) calculations, a high-accuracy data set will need only one or two projector functions for each angular moment channel of importance.

UNIVERSITAT ROVIRA I VIRGILI
FIRST-PRINCIPLES MECHANISTIC STUDIES OF AMMONIA-RELATED INDUSTRIAL PROCESSES
Jaime Gómez Díaz
ISBN:978-84-694-1247-3/T-317-2011

From the atomic frozen-core electron density $n_c^a(\vec{r})$, a new smooth-core electron density $\widetilde{n}_c^a(\vec{r})$ is constructed. This density must be identical to $n_c^a(\vec{r})$ for radii larger than r_c^a. The whole pseudoelectron density has contributions from the wave function and from atom-centered smooth-core electron densities. The true all-electron density can be obtained from the pseudoelectron density. Finally, the PAW total energy is a function of the pseudo-wavefunctions $\widetilde{\psi}_n(\vec{r})$ and the occupation numbers.

- Localized functions and grid technique

  In this grid representation, the integrals over space are turned into sums over grid points. In the PAW [36] method often is necessary to calculate the integral of a localized function, centered on an atom, multiplied by a function extended over all of space. The evaluation of this localized function on the grid is not computationally expensive, as, for each atom, is independent of the system size.

- Real-space-grid formulation of the PAW method

  The formulas for densities, potentials, and energies must be translated to a discretized form for using them with a discrete representation.

2.5.4 k-points

To optimize the calculations it is helpful to compute only the Bloch functions at a carefully selected set of points in the Brillouin zone. When a finite set of plane waves is used, each $\vec{k}$ point in the Brillouin zone is occupied with a finite number of states, but the number of $\vec{k}$ points is still infinite. As the eigenvalues in two $\vec{k}$ points close in $\vec{k}$ space, are almost the same [34], we only need to sample the eigenvalues in a finite number of $\vec{k}$ points, where each $\vec{k}$ point is representing a region in the $\vec{k}$ space. To decrease the number of $\vec{k}$ points further, special $\vec{k}$ points are often used, where the symmetry of the system is exploited. The Monkhorst-Pack grid [41] is the one usually used in the present work.

UNIVERSITAT ROVIRA I VIRGILI
FIRST-PRINCIPLES MECHANISTIC STUDIES OF AMMONIA-RELATED INDUSTRIAL PROCESSES
Jaime Gómez Díaz
ISBN:978-84-694-1247-3/T-317-2011

2.5.5 Electronic minimization

Many of the algorithms implemented in VASP use an iterative matrix-diagonalization scheme: they are based on the conjugate gradient scheme [42], block Davidson scheme [43], or a Residual MiniMization scheme-Direct Inversion in the Iterative Subspace (RMM-DIIS) [44, 45].

For the mixing of the charge density an efficient Broyden/Pulay mixing scheme [46] is used. Input charge density and wavefunctions are independent quantities. Within each self-consistency loop the charge density is used to set up the Hamiltonian, then the wavefunctions are optimized iteratively so that they get closer to the exact wavefunctions of this Hamiltonian. From the optimized wavefunctions a new charge density is calculated, which is then mixed with the old input-charge density.

The conjugate gradient and the residual minimization scheme do not recalculate the exact Kohn-Sham eigenfunctions but an arbitrary linear combination of the bands lowest eigenfunctions. Therefore it is in addition necessary to diagonalize the Hamiltonian in the subspace spanned by the trial-wavefunctions, and to transform the wavefunctions accordingly (i.e. perform a unitary transformation of the wavefunctions, so that the Hamiltonian is diagonal in the subspace spanned by transformed wavefunctions). This step is usually called sub-space diagonalization:

$$\begin{gathered}\langle\phi_j\ |\hat{H}|\phi_i\rangle = H_{ij} \\ H_{ij}U_{ij} = \epsilon_k U_{ik} \\ \phi_j \leftarrow U_{jk}\phi_k\end{gathered}$$

For GPAW package, Pulay mixing techniques are used for obtaining the self consistent density [44, 47]. Subspace diagonalizations and the residual minimization method [42, 47] using preconditioning of the electronic gradients for iteratively improving the wave function are used.

2.6 Ionic relaxation

Two numerical methods have been used to minimize the energy of the ions positions:

- A quasi-Newton (variable metric) algorithm is used to relax the ions into their instantaneous groundstate. The forces and the stress ten-

UNIVERSITAT ROVIRA I VIRGILI
FIRST-PRINCIPLES MECHANISTIC STUDIES OF AMMONIA-RELATED INDUSTRIAL PROCESSES
Jaime Gómez Díaz
ISBN:978-84-694-1247-3/T-317-2011

sor are used to determine the search directions for finding the equilibrium positions (the total energy is not taken into account). This algorithm is very fast and efficient close to local minima, but fails badly if the initial positions are a bad guess. Since the algorithm builds up an approximation of the Hessian matrix it requires very accurate forces, otherwise it will fail to converge. The implemented algorithm is the mentioned RMM-DIIS [44, 45]. It implicitly calculates an approximation of the inverse Hessian matrix by taking into account information from previous iterations. On startup, the initial Hessian matrix is diagonal. Information from old steps (which can lead to linear dependencies) is automatically removed from the iteration history, if required. The number of vectors kept in the iterations history (which corresponds to the rank of the Hessian matrix) must not exceed the degrees of freedom. Naïvely, the number of degrees of freedom is $3N - 1$, where N is the number of ions. Symmetry arguments, or constraints, can reduce this number significantly.

- A conjugate-gradient algorithm [42] is used to relax the ions into their instantaneous groundstate. In the first step ions, (and cell shape) are changed along the direction of the steepest descent (i.e. the direction of the calculated forces and stress tensor). The conjugate gradient method requires a line minimization, which is performed in several steps:

  i) First, a trial step into the search direction (scaled gradients) is done, with the length of the trial step suitable, then the energy and the forces are recalculated.

  ii) The approximate minimum of the total energy is calculated form a cubic (or quadratic) interpolation taking into account the change of the total energy and the change of the forces (three pieces of information), then a corrector step to the approximate minimum is performed.

  iii) After the corrector step the forces and energy are recalculated and it is checked whether the forces contain a significant component parallel to the previous search direction. If this is the case, the line minimization is improved by further corrector steps using a variant of Brent's algorithm [48].

UNIVERSITAT ROVIRA I VIRGILI
FIRST-PRINCIPLES MECHANISTIC STUDIES OF AMMONIA-RELATED INDUSTRIAL PROCESSES
Jaime Gómez Díaz
ISBN:978-84-694-1247-3/T-317-2011

2.6.1 Supercells

When using plane waves as basis functions, the system has to be periodic in all directions in space, in order to fulfill Bloch's theorem. As many interesting systems are not periodic, supercells are used to ensure the correct translational symmetry.

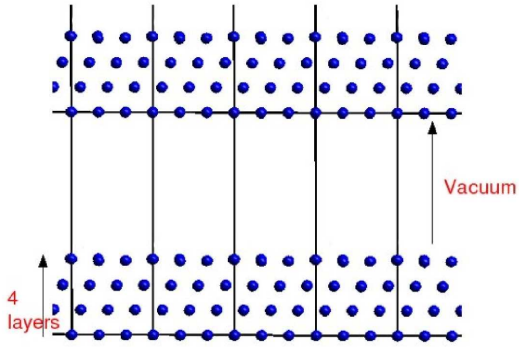

Figure 2.2: Two-dimensional representation of a four layers slab generated by the replication of a supercell. The size of the supercell is indicated by the black boxes, and the vacuum between slabs is indicated.

Figure 2.2 shows an example of such a cell, where the model system is a Pt(111) surface. As the system is periodic in all directions, a vacuum space is added to the slab in z direction. The supercell is then repeated in all three space directions in the model system.

The use of the supercell means that such a motive will be repeated in all three directions, and sometimes this might result in unrealistic situations. Usually this effect can be minimized by using large enough supercells. However, the size of the supercell must be a compromise between a realistic enough description of the system and the use of a reasonable computational time.

UNIVERSITAT ROVIRA I VIRGILI
FIRST-PRINCIPLES MECHANISTIC STUDIES OF AMMONIA-RELATED INDUSTRIAL PROCESSES
Jaime Gómez Díaz
ISBN:978-84-694-1247-3/T-317-2011

2.7 Bader analysis

Richard F.W. Bader developed an intuitive way of dividing molecules into atoms called the Quantum Theory of Atoms in Molecules (QTAIM). His definition of an atom is based purely on the electronic charge density.

The theory makes a generalization of quantum mechanics that leads to the definition of an open system and to a prediction of its properties [49, 50]. This generalization is accomplished through an extension of Schwinger's principle of stationary action [51]. That extension is possible only if a certain boundary condition is satisfied. The boundary condition demands that the flux in the gradient vector field of the charge density $n(\vec{r})$ does not exist at every point of the surface $S(\Omega, \vec{r})$ which bounds an open Ω. That is, the surface is one of zero flux in ∇n. As a consequence of the boundary

$$\nabla n(\vec{r}) \cdot \vec{n}(\vec{r}) \qquad \forall \ \vec{r} \in S(\Omega, \vec{r}) \tag{2.22}$$

being stated in terms of a property of the electronic charge density, quantum subsystems are defined in real space. This condition leads to the partitioning of the molecular system into a set of spatial regions. The result is a theory where atoms, bonds, the structure and the structural stability can be easily defined and determined, see an example in Fig. 2.3.

Bader's theory of atoms in molecules is useful for charge analysis. For example, the charge enclosed within the Bader volume is a good approximation to the total electronic charge of an atom. The charge distribution can be used to determine multipole moments of interacting atoms or molecules. Bader's analysis has also been used to define the hardness of atoms, which can be used to quantify the cost of removing charge from an atom. The theory also provides a definition for chemical bonding that gives numerical values for bond strength.

2.8 Electron Localization Function

The electron localization function (ELF) is a measure of the probability of finding an electron in the neighborhood space of a reference electron located at a given point and with the same spin. Physically, this measures the extent of spatial localization of the reference electron and provides

UNIVERSITAT ROVIRA I VIRGILI
FIRST-PRINCIPLES MECHANISTIC STUDIES OF AMMONIA-RELATED INDUSTRIAL PROCESSES
Jaime Gómez Díaz
ISBN:978-84-694-1247-3/T-317-2011

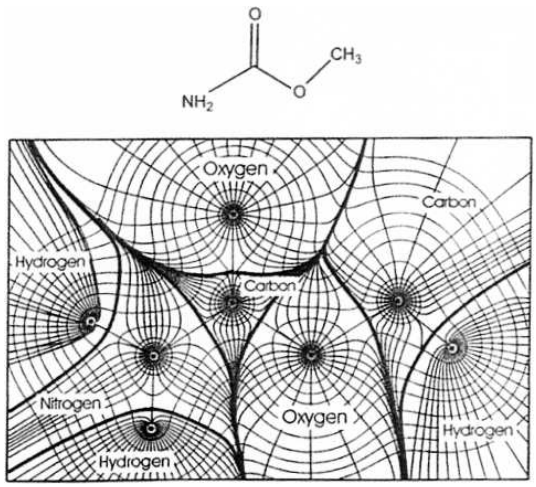

Figure 2.3: Acetamide trajectories of the gradient vector ($\vec{r}$), superimposed on the charge-density contours of ($\vec{r}$). Zero-flux surfaces defining the atomic basins and bond paths are indicated by bold lines. Their intersections correspond to the bond critical points. Taken from Ref. [52].

a method for the mapping of electron pair probability in multielectronic systems.

ELF's usefulness stems from the manner it allows the analysis of electron localization in a "chemically intuitive" way. For example, the shell structure of heavy atoms is obvious when plotting ELF against the radial distance from the nucleus. For example, the ELF for Krypton has four maxima corresponding with the electrons shell, whereas the electronic density decreases monotonically and the radially weighted density fails to show all shells.

When applied to molecules, an analysis of the ELF shows a clear separation between the core and valence electron, and also shows covalent bonds and lone pairs. Another feature of the ELF is that it is invariant with respect to transformation of the molecular orbitals.

The ELF was originally defined by Axel D. Becke and Kenneth E. Edgecombe in 1990 [53, 54]. They first argued that a measure of the electron localization is provided by

UNIVERSITAT ROVIRA I VIRGILI
FIRST-PRINCIPLES MECHANISTIC STUDIES OF AMMONIA-RELATED INDUSTRIAL PROCESSES
Jaime Gómez Díaz
ISBN:978-84-694-1247-3/T-317-2011

$$D_\sigma(\vec{r}) = \tau_\sigma(\vec{r}) - \frac{1}{4}\frac{(\nabla n_\sigma(\vec{r}))^2}{n_\sigma(\vec{r})} \tag{2.23}$$

where n is the electron spin density and τ the kinetic energy density. D is expected to be small in those regions of space where localized electron are to be found. Given the arbitrariness of the magnitude of the localization measure provided by D, it is compared to the corresponding value for a uniform electron gas with spin density equal to $n(\vec{r})$, which is given by

$$D^0_\sigma(\vec{r}) = \frac{3}{5}(6\pi^2)^{2/3} n^{5/3}_\sigma(\vec{r}) \tag{2.24}$$

The ratio

$$\chi_\sigma(\vec{r}) = \frac{D_\sigma(\vec{r})}{D^0_\sigma(\vec{r})} \tag{2.25}$$

is a dimensionless localization index that expresses electron localization with respect to the uniform electron gas. In the final step, the ELF is defined in terms of χ by mapping its values on to the range $0 \leq \mathrm{ELF} \leq 1$ by defining the electron localization function as

$$\mathrm{ELF}(\vec{r}) = \frac{1}{1 + \chi^2_\sigma(\vec{r})} \tag{2.26}$$

ELF=1 corresponding to perfect localization and ELF=1/2 corresponding to the electron gas. The original derivation was based on Hartree-Fock theory. For Density Functional Theory, the approach was generalized by Savin in 1992 [54].

2.9 Transition state searching

An important problem in theoretical chemistry and condensed matter physics is the calculation of transition rates. It is possible to obtain accurate estimates of rates using a purely statistical approach, the Transition State Theory, TST. Apart from the adiabatic approximation, TST relies on two basic assumptions, the rate is slow enough that a Boltzmann distribution is established and maintained in the reactant state, and a dividing

UNIVERSITAT ROVIRA I VIRGILI
FIRST-PRINCIPLES MECHANISTIC STUDIES OF AMMONIA-RELATED INDUSTRIAL PROCESSES
Jaime Gómez Díaz
ISBN:978-84-694-1247-3/T-317-2011

surface of dimensionality D-1, where D is the number of degrees of freedom in the system, can be identified such that a reacting trajectory going from the initial state only crosses the dividing surface once. The dividing surface must, therefore, represent a bottleneck for the transition. Because of the typical temperatures of interest, the harmonic approximation to TST can typically be used in studies of reactions at crystal surfaces. The search for the optimal transition state then becomes a search for the lowest few saddle points at the edge of the potential energy basin corresponding to the initial state. A path connecting the initial and final states that typically has the greatest statistical weight is the Minimum Energy Path (MEP). Many different methods have been presented for finding MEPs and saddle points:

2.9.1 Regular NEB method

The Nudged Elastic Band [55, 56, 57], NEB, method is an efficient method for finding the Minimum Energy Path between a given initial and final state. The MEP is found by constructing a set of images of the system between these two states. A spring interaction between adjacent images is added to ensure continuity of the path, thus mimicking an elastic band. An optimization of the band, involving the minimization of the force acting on the images, brings the band to the MEP.

For a given initial state, the substrate, and a final state, the product, a chain of n states is generated between the two end points by interpolation. Each state is described by a vector $\vec{R}$ containing all the coordinates changing during the reaction. The initial state is then described as $\vec{R}_0$ and the final state as $\vec{R}_{n+1}$. The direction along the path can be defined as an unit vector, $\vec{r}$, where

$$\vec{r}_n = \frac{\vec{R}_{n+1} - \vec{R}_{n-1}}{|\vec{R}_{n+1} - \vec{R}_{n-1}|} \tag{2.27}$$

The force on each of the n configurations can be split in the force along the path ($\vec{F}_i^s|_{\|}$) and the force perpendicular to the path ($\nabla E(\vec{R}_i)|_{\perp}$)

$$\vec{F} = \vec{F}_i^s|_{\|} - \nabla E(\vec{R}_i)|_{\perp} \tag{2.28}$$

where the true force is given by

UNIVERSITAT ROVIRA I VIRGILI
FIRST-PRINCIPLES MECHANISTIC STUDIES OF AMMONIA-RELATED INDUSTRIAL PROCESSES
Jaime Gómez Díaz
ISBN:978-84-694-1247-3/T-317-2011

$$\nabla E(\vec{R}_i)|_\perp = \nabla E(\vec{R}_i) - (\nabla E(\vec{R}_i)\hat{\tau}_i \tag{2.29}$$

where $\hat{\tau}_i$ is the normalized local tangent at image i. The second term on the right side in equation 2.28, $\nabla E(\vec{R}_i)|_\perp$, will be zero if a configuration lies in the minimum energy path. To find the reaction coordinates the energy and force for each image have to be found, and thereafter the image is moved in the direction of $\nabla E(\vec{R}_i)|_\perp$ in small steps. This is repeated until $\nabla E(\vec{R}_i)|_\perp$ approaches zero as required. Moving point n will change $\vec{r}_{n-1}$ and $\vec{r}_{n+1}$ and therefore the whole path should be iterated simultaneously.

The points have a tendency to slide down the barrier if the energy is minimized for this system, as the configurations seek the lowest energy. To prevent this a spring force

$$\vec{F}_i^s|_{||} = k(|\vec{R}_{i+1} - \vec{R}_i| - |\vec{R}_i - \vec{R}_{i-1}|)\hat{\tau}_i \tag{2.30}$$

is added to the true force, where k is the corresponding spring constant.

2.9.2 Climbing Image NEB method

The Climbing Image-NEB method [58], CI-NEB, constitutes a small modification to the NEB method. The information about the shape of the MEP is retained, but a good convergence to a saddle point is also obtained, without adding significant computational cost, see Fig. 2.4.

After a few iterations with the regular NEB, the image with the highest energy i_{max} is identified. The force on this image is not now given by equation (3.18), but rather by

$$\begin{aligned} \vec{F}_{i_{max}} &= -\nabla E(\vec{R}_{i_{max}}) + 2\nabla E(\vec{R}_{i_{max}})|_{||} = \\ &= -\nabla E(\vec{R}_{i_{max}}) + 2\nabla E(\vec{R}_{i_{max}})\hat{\tau}_{i_{max}}\hat{\tau}_{i_{max}} \end{aligned} \tag{2.31}$$

This is the full force due to the potential with the component along the elastic band inverted. The maximum energy image is not affected by the spring forces at all.

Qualitatively, the climbing image moves up the potential energy surface along the elastic band and down the potential surface perpendicular

UNIVERSITAT ROVIRA I VIRGILI
FIRST-PRINCIPLES MECHANISTIC STUDIES OF AMMONIA-RELATED INDUSTRIAL PROCESSES
Jaime Gómez Díaz
ISBN:978-84-694-1247-3/T-317-2011

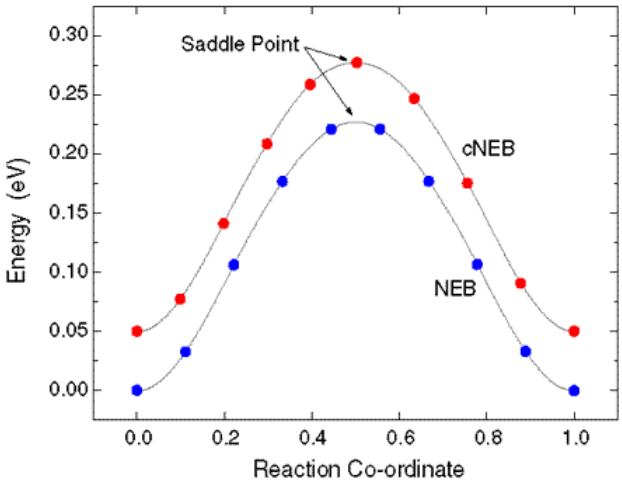

Figure 2.4: Comparison of the search for a minimum energy path with the Nudged Elastic Band method [58] and its *Climbing Image* version. Taken from Ref. [59].

to the band. The other images in the band serve the purpose of defining the one degree of freedom for which a maximization of the energy is carried out [58].

2.10 *Ab-Initio* thermodynamics

In order to extrapolate the results obtained by means of DFT, thus calculated at 0 K and p =0 atm, to real conditions of pressure and temperature, we made use of *ab-initio* thermodynamics. This approximation uses statistical and thermodynamics tools to extrapolate atomistic simulations to macroscopic systems.

In general, the Gibbs free energy G can be expressed in terms of the Hemholtz free energy F as

$$G_{solid} = F + pV \tag{2.32}$$

where p is the pressure and V the volume. This pV term is very small for solids and can be neglected. The Hemholtz free energy F can

UNIVERSITAT ROVIRA I VIRGILI
FIRST-PRINCIPLES MECHANISTIC STUDIES OF AMMONIA-RELATED INDUSTRIAL PROCESSES
Jaime Gómez Díaz
ISBN:978-84-694-1247-3/T-317-2011

be separated in two terms, $F = F_{elec} + F_{vib}$. The first term includes the electronic energy and the electrostatic energy of the ions, and the second the energy due to the lattice vibrations. For the temperatures involved in the studied processes (T<2000 K), thus much smaller than T_{Fermi}, ($\sim 10^5$ K for solids) the electronic degrees of freedom will be mainly frozen, and thus $F_{elec} \approx E_{elec}$ and then

$$G_{solid} \approx F_{solid} \approx E_{elec} + F_{vib} \tag{2.33}$$

The vibrational contributions are small in bulks, as atoms are highly confined, and then

$$G_{solid} \approx E_{elec} \tag{2.34}$$

For an ideal gas, the chemical potential $\mu_{gas}(T,p)$ can be expressed in terms of a reference pressure p^0:

$$\mu_{gas}(T,p) = \mu_{gas}(T,p^0) + k_B T \; ln\left(\frac{p}{p^0}\right) \tag{2.35}$$

The chemical potential is given by an enthalpy h and an entropy s terms:

$$\begin{aligned} \mu_{gas}(T,p^0) = h_{gas}(T,p^0) - Ts_{gas} = \\ = \Delta h_{gas}(T,p^0) + ZPVE + E_{elec} - Ts_{gas}(T,p^0) + k_B T \; ln\left(\frac{p}{p^0}\right) \end{aligned} \tag{2.36}$$

2.11 Linear relationships

Trends in chemical reactions and/or properties can often be described by linear relationships. This is the simplest possible way to reproduce trends, but makes easy its interpretation and prediction. Those relationships have been found in many reactions. I am going to deal with two of these linear relations: i) Brønsted-Evans-Polanyi [60, 61, 62] like, where the activation energy of a reaction is a function of its reaction energy and ii) those where the activation energy depends on the binding energy of an atom [63, 64].

UNIVERSITAT ROVIRA I VIRGILI
FIRST-PRINCIPLES MECHANISTIC STUDIES OF AMMONIA-RELATED INDUSTRIAL PROCESSES
Jaime Gómez Díaz
ISBN:978-84-694-1247-3/T-317-2011

2.11.1 Brønsted-Evans-Polanyi relations

Many reactions that are similar have a systematic linear dependence of the activation energy E_{act} on the reaction energy ΔE:

$$E_{act} = A + B(\Delta E) \tag{2.37}$$

Those relations with the reaction energy have been observed in many different cases. For example, N_2 dissociation barrier over several transition metals [65]; N_2, CO, NO and O_2 dissociation barrier over many transition metals [66]; and ethylene dehydrogenation over flat and stepped Pd surfaces [67].

These relations are closely related to Hammond postulate [68], literally "*If two states, as for example, a transition state and an unstable intermediate, occur consecutively during a reaction process and have nearly the same energy content, their interconversion will involve only a small reorganization of the molecular structures*". This postulate has inherent implications. Many other researchers have contributed towards expansion of the original idea of the Hammond postulate. The best known assumption is that the transition state bears the greater resemblance to the less stable species.

2.11.2 Adsorption energy with binding energy of an atom relations

Other linear relations that have been found for many transition metals [64] are the CH_x, NH_x SH_x and OH_x adsorption energy with that corresponding to the central atom (C, N, S or O). Has been as well observed NH_x, SH and OH intermediates adsorption energy dependence woth that of the central atom (N, S or O) over several transition metal and transition metal nitrides (MeN and Me_2N) [63]. This relation can be explained in terms of the *d*-band model.

Is it possible to combine both, BEP and LSR, kind of relations, which creates a powerful tool to predict potential catalysts properties. Different linear relationships are shown in Chapter 4.

UNIVERSITAT ROVIRA I VIRGILI
FIRST-PRINCIPLES MECHANISTIC STUDIES OF AMMONIA-RELATED INDUSTRIAL PROCESSES
Jaime Gómez Díaz
ISBN:978-84-694-1247-3/T-317-2011

UNIVERSITAT ROVIRA I VIRGILI
FIRST-PRINCIPLES MECHANISTIC STUDIES OF AMMONIA-RELATED INDUSTRIAL PROCESSES
Jaime Gómez Díaz
ISBN:978-84-694-1247-3/T-317-2011

Part II

Results

UNIVERSITAT ROVIRA I VIRGILI
FIRST-PRINCIPLES MECHANISTIC STUDIES OF AMMONIA-RELATED INDUSTRIAL PROCESSES
Jaime Gómez Díaz
ISBN:978-84-694-1247-3/T-317-2011

UNIVERSITAT ROVIRA I VIRGILI
FIRST-PRINCIPLES MECHANISTIC STUDIES OF AMMONIA-RELATED INDUSTRIAL PROCESSES
Jaime Gómez Díaz
ISBN:978-84-694-1247-3/T-317-2011

Chapter 3

HNO_3 synthesis: Results

In this chapter, an overview of the reactions that allow ammonia oxidation to NO is described from a theoretical point of view. This stage is the crucial step in the Ostwald process. The global reaction that takes place in the reactor [4] is the following

$$4NH_3(g) + 5O_2(g) \longrightarrow 4NO(g) + 6H_2O(g);\ \Delta H = -950\ kJ \qquad (3.1)$$

The elementary steps that govern this reaction have been studied for a set of transition metals: Au, Cu, Ir, Pd, Pt and Rh. Flat (111) and defective (211) surfaces have been considered as model catalysts. As well, the reactivity of the PtRh alloy has been studied, and an *ab-initio* thermodynamics study on the stability and volatility of Pt, Rh and their oxides under work conditions (high temperature and O_2 pressure) has been carried out.

3.1 Computational details

All the periodic calculations were performed with Density Functional Theory, DFT, applied to slabs. The calculations have been performed with the VASP code [32, 45, 47, 69, 70, 71, 72] and the exchange-correlation functional used is RPBE [33]. The inner electrons were replaced by PAW pseudopotentials [36], while the monoelectronic functions corresponding to

UNIVERSITAT ROVIRA I VIRGILI
FIRST-PRINCIPLES MECHANISTIC STUDIES OF AMMONIA-RELATED INDUSTRIAL PROCESSES
Jaime Gómez Díaz
ISBN:978-84-694-1247-3/T-317-2011

the valence electrons were expanded in plane waves with a cutoff energy of 400 eV.

The supercells employed to represent the (111) surfaces are p(2x2) and p(3x3). These cell sizes correspond to coverages of 0.25 and 0.11 monolayers (ML) respectively when a single species is adsorbed on them. The slab used to model the metal surface contains four metal layers. The two uppermost of them and the adsorbates have been allowed to relax. Vacuum space equivalent to eight metal layers has been added, and the dipole generated due to the asymmetry of the system due to adsorption has been corrected. The *k-point* sampling is based on Monkhorst-Pack scheme [41] and as dense as 5x5x1. In an equivalent way, to represent the alloy, the same slab containing four layers has been used. For the segregation study instead, a slab containing six layers has been employed. For (211) surfaces a (3x1) supercell with nine metal layers thick was employed, adding a vacuum space equivalent to 9 layers and removing the dipole generated when a species is adsorbed on one of the surfaces. The transition state (TS) search has been performed by means of CI-NEB [58], and the located structures show a single imaginary frequency.

The entropy and the thermal corrections to the energy of gas phase molecules have been calculated with DFT solved with Gaussian-09 package [73] under ideal gas approach. The exchange-correlation functional employed in this calculations is B3LYP [74] and the basis set is 6-31+g**. For heavy metals in these molecules (Pt and Rh), the large core scalar relativistic pseudopotentials by Dolg *et al.* [75] were used coupled to the double-zeta quality basis set.

To solve the *ab-initio* thermodynamics equations, the *Mathematica* software (v5.2) [76] has been employed.

3.2 A particular case: Au(111)

Let us start studying a particular metal, Au, on its most simple surface, (111), and compare the results with some previous experiments.

UNIVERSITAT ROVIRA I VIRGILI
FIRST-PRINCIPLES MECHANISTIC STUDIES OF AMMONIA-RELATED INDUSTRIAL PROCESSES
Jaime Gómez Díaz
ISBN:978-84-694-1247-3/T-317-2011

3.2.1 Previous works

Gold catalysts have been widely studied for the low-temperature CO oxidation [21, 77, 78, 79, 80]. The decomposition of N_2O have been observed over evaporated Au films at 300-425°C and over Au filaments at 830-990°C [17]. In contrast with its nanoparticles, the (111) surface of gold is known to be very noble [81]. This important structure sensitivity found for Au [82], makes ultra-high vacuum experiments on single crystals unable to retrieve the exceptional catalytic behaviour of gold nanoparticles. However, many experimental efforts have been made to perform activity experiments on Au surfaces that reproduce the results obtained with nanoparticles. For instance, to test new possible oxidation reactions on the surface of gold nanoparticles, gold crystals in ultra-high vacuum experiments can be feed directly with O atoms [83, 84, 85]. Although this approach avoids O_2 dissociation, which is the main hindering step for oxidation reactions on Au(111) surface, it can be seen as a suitable way to test new catalytic capabilities of gold-based systems. Indeed, Mullins and co. [84] have reported the oxidation of ammonia on Au(111) containing atomic O preadsorbed and the effect of the oxygen coverage on the products by this technique.

On another note, ammonia is a toxic component in waste streams that can be removed by oxidation. Many works have been performed studying the dehydrogenation of ammonia, from a theoretical point of view [64, 80, 86, 87, 88, 89, 90] or experimentally [91, 92], as well as its oxidation [91, 93, 94]. In particular for the oxidation, Pt and Ir are the most active catalysts, but they produce significant amounts of pollutant nitrogen oxides. In contrast, for oxygen precovered Au(111) at low coverages, ammonia can be selectively decomposed to form water and N_2 (90%), without any traces of nitrogen oxides. However, when the coverage of oxygen doubles that of ammonia, only 53% of ammonia reacts, and the amount of NO is 30% of that of N_2. In the TPD experiments, the recombination to give N_2 produces a peak at 460-470 K while that of NO is a broad peak at 480 K. Then, depending on the conditions, ammonia oxidation can lead to the formation of, mainly, N_2, NO and/or N_2O [95, 96].

If the objective is ammonia abatement, the key reaction is the improvement of the N_2 route, thus selectively avoiding the conversion of nitrogen into its oxides. This is the opposite objective than that in the Ostwald

UNIVERSITAT ROVIRA I VIRGILI
FIRST-PRINCIPLES MECHANISTIC STUDIES OF AMMONIA-RELATED INDUSTRIAL PROCESSES
Jaime Gómez Díaz
ISBN:978-84-694-1247-3/T-317-2011

process where NO route has to be improved.

3.2.2 Ammonia dehydrogenation on Au(111)

Dehydrogenation steps have been studied for Au(111) modeled with a p(2x2) supercell. Direct dehydrogenation on the surface has been studied, as well as O and OH assisted. N+N and N+O reactions are also considered. The p(2x2) superstructure is well-suited to represent the coverage employed in the experiments in Ref. [84]: about 0.25 ML of NH_3 and the same coverage for atomic O. The aim of this section is to investigate, through a theoretical approach, ammonia oxidation on the O-precovered Au(111) surface in order to obtain the fundamental reasons for the selectivity, in this case towards N_2, observed. In that paper, Mullins and co-workers have studied the catalytic oxidation of ammonia on oxygen precovered Au(111) surface by means of Ultra-High Vacuum, UHV, techniques. In their experiments they observe the selective formation of N_2 under different ammonia dosages and O coverages.

The adsorption of oxygen on gold has been widely reported [97, 98], and it is well known that molecular oxygen adsorption is unlikely on Au(111). On the other hand, oxidation of species without the activation of O_2 is not possible. In the experiments that are being reproduced in this section this problem is avoided by directly adsorbing O atoms on the surface. The calculated adsorption of O atoms is strongly exothermic (with respect to O ^{3}P atom), E_{ads}=-3.12 eV on *fcc* position.

The most important thermodynamic data (reaction energy and reaction barrier) for ammonia dehydrogenation are shown in Table 3.1 and the distance N-H at the transition state and its associated frequency in Table 3.2. The relevant structures of the reaction (initial, transition and final state) are shown in Fig. 3.1, 3.2 and 3.3.

Ammonia hardly adsorbs on the very inert clean Au(111) surface, its adsorption is almost thermoneutral, E_{ads}=0.05, on *top* position and the distance Au-N is 2.402 Å. The Au-N-H angle is 107°. When O atoms are on the surface, the adsorption energy of ammonia is largely increased, E_{ads}=-0.38 eV. The reason for that increase is the formation of donor-acceptor pairs in the NH_3-O substructure.

Dehydrogenation of NH_3 on the clean surface is highly endothermic, ΔE=1.52 eV, and consequently the barrier of this process is very high,

UNIVERSITAT ROVIRA I VIRGILI
FIRST-PRINCIPLES MECHANISTIC STUDIES OF AMMONIA-RELATED INDUSTRIAL PROCESSES
Jaime Gómez Díaz
ISBN:978-84-694-1247-3/T-317-2011

Table 3.1: Reaction energies, ΔE, and energy barriers, E_a, in eV, and imaginary frequencies at the transition state, ν, in cm^{-1} for the different reaction steps on Au(111) clean surface and oxygen-covered (O-assisted) and hydroxyl-covered (OH-assisted) surfaces. Positive values indicate endothermic processes while negative stand for exothermic processes. Results correspond to the calculated isolated molecular moieties in p(2x2)-Au(111), 0.25 ML coverage for each species.

	Clean surface		O-assisted		OH-assisted	
Reaction	ΔE	E_a	ΔE	E_a	ΔE	E_a
$NH_3 \rightarrow NH_2$+H	1.52	2.44	0.21	0.72	-0.07	0.51
$NH_2 \rightarrow$ NH+H	1.66	2.38	0.35	0.37	0.08	0.72
NH $\rightarrow$ N+H	1.16	2.08	-0.14	0.58	-0.42	0.29

Table 3.2: Distance between N and dissociated H, d_{N-H} in Å, at the transition state and imaginary frequencies, ν, in cm^{-1} for the different reaction steps in Table 3.1.

	Clean surface		O-assisted		OH-assisted	
Dehydrog.	d_{N-H}	ν	d_{N-H}	ν	d_{N-H}	ω
$NH_3 \rightarrow NH_2$+H	1.803	1231	2.659	279	2.380	303
$NH_2 \rightarrow$ NH+H	2.294	394	2.497	145	1.285	1196
NH $\rightarrow$ N+H	1.932	664	1.210	1238	1.256	1187

UNIVERSITAT ROVIRA I VIRGILI
FIRST-PRINCIPLES MECHANISTIC STUDIES OF AMMONIA-RELATED INDUSTRIAL PROCESSES
Jaime Gómez Díaz
ISBN:978-84-694-1247-3/T-317-2011

2.44 eV. The experiments show, in agreement with these results, low rate for this reaction. The initial, transition and final state are shown in Fig. 3.1 (top). As previously mentioned, the adsorption of NH_x species is favored by the O atoms on the surface, as NH_x hydrogens form hydrogen bonds with O atoms on the surface. The presence of these O atoms makes the reaction much less endothermic, ΔE= 0.21 eV, and facilitate the first dehydrogenation of ammonia, decreasing the barrier to 0.72 eV, see structures in Fig. 3.1, center. When hydroxyl groups are present on the surface, the dehydrogenation of ammonia becomes exothermic, ΔE= -0.07 eV, due to the formation of the highly stable water molecule. The barrier for this process is again reduced, E_a=0.51 eV, structures shown in Fig. 3.1, bottom.

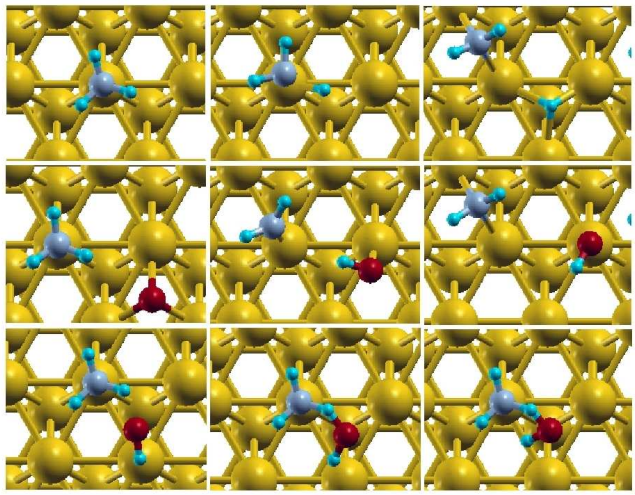

Figure 3.1: Initial, transition and final states for NH_3 dehydrogenation on Au(111) surface. Not assisted (top), O assisted (center) and OH assisted (bottom). Yellow spheres represent Au atoms, blue N, red O and small light blue H atoms.

The product of ammonia dehydrogenation, NH_2, adsorbs preferentially on a *bridge* position. Its dehydrogenation on the oxygen clean surface is very endothermic, ΔE=1.66 eV. The barrier is as well high, E_a=2.38 eV. The relevant structures of this process are shown in Fig. 3.2, top.

UNIVERSITAT ROVIRA I VIRGILI
FIRST-PRINCIPLES MECHANISTIC STUDIES OF AMMONIA-RELATED INDUSTRIAL PROCESSES
Jaime Gómez Díaz
ISBN:978-84-694-1247-3/T-317-2011

The same process when O is present on the surface becomes much more favorable, ΔE=0.35 eV, and the barrier is as well dramatically decreased, E_a=0.37 eV, see structures in Fig. 3.2, center. When the dehydrogenation is assisted by OH, it is almost thermoneutral, ΔE=0.08 eV and the barrier diminish one more time with respect to the clean surface, E_a=0.72 eV, see structures in Fig. 3.1, bottom.

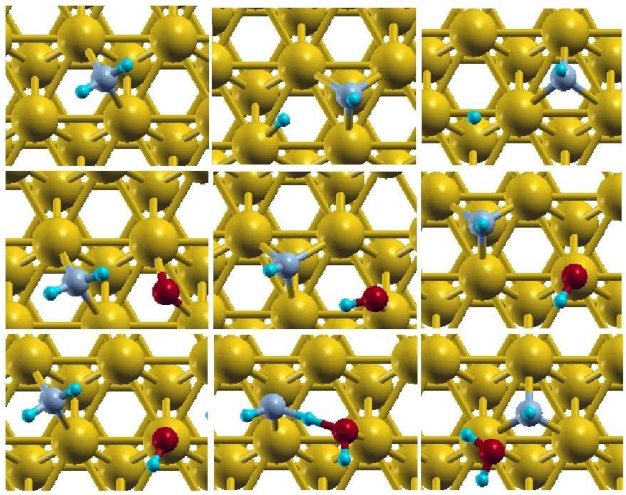

Figure 3.2: Initial, transition and final states for NH_2 dehydrogenation on Au(111) surface. Not assisted (top), O assisted (center) and OH assisted (bottom). Same color code than in Fig. 3.1

The last dehydrogenation in this set is that of NH, see structures in Fig. 3.3, top. This dehydrogenation is the least endothermic, ΔE=1.16 eV, and the one with the smallest barrier, E_a=2.08 eV, of all dehydrogenations on the clean gold surface, see structures in Fig. 3.3 (top). The presence of oxygen makes the reaction exothermic, ΔE=-0.14 eV, and decreases the barrier to E_a=0.58 eV. When OH appears on the surface the reaction is even more exothermic, ΔE=-0.42 eV, and the barrier is smaller, E_a=0.29 eV, see structures in Fig. 3.1 (bottom).

Summarizing, all the dehydrogenation barriers are decreased between 1.5-2.0 eV when O is present on the surface, and between 1.9-1.7 eV when later OH is on the surface, with respect to the barriers on the clean surface.

UNIVERSITAT ROVIRA I VIRGILI
FIRST-PRINCIPLES MECHANISTIC STUDIES OF AMMONIA-RELATED INDUSTRIAL PROCESSES
Jaime Gómez Díaz
ISBN:978-84-694-1247-3/T-317-2011

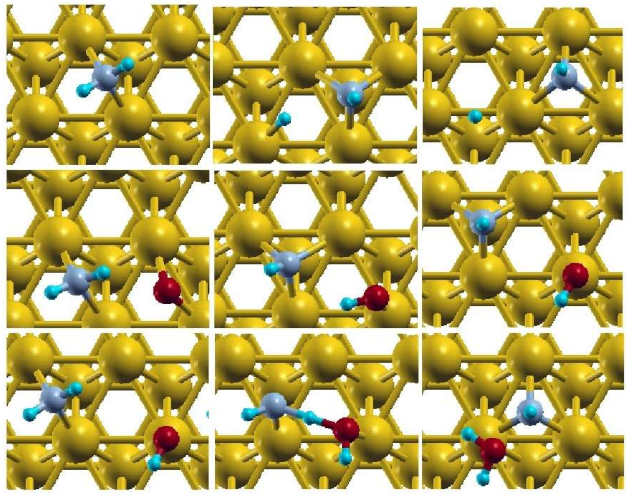

Figure 3.3: Initial, transition and final states for NH dehydrogenation on Au(111) surface. Not assisted (top), O assisted (center) and OH assisted (bottom). Same color code than in Fig. 3.1

The presence of O makes ammonia dehydrogenation fast in a wide range of temperatures on Au(111), otherwise, very low on the clean surface.

3.2.3 NO and N_2 formation on Au(111)

Once ammonia has been dehydrogenated, N atoms can be eliminated from the surface through both N_2 or NO routes. If the coverage is low, the atoms have to move on the surface to approach each other. This diffusion is generally hindered by low barriers, see in Table 3.3.

Therefore, N-N or N-O repulsion is, as expected, dependent on the surface coverage. The range of lateral interactions is 0.52 eV (for N+N approach) and 0.62 (for N+N approach) when the energy computed is the difference between N and X in two separated p(2x2) supercells and in the same p(2x2) supercell. If this difference is calculated in p(3x3) supercells the barrier found is very small, 0.04 eV for both approaches, being the atoms in the final state separated by a distance of two holes. The first diffusion is hindered by 0.24 eV for N+N and 0.40 for N+O. The

UNIVERSITAT ROVIRA I VIRGILI
FIRST-PRINCIPLES MECHANISTIC STUDIES OF AMMONIA-RELATED INDUSTRIAL PROCESSES
Jaime Gómez Díaz
ISBN:978-84-694-1247-3/T-317-2011

Table 3.3: Diffusion energies, E_{diff} in eV, for N and O atoms at several coverages.

System	X=N	X=O
N (0.25 ML)+X (0.25 ML) → N+X (0.50 ML)	0.52	0.62
N (0.11 ML)+X (0.11 ML) → N+X (0.22 ML)	0.04	0.04
N+X_{far} (0.22 ML) → N+X_{close} (0.22 ML)	0.24	0.40
N+X_{far} (0.22 ML) → N+X_{close} (0.22 ML) (2^{nd} diff.)	0.64	0.70

second diffusion, which gives contiguous atoms, is hindered by 0.64 and 0.70 eV for N+N and N+O respectively. The strong repulsion found at high coverages is due to two factors. First, the *pure* lateral interaction and second, that in the initial configuration, each N atom shares two metal atoms with other two N atoms [99] and this unfavorable situation is presented twice for each p(2x2) unit cell. However, such approach has been employed extensively [87] to obtain lateral interactions. These values are similar to those obtained for NO on Rh(100) [100, 101], and illustrates how Density Functional Theory results can help in the determination of lateral interactions.

Selectivity

The issue of selectivity is related to the competition between N+O and N+N recombinative steps. In Fig. 3.4 the energy profile for N-N recombination (and previous diffusion) on Au(111) surface for p(2x2) and p(3x3) supercells are shown. The recombination is exothermic by about 5.5 eV in both cells, and the resulting N_2 molecule readily leaves the surface. The barrier for recombination has been calculated in both the p(2x2) and p(3x3) unit cell (0.5 and 0.22 ML when 2 N atoms are adsorbed). The N-N coupling barrier from the high coverage 0.50 ML initial configuration is only 0.68 eV and at low coverage conditions (0.22 ML), close to the 0.25 ML used in the experiments, is 0.96 eV. This barrier is smaller than that reported for other metals, as we will see in next sections.

Finally, as for the geometries at the transition state the N-N distance is 2.080 Å for the p(2x2) unit cell and the N atoms are sitting almost at two contiguous bridging sites. For the lower coverage the structure is

UNIVERSITAT ROVIRA I VIRGILI
FIRST-PRINCIPLES MECHANISTIC STUDIES OF AMMONIA-RELATED INDUSTRIAL PROCESSES
Jaime Gómez Díaz
ISBN:978-84-694-1247-3/T-317-2011

qualitatively similar (both atoms at neighbouring bridging sites) but the N-N distance is further reduced to 1.921 Å. Moreover, at high coverage the Au in contact with both N atoms is lifted from the surface plane by about 0.65 Å. A smaller extraction from the surface plane, 0.58 Å, is found when the larger supercell is employed. Similar effects have been found for CH_4 dissociation on Ir(111) [102].

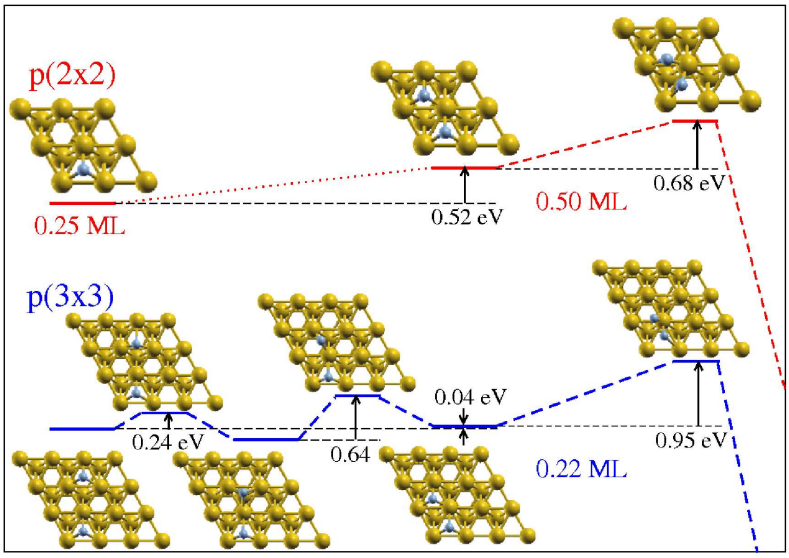

Figure 3.4: Energy profile for diffusion and formation of N_2 on Au(111) p(2x2) and p(3x3) supercells. The position of atoms for NO formation is almost identical.

3.2.4 Kinetic modeling

Once the thermodynamic and energy barriers are obtained from Density Functional Theory, they can be employed in micro-kinetic models in order to obtain the reaction rates. This has been successfully applied before to other processes as the ammonia synthesis [86]. In the present case, the required result is not directly the reaction rate but the selectivity, S_{NO/N_2} of the process. In order to investigate the selectivity, description on the Langmuir-Hinshelwood kinetics applied to the oxidation of ammonia is described in the following.

UNIVERSITAT ROVIRA I VIRGILI
FIRST-PRINCIPLES MECHANISTIC STUDIES OF AMMONIA-RELATED INDUSTRIAL PROCESSES
Jaime Gómez Díaz
ISBN:978-84-694-1247-3/T-317-2011

Table 3.4: Energy barriers for each elementary step, E_a in eV, and imaginary frequencies at the transition state, ν, in cm^{-1}. The coverages of NH_x, oxygen and hydroxyl groups are 0.25 ML, p(2x2) and 0.11 ML, p(3x3).

System	Coverage	ΔE	E_a	ν
N+N $\rightarrow$ N_2	p(2x2)	-5.43	0.68	464
N+O $\rightarrow$ NO	p(2x2)	-1.45	0.86	411
N+N $\rightarrow$ N_2	p(3x3)	-5.57	0.96	486
N+O $\rightarrow$ NO	p(3x3)	-2.22	1.01	399

Langmuir-Hinshelwood kinetics

The defining point in the Langmuir-Hishelwood kinetics is that all species are adsorbed and accommodated (thermal equilibrium) on the surface before they take part in any reaction. This is the prevailing situation in heterogeneous catalysis. Keeping this in mind, the set of reactions in the ammonia oxidation mechanism can be summarized as follows:

$$NH_3... \rightleftharpoons NH_2... \rightleftharpoons NH... \rightleftharpoons N* \tag{3.2}$$

$$O_2 + 2* \rightleftharpoons 2O* \tag{3.3}$$

$$N* + O* \rightleftharpoons NO* + * \tag{3.4}$$

$$NO* \rightleftharpoons NO + * \tag{3.5}$$

$$N* + N* \longrightarrow N_2 + 2* \tag{3.6}$$

The dehydrogenation of ammonia can be assisted by O atoms or OH groups

$$NH_3 + O \rightleftharpoons ... \rightleftharpoons N* + OH \tag{3.7}$$

$$NH_3 + OH \rightleftharpoons ... \rightleftharpoons N* + H_2O \tag{3.8}$$

Now we turn into the reaction rate expressions. For reaction 3.3 the rate r_{O*} can be written as:

$$r_{O*} = k^+_{O*} p_{O_2} \theta^2_* - k^-_{O*} \theta^2_O \tag{3.9}$$

UNIVERSITAT ROVIRA I VIRGILI
FIRST-PRINCIPLES MECHANISTIC STUDIES OF AMMONIA-RELATED INDUSTRIAL PROCESSES
Jaime Gómez Díaz
ISBN:978-84-694-1247-3/T-317-2011

where k^+_{O*} is the rate constant for the direct reaction 3.3 (O* formation), p_{O_2} is partial O_2 pressure, θ_* is the fraction of free sites, k^-_{O*} is the rate constant for the O*+O* recombination (inverse reaction 3.3), and θ_O is oxygen coverage. Following an equivalent nomenclature, the rates for the other reactions can be written as:

$$r_{NO*} = k^+_{NO*}\theta_N\theta_O - k^-_{NO*}\theta_{NO}\theta_* \tag{3.10}$$

$$r_{NO} = k^+_{NO}\theta_{NO} - k^-_{NO}p_{NO}\theta_* \tag{3.11}$$

$$r_{N_2} = k^+_{N_2}\theta_N\theta_N \tag{3.12}$$

Due to the high barrier found for N_2 dissociation and its Eley-Rideal character (i.e. N_2 is not adsorbed on the surface), the inverse reaction of N_2 formation is not considered.

- Complete solution

The complete solution for the above equations is the set of differential equations:

$$\frac{d\theta_N}{dt} = r_{N*} - r_{NO*} - r_{N_2} \tag{3.13}$$

$$\frac{d\theta_O}{dt} = r_{O*} - r_{NO*} \tag{3.14}$$

$$\frac{d\theta_{NO}}{dt} = r_{NO*} - r_{NO} \tag{3.15}$$

$$\frac{d\theta_*}{dt} = -r_{N*} - r_{O*} + r_{NO*} + r_{NO} + r_{N_2} \tag{3.16}$$

which can, in principle, be solved numerically given that all parameters needed are known or estimated.

- The Steady State Approximation

Most often, we are in a situation where a constant flow of reactants leads to a constant output of products. In this case coverages and rates have reached a constant value. Hence we can apply the steady state approximation, and set all differentials in Eqs. 3.13-3.16 equal to zero:

UNIVERSITAT ROVIRA I VIRGILI
FIRST-PRINCIPLES MECHANISTIC STUDIES OF AMMONIA-RELATED INDUSTRIAL PROCESSES
Jaime Gómez Díaz
ISBN:978-84-694-1247-3/T-317-2011

$$\frac{d\theta_N}{dt} = r_{N*} - r_{NO*} - r_{N_2} = 0 \tag{3.17}$$

$$\frac{d\theta_O}{dt} = r_{O*} - r_{NO*} = 0 \tag{3.18}$$

$$\frac{d\theta_{NO}}{dt} = r_{NO*} - r_{NO} = 0 \tag{3.19}$$

$$\frac{d\theta_*}{dt} = -r_{N*} - r_{O*} + r_{NO*} + r_{NO} + r_{N_2} = 0 \tag{3.20}$$

In our case, this complete solution is only taken regarding adsorbed species and thus no information on the binding energy of reactants is taken into account. Therefore, the set of equations is indeterminated. However, a picture on the behaviour of the different surfaces can be extracted.

3.2.5 Kinetic model for the Au(111) surface.

In the particular case of Au, the values for the adsorption and reaction barriers can enlighten the issue of selectivity. As none NO and N_2 are not bonded to the surface the selectivity can be written just in terms of the direct recombination steps: N+O and N+N. Then the selectivity can be expressed as follows:

$$\begin{aligned} S_{NO/N_2} &= \frac{k^+_{NO}\theta_{NO} - k^-_{NO}p_{NO}\theta_*}{k^+_{N_2}\theta_N^2} = \\ &= \frac{k^+_{NO*}\theta_N\theta_O - k^-_{NO*}\theta_{NO}\theta_*}{k^+_{N_2}\theta_N^2} \approx \\ &\approx \frac{k^+_{NO*}\theta_N\theta_O}{k^+_{N_2}\theta_N^2} \end{aligned} \tag{3.21}$$

That contains the formation of NO and that of N_2 without any further contributions.

Then, to compare with the experiments we will define the selectivity towards N_2, S'_{N_2} as:

$$S'_{N_2} = \frac{r_{N_2}}{r_{N_2} + r_{NO}} = \frac{1}{1 + S_{NO/N_2}} \tag{3.22}$$

UNIVERSITAT ROVIRA I VIRGILI
FIRST-PRINCIPLES MECHANISTIC STUDIES OF AMMONIA-RELATED INDUSTRIAL PROCESSES
Jaime Gómez Díaz
ISBN:978-84-694-1247-3/T-317-2011

Where in the last term we indicate the relation to the S_{NO/N_2} defined before and r_{N_2} and r_{NO} are the rates for the N_2 and NO formation respectively. The kinetic constants can be written as Arrhenius equations in the form: $k = A\,exp(-E_a/RT)$. If we assume that the prefactors in the rate constants are similar, a reasonable assumption given the similarities of these elementary steps, the simplest expression for the selectivity can be written as:

$$\begin{aligned} S'_{N_2} &= \frac{k_{N_2}}{k_{N_2} + k_{NO}(\frac{\theta_O}{\theta_N})} = \\ &= \frac{exp(-E_{aN_2}/RT)}{exp(-E_{aN_2}/RT) + exp(-E_{aNO}/RT)(\frac{\theta_O}{\theta_N})} \end{aligned} \tag{3.23}$$

Therefore, we can describe the selectivity as a function of the relative oxygen to nitrogen coverage. The values for the barriers, E_a, are taken from the DFT calculations described above and the temperature employed is 450 K following the experimental conditions described in reference [103]. The results are shown in Fig. 3.5.

In order to compare to the values in Ref. [103] we have studied the two experimental conditions with initial coverages of 1) 0.25 ML and ammonia 0.18 ML and 2) 0.64 ML O and 0.25 ML ammonia. In the first case, the experiment indicate that 89% of the ammonia reacts giving 100% selectivity towards N_2, whereas in the second set of experiments only a 53% of ammonia is oxidized. In any case, O and OH groups are needed for the complete ammonia dehydrogenation. In the first case, this would mean that the surface is no longer covered by O as all has been employed in the dehydrogenations and thus the selectivity is 100%. In the second case, the total amount of oxygen on the surface comes from the O atoms that have not reacted to ammonia and thus is smaller than the nominal 0.64 ML. The figure shows how the selectivity at low O coverages leads exclusively to the formation of nitrogen, and thus this would be the desired regime for the selective ammonia oxidation towards N_2 in agreement with the experiments [103]. However, when the relative oxygen coverage increases on the surface the selectivity decreases by 20%. Our model, represented in Fig. 3.5 by the black line, is in reasonable agreement with the experimental results represented by the two black boxes in the figure. One of the reasons

UNIVERSITAT ROVIRA I VIRGILI
FIRST-PRINCIPLES MECHANISTIC STUDIES OF AMMONIA-RELATED INDUSTRIAL PROCESSES
Jaime Gómez Díaz
ISBN:978-84-694-1247-3/T-317-2011

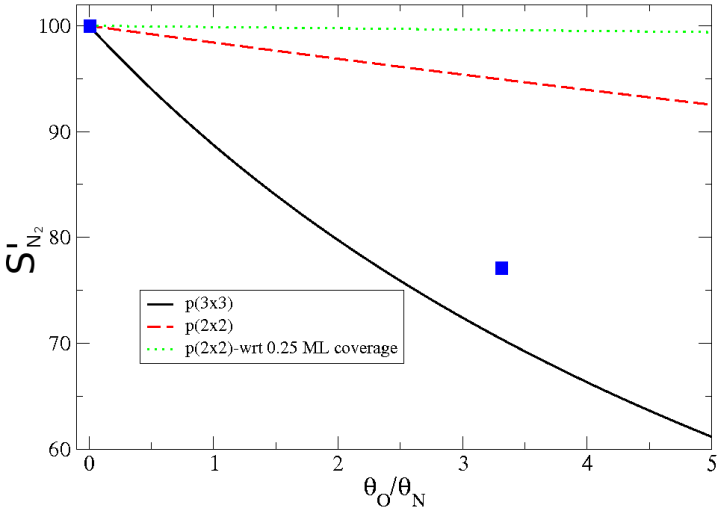

Figure 3.5: Selectivity towards N_2 in Au(111) at 450 K is expressed as a function of the relative O/N coverages. The continuous black line represents the model described in the p(3x3) cell, the dashed one in the p(2x2) cell and the dotted one in the p(2x2) cell including the initial repulsion. The blue boxes represent the experimental values obtained in Ref. [103].

UNIVERSITAT ROVIRA I VIRGILI
FIRST-PRINCIPLES MECHANISTIC STUDIES OF AMMONIA-RELATED INDUSTRIAL PROCESSES
Jaime Gómez Díaz
ISBN:978-84-694-1247-3/T-317-2011

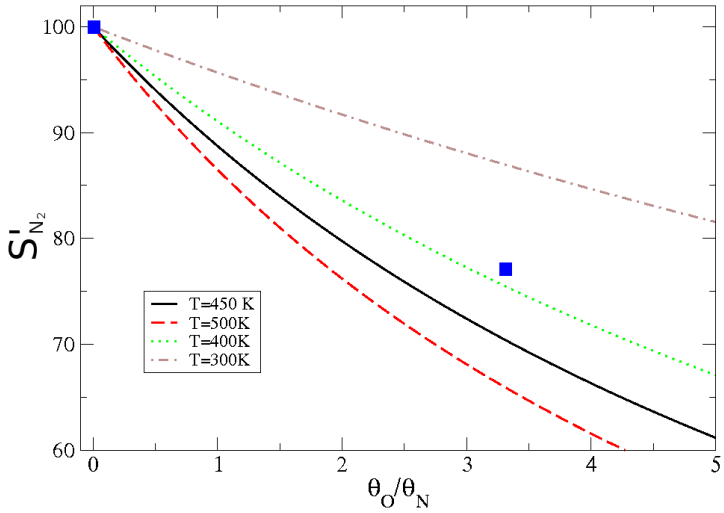

Figure 3.6: Selectivity towards N_2 in Au(111) at different temperatures expressed as a function of the relative O/N coverages. The blue boxes the experimental results from Ref. [103].

for the deviations with respect to the experiments at high O coverage is that oxygen recombination to form O_2 is neglected in our model.

3.3 A more general case: Transition Metals

Equation 3.2 wraps up the set of reactions that lead to the decomposition of ammonia and subsequent nitrogen formation on the surface. Those reactions have been previously studied [64, 86, 87, 88, 89, 90, 104]. It is well known that oxygen presence lower the barrier for dehydrogenations [87, 104], same examples can be found in Chapter 4. Since the main aim of our study is to focus on the competitive NO and N_2 formation, the fine details that drive ammonia decomposition will not be addressed.

3.3.1 Previous works

NO adsorption, formation and dissociation has been extensively reviewed in the literature.

UNIVERSITAT ROVIRA I VIRGILI
FIRST-PRINCIPLES MECHANISTIC STUDIES OF AMMONIA-RELATED INDUSTRIAL PROCESSES
Jaime Gómez Díaz
ISBN:978-84-694-1247-3/T-317-2011

They report a high temperature dependency of the product selectivity as below ≈ 800 K the reaction mainly produces N_2, but at above 850 K it is superseded by NO production. The system has been studied on supported Pt [105, 106], polycrystalline Pt [107, 108] and single crystals [109, 110]. The first comprehensive study on this behavior was performed by Bradley, Hopkinson and King, thereafter indicated as BHK model, in 1995 [91]. In their TPD experiments they analyzed the temperature dependence of steady-state products and proposed the following mechanism

$$NH_3 * + O* \rightarrow NO(g) + H_2(g) + H *$$
$$NH_3 * + NO* \rightarrow N_2(g) + H_2O(g) + H*$$

Indeed, they identified that with a 98% O_2 in the bam mixture, the surface produces NO with a 100% efficiency. Moreover, they proposed a mechanism involving the adsorption of ammonia and the dissociative adsorption of oxygen and indicating a positive effect of oxygen in H stripping from ammonia. Temperature Programmed Reaction, TPD, experiments showed that NO is formed at low surface temperatures and its formation is facile. Similar experiments denoted also that, above 350 K, NO will dissociated on the clean Pt(100) surface, and that this step will compete with NO desorption and N_2 formation. Isotope labeling have shown that N_2 can be formed from NO dissociation, NH_3 dissociation or from both [111, 112, 113]. Therefore, BHK proposed that NO dissociation has the control over ammonia oxidation reaction. Later in 2000, Prof. King and his group carried out TPD and TPD-RAIRS experiments on Pt(100) surface [92], determining that the reaction selectivity between NO and N_2 was determined by the O adatom coverage.

From a computational point of view, the number of works related to N_2 activation and NO adsorption and dissociation is very large. In here, a very brief discussion on the most important works will be described. Regarding N_2, its dissociation is the most difficult step in ammonia synthesis. The group of Prof. Nørskov has been very active in the field, and extensive studies regarding this particular step have been put forward. Two of the most interesting works are the first indication of the role of steps in the activation of N_2 [114] and the combined Monte-Carlo DFT study [86] that allowed to compare the calculated rates to the experimental ones.

UNIVERSITAT ROVIRA I VIRGILI
FIRST-PRINCIPLES MECHANISTIC STUDIES OF AMMONIA-RELATED INDUSTRIAL PROCESSES
Jaime Gómez Díaz
ISBN:978-84-694-1247-3/T-317-2011

In addition, Prof. Hammer performed a series of studies regarding the adsorption and dissociation of NO on different stepped surfaces including Pd and Ru [99, 115]. In these works, a model to understand the role of coordination in the contribution to the transition state energy ordering was stated, indicating that when in the final state the adsorbates do not share any surface atoms the barrier for dissociation is lower. A description of all possible dissociation routes for NO at Pt(211) steps was performed in the group of Prof. Neurock [116]. More recently, the same authors have complemented the DFT analysis by a kinetic Monte Carlo study on the reduction of NO on Pt nanoparticles [117]. Bogicevic and Hass studied NO and N_2O formation on Cu(111) and Pt(111) [118], and they found negligible the dissociation of NO. More recently, Hafner *et al.* [119, 120] studied the molecular adsorption of NO on transition (Co, Ni, Ru, Rh, Pd, Ir, Pt, Cu, Ag, Au) metals. The adsorption energies and the relative positions of the adsorbates were carefully considered in these works.

However, due to its complexity, the analysis of the selectivity only partially be taken into account. Seminal papers by the group of Prof. Pérez-Ramírez [121] was recently published. There, a scale with the activity of Rh, Pd and Pt under different reaction conditions was proposed from a microkinetic analysis based on DFT calculations for the (100) surface of these metals.

Regarding the appearance of N_2O, by isotopically-labeled molecular beams and TPD analysis on Rh(111), Zaera and co-workers [122, 123, 124] found evidences of N_2O intermediate in the catalytic reduction of NO to N_2 at UHV conditions in presence of CO. As previously mentioned, Pérez-Ramírez and co-workers have studied the recombination of N and O atoms to form NO and N_2O [121] theoretical (periodic DFT calculations) and experimentally (TPD experiments). They observed Pt>Pd>Rh NO selectivity and the possibility of increase the selectivity with larger oxygen/ammonia ratios.

3.3.2 NO and N_2 formation on transition metals

The adsorption energies of atomic oxygen and nitrogen, NH_3, NO and N_2O on flat metal surfaces Me(111) with respect to the corresponding gas phase molecule are reported in Table 3.5. N, O and NO adsorb preferably on *fcc* sites on the flat surfaces, except on N on Rh, that shows small

UNIVERSITAT ROVIRA I VIRGILI
FIRST-PRINCIPLES MECHANISTIC STUDIES OF AMMONIA-RELATED INDUSTRIAL PROCESSES
Jaime Gómez Díaz
ISBN:978-84-694-1247-3/T-317-2011

preference for *hcp* site. NH_3 and N_2O adsorb preferably on *top* position.

Table 3.5: Adsorption energies of N and O (with respect to half gas-phase molecule), NH_3, NO, N_2 and N_2O (with respect to gas phase species). All energies in eV.

	Au	Cu	Ir	Pd	Pt	Rh
(111)						
N	2.70	1.58	0.27	0.52	0.57	-0.02 [1]
O	0.01	-1.44	-1.48	-0.91	-0.89	-1.67
NH_3	-0.17	-0.87	-0.68	-0.50	-0.97	-0.58
NO	-0.12	-0.86	-1.62	-1.99	-1.43	-2.06
N_2O	0.11	0.27	0.08	0.06	0.26	-0.07
(211)						
NO_{step}	-0.18	-1.01	-2.31	-1.99	-2.22	-2.34

[1] *hcp*

Gold is, by far, the most noble of these metals, and adsorption of these species are all between endothermic and slightly exothermic. On the other hand, Ir and Rh show the strongest interactions. Remarkable is the case of Cu, that have a highly endothermic adsorption energy for N (1.58 eV) but a very exothermic for O (-1.44 eV), reflexing the ability of Cu metal to form oxides but not nitrides. For ammonia, all the binding energies are similar (except for Au) and exothermic in the range from 0.5-1 eV.

3.3.3 Reactivity on Me(111) flat surfaces

The most relevant reactions in the selectivity of NO/N_2 are those following:

$$N* + O* \rightleftharpoons NO* + * \tag{3.24}$$

$$NO* \rightleftharpoons NO(g) + * \tag{3.25}$$

$$N* + N* \longrightarrow N_2(g) + 2* \tag{3.26}$$

The thermodynamic and kinetic data, as well as some relevant geometrical parameters for the transition states, for these reactions on a p(3x3)

UNIVERSITAT ROVIRA I VIRGILI
FIRST-PRINCIPLES MECHANISTIC STUDIES OF AMMONIA-RELATED INDUSTRIAL PROCESSES
Jaime Gómez Díaz
ISBN:978-84-694-1247-3/T-317-2011

supercell are shown in Table 3.6. The corresponding structures are shown in Figs. 3.7-3.11.

NO formation:

At the initial configuration N and O atoms are sitting in neighboring *fcc* positions on the surfaces. The reaction takes place by the activation of oxygen, and the resulting NO is sited N-down on *fcc* position, see Fig. 3.7. The smallest barrier for N+O recombination is that of Au, E_a=1.01 eV, the reaction being very exothermic, ΔE=-2.22 eV. The second lowest barrier for this step is found for Cu, 1.28 eV, where the reaction is as well exothermic, ΔE=-0.53 eV. Pt, 2.12 eV, and Rh, 2.39 eV, show the highest barriers for this coupling. For both metals the reaction is endothermic (around 0.5 eV). Notice that the largest barriers for N+O coupling are found on those metals used in the industrial catalyst (that tries to maximize NO production).

Figure 3.7: Initial (left), transition (centre) and final (right) states for N+O coupling on Pd(111) surface. Grey spheres represent Pd atoms, blue N and red O.

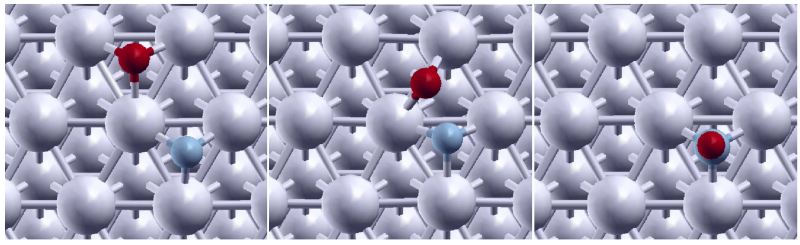

N_2 formation:

The same initial configuration is taken as the starting point for N_2 recombination. In this case, both atoms are activated equally. The resulting N_2 molecule is physisorbed (N-Me distance $\approx$ 3 Å), see Fig. 3.8. The lowest barriers for N_2 evolution correspond to Cu, 0.71 eV, and Au, 0.96 eV. These low barriers and large exothermicity are due to the weak interaction than N atoms have with those surfaces. The barriers for other metals are

UNIVERSITAT ROVIRA I VIRGILI
FIRST-PRINCIPLES MECHANISTIC STUDIES OF AMMONIA-RELATED INDUSTRIAL PROCESSES
Jaime Gómez Díaz
ISBN:978-84-694-1247-3/T-317-2011

around 2 eV, but with large differences in the reaction energy, that goes from -1.55 eV for Pd, to -0.32 eV and -0.14 eV for Ir and Rh respectively.

Figure 3.8: Initial (left), transition (centre) and final (right) states for N+O coupling on Au(211) surface. Coppery spheres represent Cu atoms and blue N.

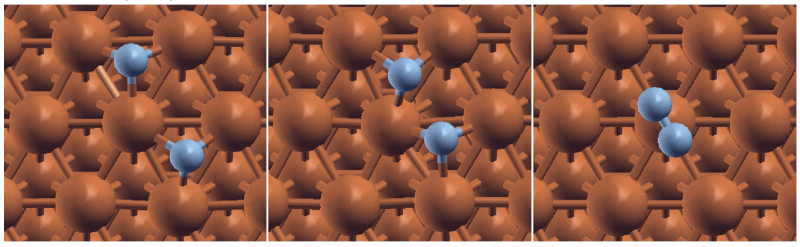

N_2O formation:

For this elementary steps both N atom and NO are sitting in neighboring *fcc* positions . The reaction takes place by the activation of both species activation, and the final configuration is a N_2O species sited N-down on *top* position, see Fig. 3.9. Again the lowest barriers correspond to Au and Cu, about 0.5 eV. Larger barriers are found for Pd, 1.70 eV, Rh, 1.65 eV, and Ir, 1.54 eV.

Figure 3.9: Initial (left), transition (centre) and final (right) states for N+O coupling on Ir(211) surface. Grey spheres represent Ir atoms, blue N and red O.

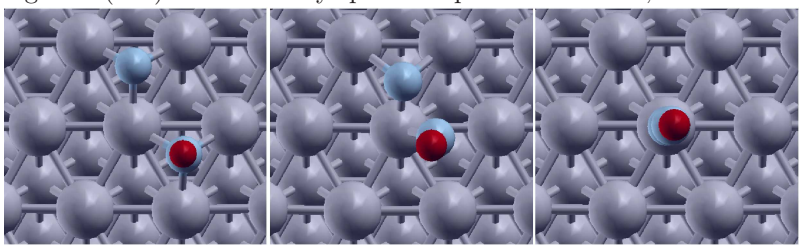

UNIVERSITAT ROVIRA I VIRGILI
FIRST-PRINCIPLES MECHANISTIC STUDIES OF AMMONIA-RELATED INDUSTRIAL PROCESSES
Jaime Gómez Díaz
ISBN:978-84-694-1247-3/T-317-2011

3.3.4 Reactivity on Me(211) stepped surfaces

NO formation:

When moving to the stepped surface all the barriers for N+O coupling are reduced except on that for Pd where both are very similar. The lowest barrier found corresponds to a path where in the initial configuration, N is placed on a *bridge* position at the edge while the O atom is adsorbed on a *fcc* site at the lower (111) terrace, see Fig. 3.10. Then oxygen gets activated close to the edge and produces NO sitting right at the edge. The smallest barrier found is again that for Au, 0.13 eV, now followed by Pd, 0.39 eV. Cu is the metal showing a lowest reduction of the overall barrier when moving from the (111) to the (211) surface. The largest barrier on the stepped surface corresponds to Ir, 1.55 eV. The large reduction found agrees with the large structure sensitivity found for the reaction on Pt and explains why the Pt catalysts needs some time for activation related to the formation of most active facets under reaction conditions.

Figure 3.10: Initial (left), transition (centre) and final (right) states for N+O coupling on Au(211) surface. Yellow spheres represent Au atoms, blue N and red O. Lateral and top views are shown for clarity.

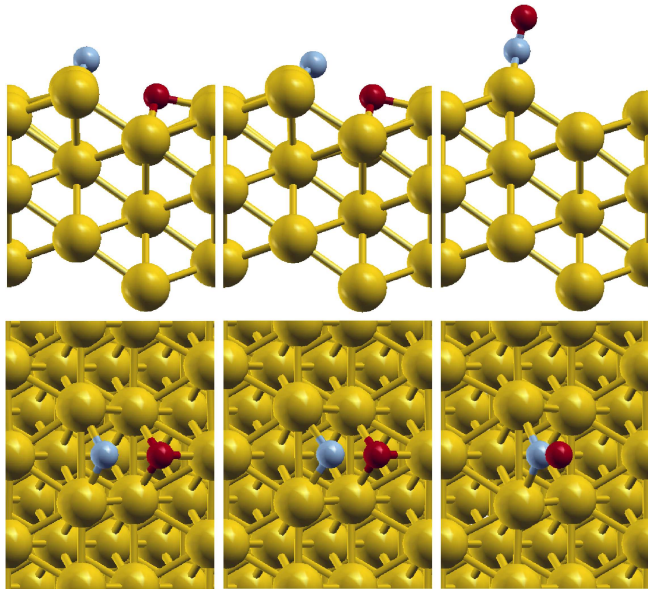

UNIVERSITAT ROVIRA I VIRGILI
FIRST-PRINCIPLES MECHANISTIC STUDIES OF AMMONIA-RELATED INDUSTRIAL PROCESSES
Jaime Gómez Díaz
ISBN:978-84-694-1247-3/T-317-2011

N_2 formation:

The reaction mechanism is very similar to that for N+O reaction at the edge, with one N atom on the edge and second at the *fcc* site. I have not found a significant barrier for the formation of N_2 at the gold step. On Pd, the barrier becomes much smaller than on the flat surface, 0.18 eV while Rh shows a larger barrier than that corresponding to the surface, E_a=2.16 eV.

Figure 3.11: Initial (left), transition (centre) and final (right) states for N+O coupling on Rh(211) surface. Dark grey spheres represent Rh atoms and blue N. Lateral and top views are shown for clarity.

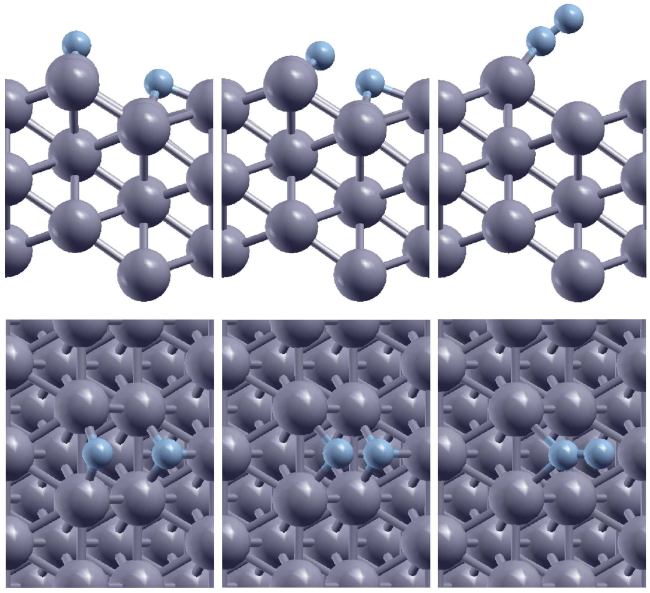

3.3.5 Kinetics on transition metals

We now summarize the results on the different surfaces. For the recombination of N_2, all the presented metals show a similar profile, where recombination is a single step leading to a free molecule, see Fig. 3.12. Thus, only the direct reaction needs to be taken into account.

UNIVERSITAT ROVIRA I VIRGILI
FIRST-PRINCIPLES MECHANISTIC STUDIES OF AMMONIA-RELATED INDUSTRIAL PROCESSES
Jaime Gómez Díaz
ISBN:978-84-694-1247-3/T-317-2011

Table 3.6: Reaction energy, ΔE in eV; activation energy, E_a in eV; desorption energy, E_d in eV; X-Y distance at the transition state, d_{X-Y} in Å; and its associated imaginary frequency, ν in cm^{-1}.

	Au	Cu	Ir	Pd	Pt	Rh
NO (111)						
ΔE	-2.22	-0.53	-0.36	0.84	0.48	0.31
$E_{a,\,N+O}$	1.01	1.28	1.90	1.61	2.12	2.39
d_{N-O}	2.037	1.895	1.881	1.809	1.814	1.679
ν	399	396	491	488	483	494
E_d	0.12	0.86	1.62	1.99	1.43	2.06
N_2 (111)						
ΔE	-5.57	-3.38	-0.32	-1.55	-1.42	-0.14
$E_{a,\,N+N}$	0.96	0.71	1.95	1.82	2.13	1.98
d_{N-N}	2.141	2.033	1.800	1.893	1.923	1.855
ν	486	403	548	590	565	570
N_2O (111)						
ΔE	-1.99	-0.71	0.85	+0.94	+0.88	1.24
$E_{a,\,N+O}$	0.38	0.54	1.54	1.70	1.30	1.65
d_{N-N}	2.396	2.186	1.730	1.928	1.918	1.903
d_{N-O}	1.171	1.170	1.192	1.183	1.181	1.186
ν	260	293	376	352	285	352
NO (211)						
ΔE	-3.09	-0.41	-0.13	-1.19	-1.16	-0.17
$E_{a,\,N+O}$	0.13	1.10	1.55	0.39	0.80	0.98
d_{N-O}	2.198	2.243	1.809	1.809	1.652	1.689
ν	228	193	185	420	543	516
E_d	0.18	1.01	2.31	1.99	2.22	2.34
N_2 (211)						
ΔE	-6.88	-3.65	-0.77	-2.38	-1.81	-0.85
$E_{a,\,N+N}$	–	0.92	0.82	0.18	1.14	2.16
d_{N-N}	–	2.417	1.800	2.158	1.927	1.849
ν	–	223	476	230	471	485

UNIVERSITAT ROVIRA I VIRGILI
FIRST-PRINCIPLES MECHANISTIC STUDIES OF AMMONIA-RELATED INDUSTRIAL PROCESSES
Jaime Gómez Díaz
ISBN:978-84-694-1247-3/T-317-2011

Figure 3.12: Thermodynamic profile for N+N coupling on transition metals (111) surface.

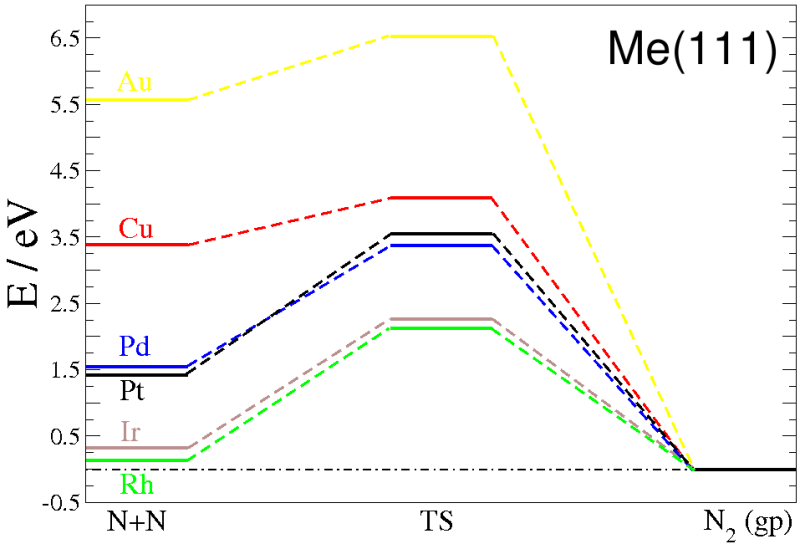

As for NO, the situation is far more complex. NO is not adsorbed on Au and, as explained in Section 3.13 of this chapter, the same discussion as for N_2 can be applied. The rest of the metals can be grouped as follows, see Fig. 3.13. For Cu, Ir and Pt; the N+O formation shows a lower barrier than its dissociation from the transition state, but the lowest one corresponds to the evolution to the gas-phase.

The proper way to describe the reaction mechanism leading to NO for these (111) surfaces is then:

$$N* + O* \rightarrow NO* \rightarrow NO \tag{3.27}$$

Thus N+O formation is the rate determining step for NO formation on the surface. For Cu, the competition of the N+O and the N+N bond favours the second, thus the selectivity under similar O and N coverages would favour N_2 formation. For Ir and Pt the N+O and N+N reactions are comparable and thus selectivity is a strong function of the coverages as for these surfaces both N+O or N+N controls can be possible in principle. This correlates with the biphasic nature found for ammonia oxidation

UNIVERSITAT ROVIRA I VIRGILI
FIRST-PRINCIPLES MECHANISTIC STUDIES OF AMMONIA-RELATED INDUSTRIAL PROCESSES
Jaime Gómez Díaz
ISBN:978-84-694-1247-3/T-317-2011

Figure 3.13: Thermodynamic profile for N+O coupling and NO* desorption on transition metals (111) surface.

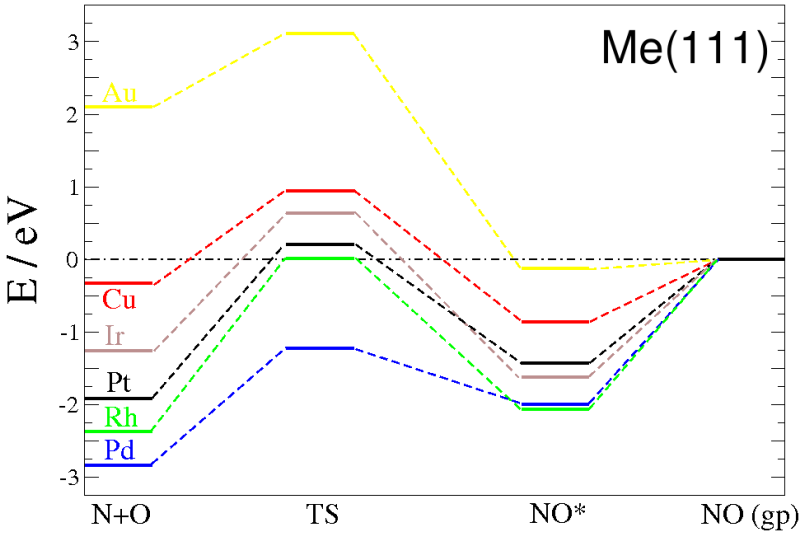

on Pt. The third group is constituted by Pd and Rh. In these cases, the evolution of NO towards the surface is comparable to the barriers required to form the N+O or N+N bond. In addition, the NO dissociation for Pd from the adsorbed precursor shows a very small barrier (about 0.8 eV), thus, this process is responsible for the decrease of selectivity provided that the long contact times or a significant amount of NO pressure is present. In this case the reaction scheme is better described as follows:

$$N* + O* \rightleftharpoons NO* \rightleftharpoons NO \tag{3.28}$$

If we now consider the stepped surfaces, some important differences arise. Now, bond formation both N+O and N+N is easier, but the binding energy of NO to the steps is larger, see Figs. 3.14 and 3.15.

It is clearly shown in the picture how now the situation has changed for Pt and Ir. Both metals then belong to the third class described above, when NO desorption is the rate determining step. In addition the dissociation of NO is possible at the high temperatures employed in the reaction mixture. Thus the strong structure sensitivity found for the reaction af-

UNIVERSITAT ROVIRA I VIRGILI
FIRST-PRINCIPLES MECHANISTIC STUDIES OF AMMONIA-RELATED INDUSTRIAL PROCESSES
Jaime Gómez Díaz
ISBN:978-84-694-1247-3/T-317-2011

Figure 3.14: Thermodynamic profile for N+N coupling on transition metals (211) surface.

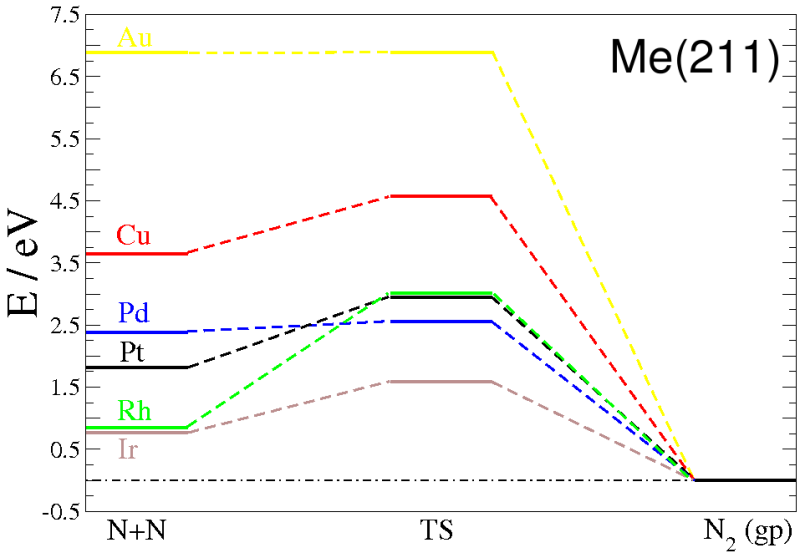

Figure 3.15: Thermodynamic profile for N+O coupling and NO* desorption on transition metals (211) surface.

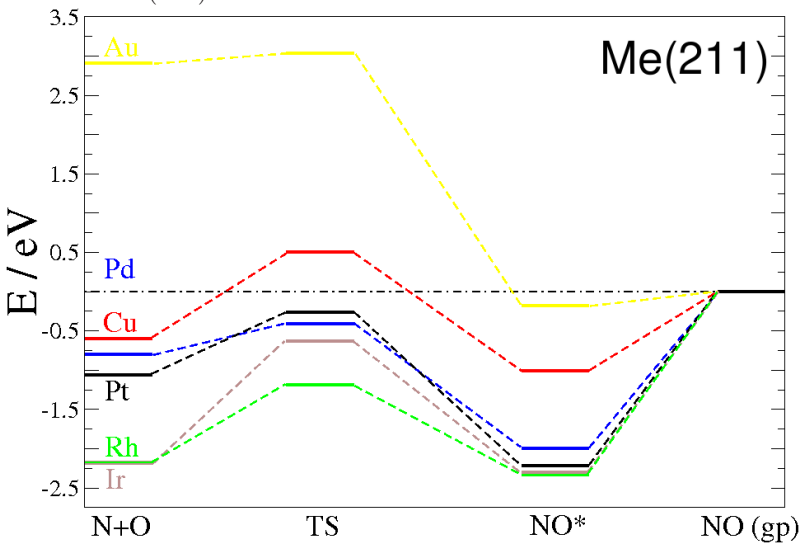

UNIVERSITAT ROVIRA I VIRGILI
FIRST-PRINCIPLES MECHANISTIC STUDIES OF AMMONIA-RELATED INDUSTRIAL PROCESSES
Jaime Gómez Díaz
ISBN:978-84-694-1247-3/T-317-2011

fects the reaction scheme and both the selectivity and activity determining steps. Our results are in good agreement with the results in the BHK model [91] indicating that NO readsorption affects the selectivity of the process by readsorption and dissociation, thus being responsible at the same time for the raise in the activity of the process and the reduction of the selectivity.

3.4 A model for the catalyst in industry: the PtRh alloy

3.4.1 Previous works.

Due to the industrial importance of the process, many studies have been made focusing on the behavior of the PtRh catalyst under ammonia oxidation conditions, but very few focus on the intrinsic mechanism or the perturbations introduced by the presence of Rh in the samples. Recently, studies in the activity of PtRh in NO_x reduction (for example in exhaust gas treatment) have been presented [125, 126], showing the versatility of this catalyst. Up to date, very little is known about the role of Rh in the alloy. As Rh is a much more expensive component than Pt two possibilities for its need in the catalyst have been raised:

- It improves the selectivity of the gauzes
- It improves the stability of the gauzes under reaction conditions

It is well-known that the catalyst under reaction conditions suffers strong degragation affecting the whole tridimensional structure. This is clearly seen in Fig. 3.16. In spite of the complexity shown in this figure, theoretical simulations can shed some light in the two options described above. Indeed, this is the aim of the present chapter: to identify which option, either the increase of selectivity or the improvement of the stability, is more likely.

To do this we have performed two types of studies, first describing the reaction network for the competitive N+N and N+O reactions on a model alloy and second by identifying the stability of different Pt and Rh materials at high pressures and temperatures.

UNIVERSITAT ROVIRA I VIRGILI
FIRST-PRINCIPLES MECHANISTIC STUDIES OF AMMONIA-RELATED INDUSTRIAL PROCESSES
Jaime Gómez Díaz
ISBN:978-84-694-1247-3/T-317-2011

Figure 3.16: SEM images of reconstructed surfaces on catalyst wires after ammonia oxidation for 336 h at 900°C: facets on surfaces of (a) Pt/10% Rh and (b) Pt/13% Rh, at location ca. 2 mm from gas inlet. Reconstructed surfaces from the reaction zone, at location ca. 20 mm down the catalyst wire: (c) Pt, (d) Pt/5% Rh, (e) Pt/10% Rh, (f) Pt/13% Rh, (g) Pt/20% Rh, (h) Pt/30% Rh, (i) Pt/40% Rh (bar-shaped cross-section), and (j) Rh (note only 60 h duration). Taken from Ref. [127].

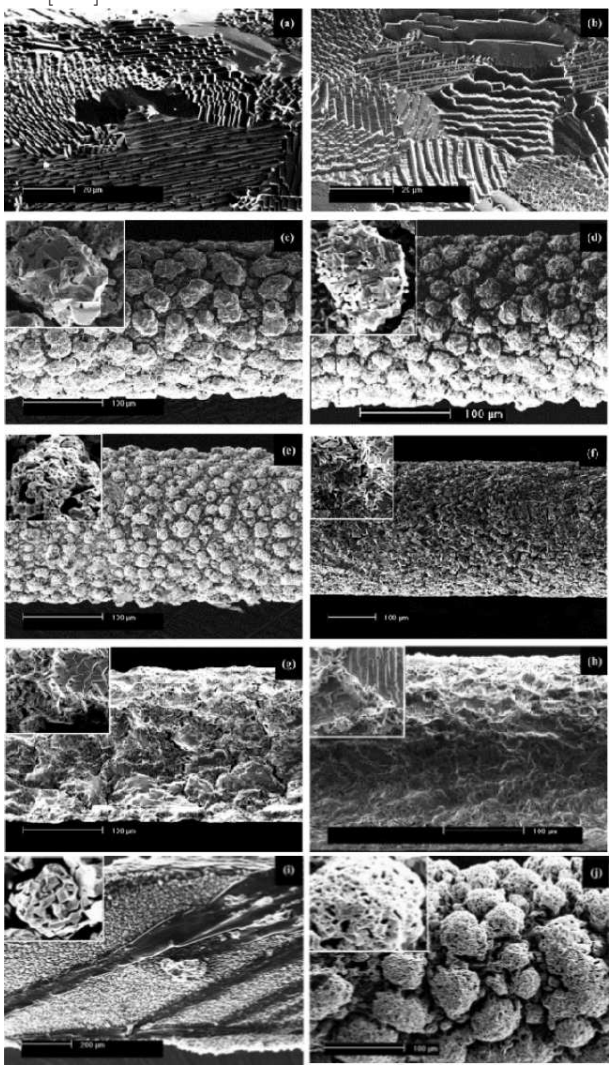

UNIVERSITAT ROVIRA I VIRGILI
FIRST-PRINCIPLES MECHANISTIC STUDIES OF AMMONIA-RELATED INDUSTRIAL PROCESSES
Jaime Gómez Díaz
ISBN:978-84-694-1247-3/T-317-2011

3.4.2 Rh in Pt segregation and islanding.

In order to model the catalyst, we have employed a model representing the Pt surface with Rh present as an impurity. This system is the one representing the experimental $Pt_{100-x}Rh_x$ composition in a most adequate way. First, we have identified the local structure. To do this we have employed the segregation energy, this is the energy obtained when the impurity is placed on the surface of the metal compared to the impurity at the bulk. The segregation of Rh in Pt has been studied with a p(3x3) 6-layers slab, see Fig. 3.17. Calculations show that the most likely position at for the impurity corresponds to positions in the subsurface. The energy difference between surface and subsurface positions is close to -0.35 eV. Therefore, given the high temperatures employed in the reaction and the potential induced segregation effects caused by oxygen we cannot discard surface positions for Rh. With respect to islanding, there is no significant difference between separated and adjoining Rh atoms on Pt surface.

Figure 3.17: Schematic representation of the segregation of a Rh atom (grey large sphere) into a Pt surface (blue small spheres) and segregation energies, E_{seg} in eV, of Rh into Pt.

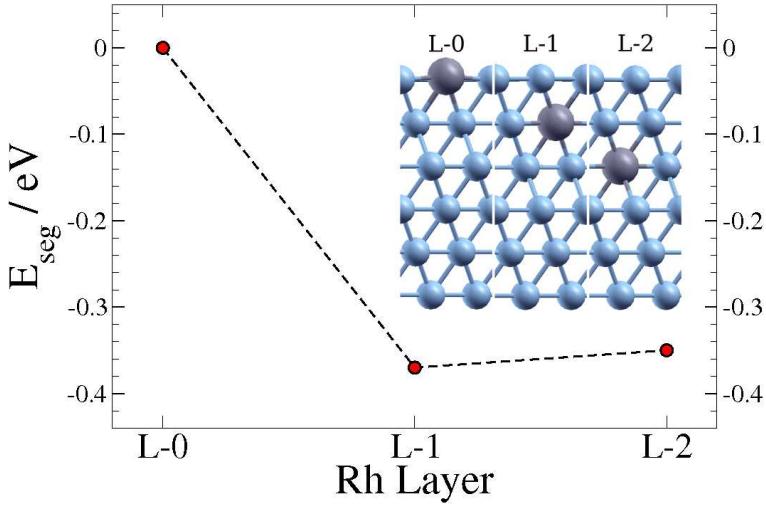

UNIVERSITAT ROVIRA I VIRGILI
FIRST-PRINCIPLES MECHANISTIC STUDIES OF AMMONIA-RELATED INDUSTRIAL PROCESSES
Jaime Gómez Díaz
ISBN:978-84-694-1247-3/T-317-2011

3.4.3 NO and N_2 formation on PtRh alloy

The recombination of N and O has been studied using a p(3x3) 4-layers slab with one Rh atom on surface. This represents one Rh atom on the surface for each eight Pt surface atoms. If we analyze the percentage in atomic ratio of the surface layer we find a 6% in weight, close to the 5-10 % employed in industry. In order to show the effect of surface rhodium atoms on the reactions studied, several adsorbate positions with respect to impurities have been considered. In Fig. 3.18, we observe on the left the cell with the adsorbate adjacent to the Rh atom (close) and on the right the adsorbate separated (far) from Rh.

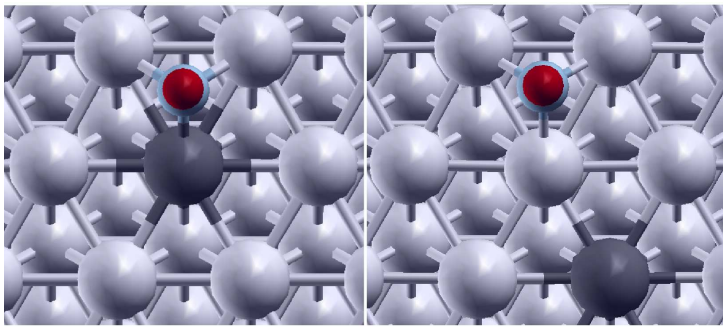

Figure 3.18: PtRh(111) alloy with an adsorbate on the surface. Light grey spheres represent Pt atoms, dark grey one the Rh impurity, red one O and blue one N atom. On the left, the adsorbate is adjacent to the impurity (*close*) and on the right the adsorbate is separated (*far*).

The adsorption energies are shown in Table 3.7. On the neighboring of the Rh atom, the adsorption energy of species is always larger than those at bigger distances. As well, the interaction on this adjoining Rh sites is in general higher than for pure Pt, but for the sites far away from Rh there is not significant change. An exception to this is NH_3, that has smaller adsorption energy than on pure Pt. It can be also seen that the adsorption energy on the alloy can be in general approximated as the sum of the averaged contributions for each bond to the surface [128]. This can be written as follows:

UNIVERSITAT ROVIRA I VIRGILI
FIRST-PRINCIPLES MECHANISTIC STUDIES OF AMMONIA-RELATED INDUSTRIAL PROCESSES
Jaime Gómez Díaz
ISBN:978-84-694-1247-3/T-317-2011

$$E_{ads}^{XY_{alloy}} = \frac{E_{ads}^{X} \cdot N_{bonds}^{X} + E_{ads}^{Y} \cdot N_{bonds}^{Y}}{N_{bonds}^{TOTAL}} \tag{3.29}$$

where E_{ads}^{X} is the adsorption energy of the adsorbate on pure X metal, N_{bonds}^{X} is the number of bonds to X when on this site, and N_{bonds}^{TOTAL} is the total number of bonds to the site (N_{bonds}^{TOTAL}=N_{bonds}^{X}+N_{bonds}^{Y}), see results in Table 3.7. The approximation is reasonable except for the ammonia case.

Table 3.7: Adsorption energies, E_{ads} in eV; for N, O (with respect to half the gas-phase molecules), NH_3 and NO (with respect to the gas-phase molecule) on PtRh. Energies on pure Pt and Rh are also shown for comparison as well as the values estimated by averaging the bond energies with Eq. 3.29.

	PtRh close	PtRh far	Pt	Rh	Average
$E_{ads\,N}$ (fcc)	0.26	0.56	0.57	-0.02	0.37
$E_{ads\,O}$ (fcc)	-1.24	-0.94	-0.59	-1.67	-0.95
$E_{ads\,NH_3}$ (top)	-0.82	-0.59	-0.97	-0.58	-0.58
$E_{ads\,NO}$ (fcc)	-1.74	-1.47	-1.43	-2.06	-1.64

The reactions on the alloy have been studied with several different configurations to determine the effect of Rh atoms, see Fig. 3.19. In the first configuration, X-Rh-Y, both species X and Y are contiguous to Rh atom while in the second, Rh-X-Y, one of the reactants, X, is bonded to the impurity and the second species, Y, is on the second vicinity. Respect to the position of the species resulting from the coupling, the two previously indicated configurations, *close*(-XY) and *far*(-XY), are possible. Thus, for example, in a "X-Rh-Y/close-XY" case, the reactants (X and Y) are located contiguous to the Rh atom, see Fig. 3.19 as well as the coupling resulting XY. In the "Rh-X-Y/close-XY" one of the reactants (X) is adjoin the Rh atom and the other one (Y) is far from it, see Fig. 3.19 and product "XY" is bonded to Rh (*close*). The "Rh-X-Y/far-XY" and "Rh-Y-X/far-XY" reaction have X and Y atoms adjoin Rh respectively and both have the product "XY" not bonded to Rh, see Fig. 3.19. The more relevant thermodynamic, kinetic and geometrical parameters for these reactions are shown in Table 3.8. As for N+N reaction both reactants are the same there are only two possible configurations (N-Rh-N/close-N_2 and Rh-N-

UNIVERSITAT ROVIRA I VIRGILI
FIRST-PRINCIPLES MECHANISTIC STUDIES OF AMMONIA-RELATED INDUSTRIAL PROCESSES
Jaime Gómez Díaz
ISBN:978-84-694-1247-3/T-317-2011

N/far-N_2). Structures for N+N coupling (not shown) are basically the same than those for N+O one.

Table 3.8: Calculated reaction energies, ΔE and activation energies, E_a, both in eV. The distances at the transition state structures are denoted by d and shown in Å, and the corresponding imaginary frequency, ν in cm^{-1} for all the configurations investigated in the model PtRh alloys

	X-Rh-Y close	Rh-X-Y close	Rh-X-Y far	Rh-Y-X far
NO				
ΔE	-0.08	-0.39	-0.12	-0.14
$E_{a,N+O}$	2.17	2.22	2.44	2.41
d_{N-O}	1.775	1.885	1.787	1.766
ν	517	420	517	483
N_2				
ΔE	-0.82	–	-1.17	–
E_{a,N_2}	2.24	–	2.14	–
d_{N-N}	1.881	–	1.889	–
ν	603	–	562	–

The calculated activation energies are similar to those reported in Table 3.8, but since NO adsorption is also higher Rh does not seem to promote the selectivity towards NO when present in the catalyst. Therefore, an alternative explanation is needed.

3.5 Pt, Rh and PtRh alloy stability

Pt and Rh on aerobic conditions form different oxides depending on the temperature and the pressure of oxygen. The behavior of the alloy at working conditions is important to know which phases are present in the reactor and which are the main causes responsible for Pt losses along the reaction.

3.5.1 Previous works

Due to the difficulties present in the experimental studies [129], the determination of the phases and their transition are not accurately determined.

UNIVERSITAT ROVIRA I VIRGILI
FIRST-PRINCIPLES MECHANISTIC STUDIES OF AMMONIA-RELATED INDUSTRIAL PROCESSES
Jaime Gómez Díaz
ISBN:978-84-694-1247-3/T-317-2011

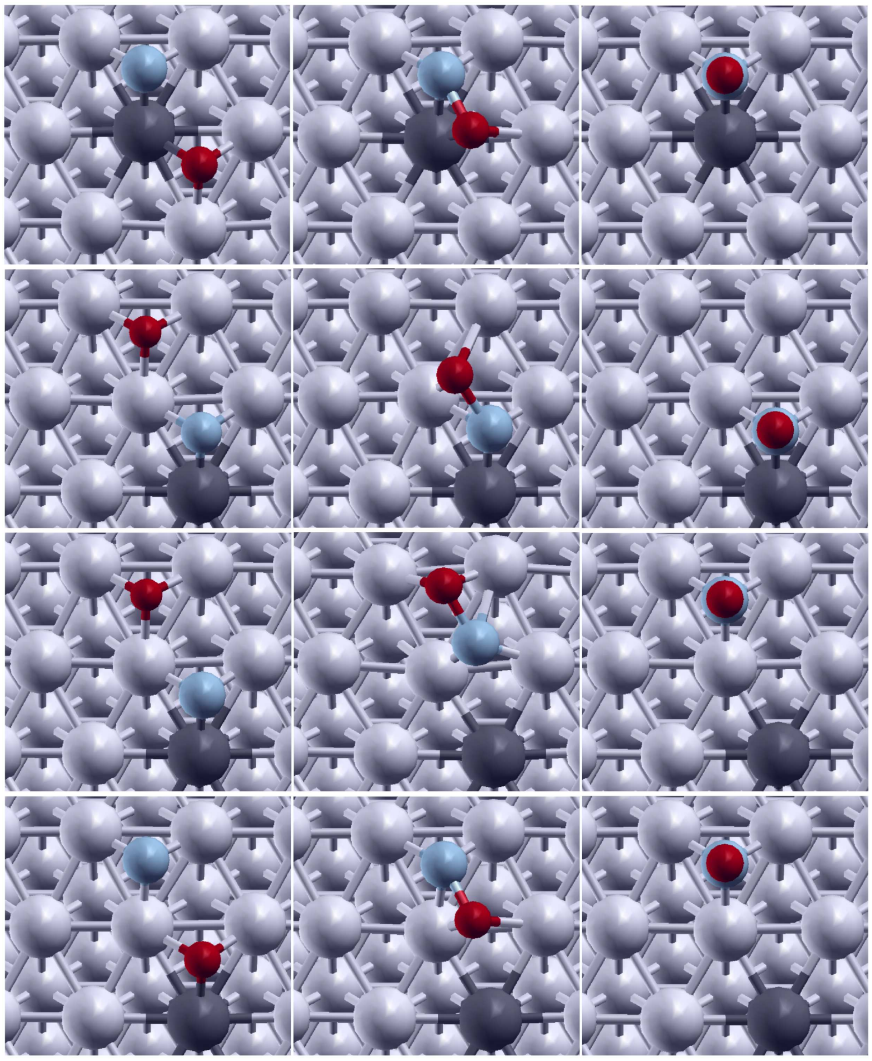

Figure 3.19: Schematic representation of the reactions on PtRh(111) surface. The column on the left contains the structures of the initial states, column on the middle the transition states and right column the final states. Top row represent the N-Rh-O/close-NO reaction, middle-top the Rh-N-O/close-NO, middle-bottom the Rh-N-O/far-NO and bottom the Rh-O-N/far-NO one. Same color code than in Fig. 3.18.

UNIVERSITAT ROVIRA I VIRGILI
FIRST-PRINCIPLES MECHANISTIC STUDIES OF AMMONIA-RELATED INDUSTRIAL PROCESSES
Jaime Gómez Díaz
ISBN:978-84-694-1247-3/T-317-2011

These problems are mainly due to the frequent mixture of oxides and free platinum present in the samples and the presence of partly hydrated oxides. Such uncertainties are inevitably important due to the nature of the binding forces in the materials when so close to dissociation. Rubel and coworkers claimed [130] that the changes observed in the industrial catalysts during NH_3 oxidation are mainly due to the presence of high oxygen pressures. They observed that the losses in catalytic mass are due to both the volatile PtO_2 molecule and also RhO_2 volatility. The presence of α-PtO_2 and RhO_2 was confirmed in these experiments. As well, β-PtO_2 was excluded to be present and other complex phases such as Rh_2O_2 were not completely ruled out. These authors proposed the following description of the process that occurs during the first stage of the interaction with the oxidizing atmosphere:

- Oxidation of platinum to volatile PtO_2 and rhodium to nonvolatile, surface Rh_2O_3 and volatile RhO_2.
- Rh diffusion to the alloy surface along the grain boundaries, the process is continuously stimulated by rhodium oxidation to Rh_2O_3 in the subsurface region.

As a consequence, they found a decrease in the ammonia oxidation rate with the increase in Rh concentration. More recently, Hennevold *et al.* carried out a similar study on the reconstruction of Pt, Rh and Pt-Rh catalysts during the ammonia oxidation process [127]. The experiments provided detailed Scanning Electron Microscopy images and mass spectrometric surveys of the gases formed and X-ray powder characterization of the structures, see Fig. 3.16 (PtRh alloy). Rdzawski *et al.*, also analyzed the phenomena taking place at the catalyst during the process [131], with the aim of increasing its performance. They found several improvements in the addition of yttrium or boron to the classical PtRh catalyst with comparable costs. They also pointed out the necessity of fully elucidate the process taking place at the catalyst surface.

Theoretical investigations cannot take into account all the complexity derived from the large time and lenght scales related to the massive structural transformation experimented by the catalyst and clearly shown in Fig. 3.16. However, some studies on the determination of phase diagrams from a theoretical point of view [132, 133, 134] have been carried

UNIVERSITAT ROVIRA I VIRGILI
FIRST-PRINCIPLES MECHANISTIC STUDIES OF AMMONIA-RELATED INDUSTRIAL PROCESSES
Jaime Gómez Díaz
ISBN:978-84-694-1247-3/T-317-2011

out. For instance, Seriani *et al.* published two papers reporting a DFT study [133, 134] on the structures of the most important platinum oxides and they constructed their corresponding phase diagram through *ab-initio* thermodynamics. In our case, not only the structures and phase diagrams of the phases will be analyzed in detail by DFT and the extension to *ab initio* thermodynamics but also the role of the gas-phase species will be described.

3.5.2 Platinum and rhodium structures

The more relevant Pt and Rh oxides have been studied, to determine which phases are present at catalyst working conditions and the influence of adding rhodium to the catalyst.

- α-PtO_2: crystallizes in the hexagonal CdI_2 structure and presents a laminar structure that is bonded through Van der Waals interactions. The space group is P-3m1 (164), see Fig. 3.20. The agreement of the calculated structure with the experimental results is very good, see Table 3.9. Surprisingly, even the calculated interplane distance 4.465 Å is in rather good agreement with the experimentally determined, 4.34 Å [135].

- Pt_3O_4: there are two proposed crystal structures for Pt_3O_4: body centered cubic and simple cubic. Previous calculations [134], found the formation of the simple cubic structure more favorable. The space group is lm-3m (229). This is the only structure that we have considered in the calculations. As for the previous case, the agreement with the experimental data is good, see Table 3.9.

- RhO_2: crystallizes in rutile structure, see Fig. 3.20. The corresponding space group is $P4_2/mnm$ (136). The agreement in the geometrical parameters with the experimentally determined is very good.

- Rh_2O_3: the structure of Rh_2O_3 is corundum-like, see Fig. 3.20. The corresponding space group is R-3C (167). Like for the other structures, there agreement in the geometrical parameters is very good.

UNIVERSITAT ROVIRA I VIRGILI
FIRST-PRINCIPLES MECHANISTIC STUDIES OF AMMONIA-RELATED INDUSTRIAL PROCESSES
Jaime Gómez Díaz
ISBN:978-84-694-1247-3/T-317-2011

Figure 3.20: (a) α-PtO_2 hexagonal, (b) Pt_3O_4 simple cubic, (c) RhO_2 rutile, and (d) Rh_2O_3 corundum structures. Light grey spheres represent Pt atoms, dark grey Rh and small red O atoms.

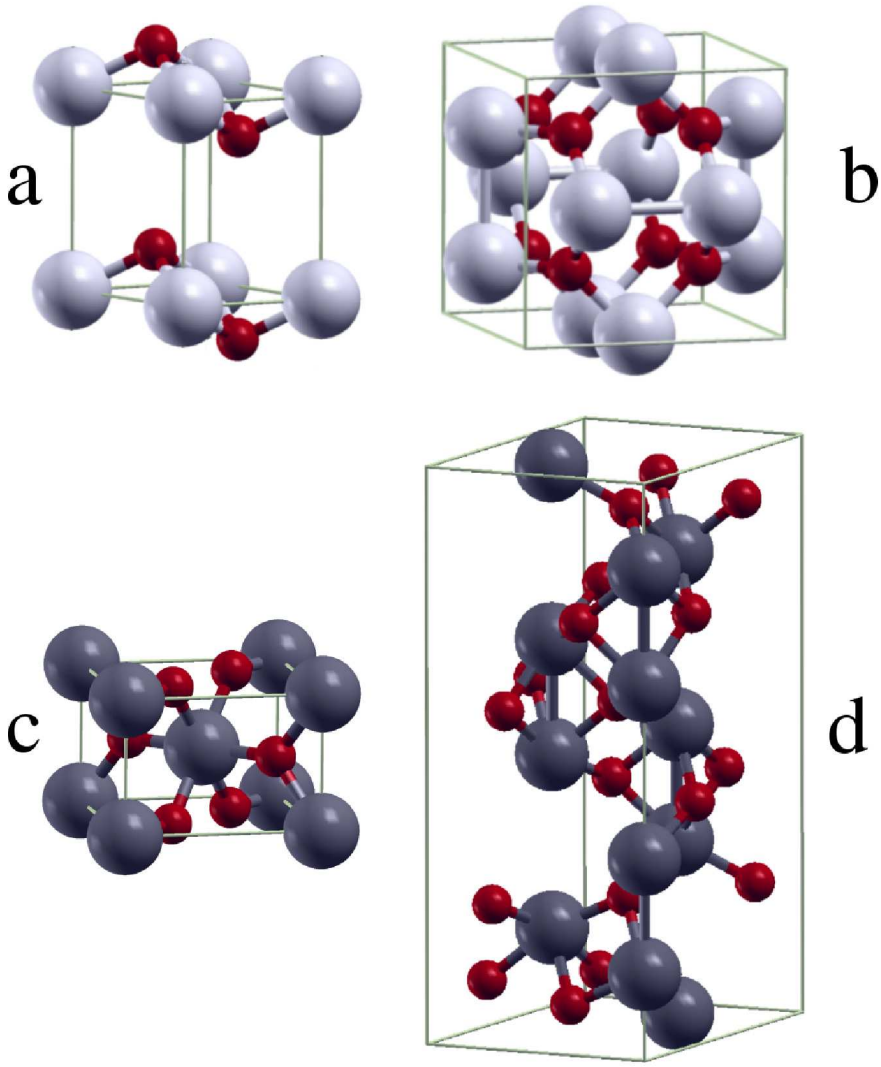

UNIVERSITAT ROVIRA I VIRGILI
FIRST-PRINCIPLES MECHANISTIC STUDIES OF AMMONIA-RELATED INDUSTRIAL PROCESSES
Jaime Gómez Díaz
ISBN:978-84-694-1247-3/T-317-2011

Table 3.9: DFT calculated geometrical parameters compared with other DFT and experimental data for PtO_2, Pt_3O_4, RhO_2 and Rh_2O_3. Pt oxides data from Ref. [133] and Rh oxides from Ref. [136].

	α-PtO_2			Pt_3O_4		
Structure	hexagonal			cubic		
	This work	DFT	Exp	This work	DFT	Exp
a	3.160	3.14	3.10	5.670	5.65	5.585
c/a	1.413	1.85	1.38-1.42	–	–	–
d_{Pt-O}	2.059	2.05	–	2.005	2.00	1.974
d_{Pt-Pt}	3.160	3.14	3.10	2.835	2.83	2.792

	RhO_2			Rh_2O_3		
Structure	rutile			corundum		
	This work	DFT	Exp	This work	DFT	Exp
a	4.542	4.589	4.490	5.210	5.293	5.126
c/a	0.691	0.686	0.689	2.683	2.718	2.734
d_{Rh-O}	1.974	–	–	2.097	–	–
d_{Rh-Rh}	3.140	–	–	2.797	–	–

Table 3.10: PtO_2, Pt_3O_4, RhO_2 and Rh_2O_3 Gibbs free energy of formation, ΔH_f, at 0 K and p=0 atm, in eV/Pt atom compared with previous results in the literature: Ref. [133] for Pt oxides data and Ref. [136] for Rh oxides ones.

	α-PtO_2	Pt_3O_4
This work	-1.04	-0.74
Seriani (PW91)	-2.05	-1.42
Other DFT	-1.24	–
Experimental	-1.73, -1.97, -2.30	-1.13, -1.27

	RhO_2	Rh_2O_3
This work	-1.84	-1.31
Grillo (PBE)	-1.96	-1.83
Experimental	-1.96	-1.78

UNIVERSITAT ROVIRA I VIRGILI
FIRST-PRINCIPLES MECHANISTIC STUDIES OF AMMONIA-RELATED INDUSTRIAL PROCESSES
Jaime Gómez Díaz
ISBN:978-84-694-1247-3/T-317-2011

3.5.3 *Ab-initio* thermodynamics

An *ab-initio* thermodynamic analysis of Pt and Rh have been carried out. Let us develop the model for one of the diagrams calculated, the equilibrium corresponding to

$$Pt_3O_4 \rightleftharpoons 3Pt + 2O_2 \tag{3.30}$$

The line that represents the equilibrium between these phases is that which fulfill

$$g^{bulk}_{Pt_3O_4} = 3g_{Pt} + 2\mu_{O_2} \tag{3.31}$$

Where $g^{bulk}_{Pt_3O_4}$ is the Gibbs free energy of a formula unit of Pt_3O_4, g_{Pt} is corresponding one for Pt bulk and μ_{O_2} is the chemical potential of O_2. For a solid, $g \approx E_{DFT}$ is a good approximation, (see for example Ref. [132] or Section 2.10). The influence of this approximation, not to take into account the vibrational free energy (f_{vib}), has been estimated for this equilibrium [134] as a difference in the temperature of transition around 30 K, small enough to be neglected.

The chemical potential, derived from statistical thermodynamics, for a gas species, in this case, O_2, is

$$\mu_{O_2} = h_{O_2} + E_{O_2} + ZPVE_{O_2} - (Ts_{O_2}) + k_bT\ ln[p_{O_2}/p_0] \tag{3.32}$$

where h_{O_2} is the thermal correction to the enthalpy of O_2, E_{O_2} is its electronic energy, $ZPVE_{O_2}$ the corresponding zero point vibrational energy, T the temperature, s_{O_2} is O_2 entropy, k_b is Boltzmann's constant and p_{O_2} and p_0 are the pressure of O_2 and the pressure of reference respectively. For E_{O_2}, the DFT energy (at 0 K and p=0 atm) is employed. The enthalpy of molecules, ZPVE and entropy (at 873 K) has been calculated under the ideal gas approximation plus a thermal correction estimated with Gaussian-09.

The equilibrium lines have been calculated in a similar way for the following reactions:

$$3\alpha{-}PtO_2 \rightleftharpoons Pt_3O_4 + O_2 \tag{3.33}$$

UNIVERSITAT ROVIRA I VIRGILI
FIRST-PRINCIPLES MECHANISTIC STUDIES OF AMMONIA-RELATED INDUSTRIAL PROCESSES
Jaime Gómez Díaz
ISBN:978-84-694-1247-3/T-317-2011

$$Pt_3O_4 \rightleftharpoons 3Pt + 2O_2 \tag{3.34}$$

$$2RhO_2 \rightleftharpoons Rh_2O_3 + 1/2O_2 \tag{3.35}$$

$$Rh_2O_3 \rightleftharpoons 2Rh + 3/2O_2 \tag{3.36}$$

and the resulting phase diagrams for Pt and Rh are shown in Fig. 3.21 and 3.23. In the platinum phase diagram the β-PtO_2 phase has not been included, as it is present only under extremely high oxygen pressures. The agreement between the calculated phase diagram with the experimental one [137] is reasonable. At an oxygen pressure of about 10 atmospheres, the transition between Pt and Pt_3O_4 takes place at about 525°C. This qualitatively agrees with the 625°C observed in the experimental phase diagram [137]. The transition between Pt_3O_4 and α-PtO_2 occurs at 120 atmospheres of oxygen and 500°C while the experimental estimate is around 575°C .

In the rhodium phase diagram Rh, corundum Rh_2O_3 and rutile RhO_2 structures have been included. Rh_2O_3 orthorhombic phase has not been considered, as it is present only at extremely high oxygen pressures. The agreement between the calculated phase diagram with the experimental one is reasonable, see Figs. 3.23 and 3.24. At an oxygen pressure of 0.1 atmospheres, the transition RhO_2/Rh_2O_3 takes place at around 485°C, which compares well with the 650°C found experimentally.

In order to measure the volatility of the oxides, the equilibrium pressure of gaseous PtO_2 and RhO_2 for Pt and Rh in equilibrium with 1 atm. oxygen pressure has been calculated, see Fig. 3.25. Rh is found to be much less volatile, with partial pressures of RhO_2 molecule around 100 times smaller than the PtO_2 value.

Even when the trends observed are good, the temperatures for the transitions are not accurately determined. This is due to several points. First, it is well known that the ground state energy of the gas-phase molecule O_2, $^3\Sigma_g^-$, is not well described by DFT methods. Second, the conditions that the diagrams are reproduced (high pressure and temperature) are far from those in which the ideal gas approximation is reliable. Third, the vibrational entropy of solids has not been taken into account, although this might be a good approximation at low termperatures it is less accurate at high temperatures. Fourth, the thermal corrections to enthalpy and entropy, that have been considered constant at 873 K values, change with the temperature.

UNIVERSITAT ROVIRA I VIRGILI
FIRST-PRINCIPLES MECHANISTIC STUDIES OF AMMONIA-RELATED INDUSTRIAL PROCESSES
Jaime Gómez Díaz
ISBN:978-84-694-1247-3/T-317-2011

Figure 3.21: Calculated phase diagram for Pt at O_2 pressure.

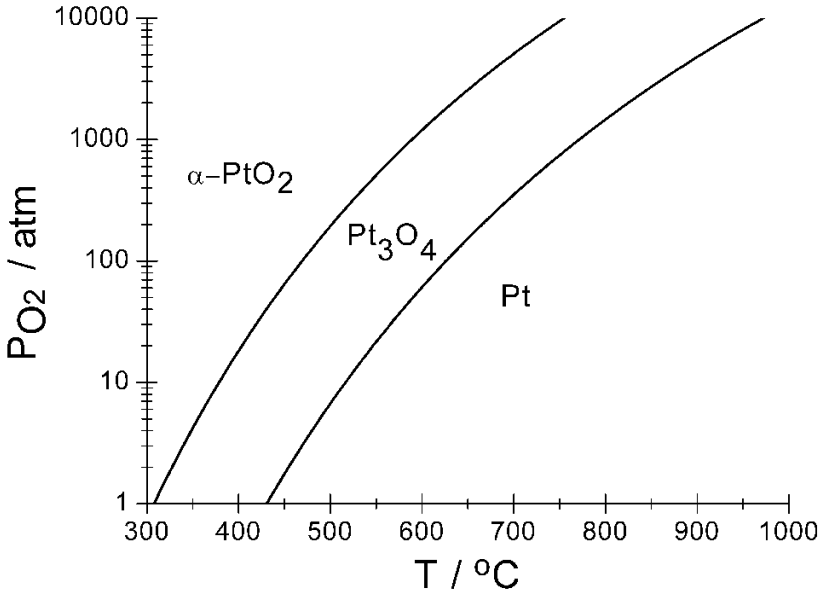

Figure 3.22: Experimental phase diagram for Pt at high O_2 pressures, from Ref. [137]. No better resolution available.

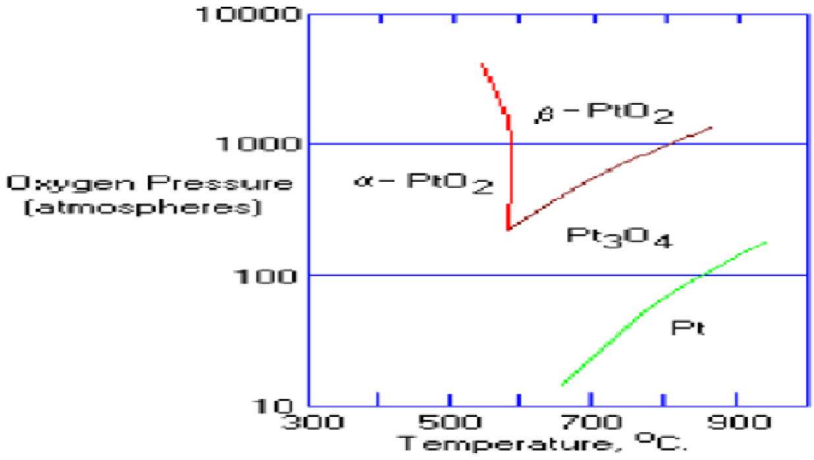

UNIVERSITAT ROVIRA I VIRGILI
FIRST-PRINCIPLES MECHANISTIC STUDIES OF AMMONIA-RELATED INDUSTRIAL PROCESSES
Jaime Gómez Díaz
ISBN:978-84-694-1247-3/T-317-2011

Figure 3.23: Calculated phase diagram for Rh at O_2 pressure.

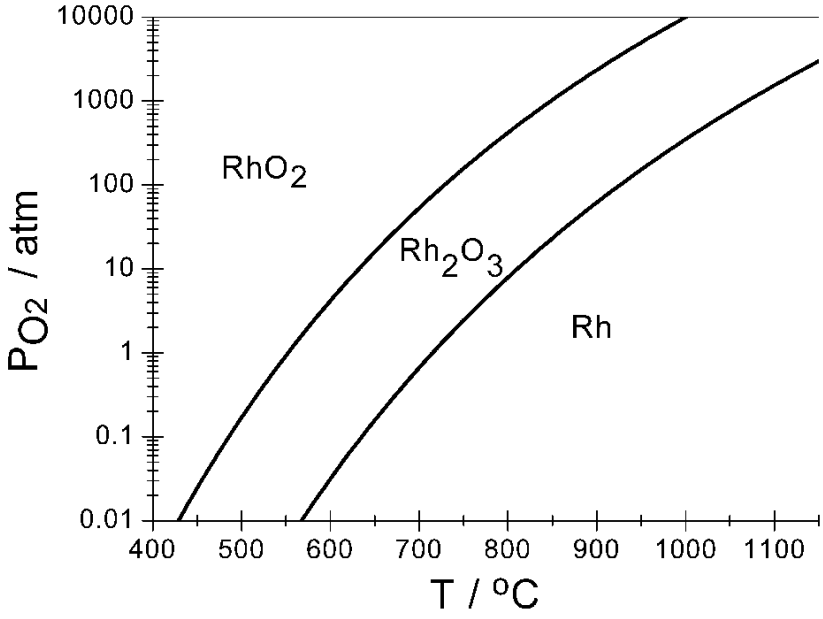

Figure 3.24: Phase diagram for Rh at low O_2 pressures, from Ref. [137]. No better resolution available.

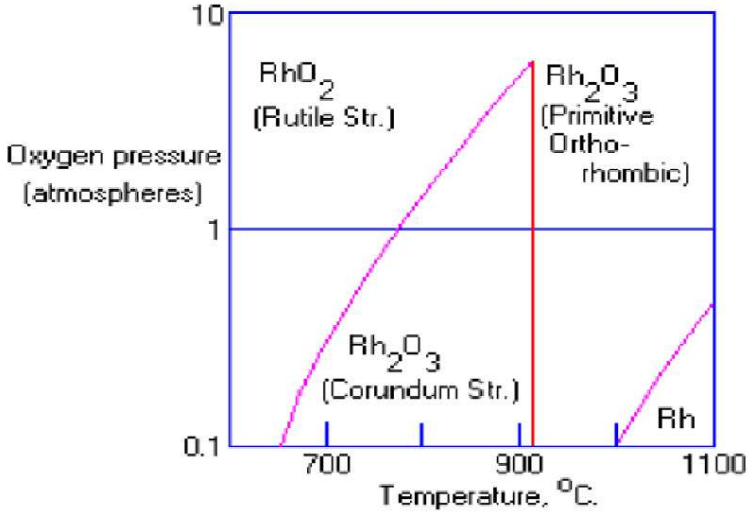

UNIVERSITAT ROVIRA I VIRGILI
FIRST-PRINCIPLES MECHANISTIC STUDIES OF AMMONIA-RELATED INDUSTRIAL PROCESSES
Jaime Gómez Díaz
ISBN:978-84-694-1247-3/T-317-2011

In summary, since the binding energy of oxygen to the Rh-containing centers is larger than for Pt this explains the induced segregation of Rh towards the surface, once there Rh acts as an oxygen sink as most of the oxygen would be neighboring these impurities on the surface. This will reduce the effective oxidative potential exerted on the Pt atoms on the surface. Then, since Rh is less likely to produce volatile species than Pt, as seen in Fig. 3.25, the result is that the PtRh alloy is more resistant to oxidation and Pt losses in the form of PtO_2.

Figure 3.25: Gas phase PtO_2 and RhO_2 pressures in equilibrium with Pt and Rh solid and 1 atmosphere oxygen pressure.

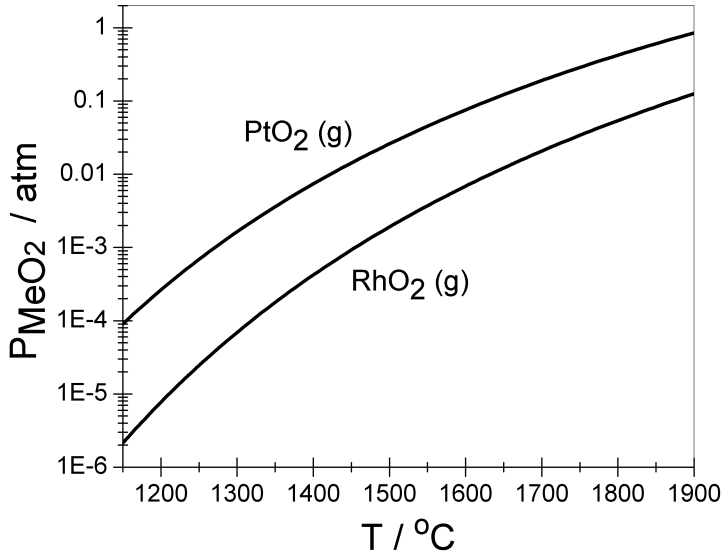

3.6 Conclusions

We have studied the most relevant steps on the Ostwald process reaction for several materials including metals, and the PtRh alloy. For the latter, an analysis of the stability has been performed.

UNIVERSITAT ROVIRA I VIRGILI
FIRST-PRINCIPLES MECHANISTIC STUDIES OF AMMONIA-RELATED INDUSTRIAL PROCESSES
Jaime Gómez Díaz
ISBN:978-84-694-1247-3/T-317-2011

Au(111)

-Oxygen atoms or hydroxyl groups have been revealed as crucial in ammonia dehydrogenation on this surface. In addition, all oxygen or hydroxyl assisted dehydrogenation steps have lower barriers than the recombination processes under relevant conditions. N_2 recombination is hindered by a barrier of 0.95 eV, whereas that of NO is 1.03 eV.

-NO adsorbs only weakly on the metal surface and readsorption or recombination with other N, O atoms on the surface are unlikely events. Our DFT combined with the detail balance of the species on the surface can account for the experimental observations regarding the preferred N_2 selectivity in the group of Prof. Mullins.

Transition metals (111 and 211)

-On the flat surfaces, the smaller coupling barriers are found for Au and Cu. In these metals, the recombinations are much more exothermic than for the other metals. The adsorption of species is among the smallest.

-Different case regarding the extension of the reaction involved in the selectivity problem have been established. In particular for the Pt (211) surface it is seen that the reasorption of NO is possible and even the dissociation towards N+O can be a route to reduce the high selectivity otherwise observed by the comparison of the N+O versus the N+N reaction routes. Our results are in agreement with the BHK model.

PtRh reactivity and stability

-The electronic influence of a Rh impurity on a Pt slab is weak out of its vicinity. The only remarkable difference concerns the high adsorption energy of oxygen in mixed sites containing Rh. Given the present results it is unlikely that a large perturbation on the selectivity takes place under reaction conditions for the gauzes containing the Rh impurity.

-Instead, the present calculations support the role of Rh in improving the oxygen tolerance of the PtRh alloy when compared to pure Pt. This is based in several factors: regeneration from the bulk, easy extraction in the presence of oxygen, and the fact that Rh acts as a sink for oxygen atoms on the surface, thus reducing the effective pressure on the Pt atoms

UNIVERSITAT ROVIRA I VIRGILI
FIRST-PRINCIPLES MECHANISTIC STUDIES OF AMMONIA-RELATED INDUSTRIAL PROCESSES
Jaime Gómez Díaz
ISBN:978-84-694-1247-3/T-317-2011

on the surface. This is complemented by the fact that Rh species are less volatile than Pt ones.

UNIVERSITAT ROVIRA I VIRGILI
FIRST-PRINCIPLES MECHANISTIC STUDIES OF AMMONIA-RELATED INDUSTRIAL PROCESSES
Jaime Gómez Díaz
ISBN:978-84-694-1247-3/T-317-2011

UNIVERSITAT ROVIRA I VIRGILI
FIRST-PRINCIPLES MECHANISTIC STUDIES OF AMMONIA-RELATED INDUSTRIAL PROCESSES
Jaime Gómez Díaz
ISBN:978-84-694-1247-3/T-317-2011

Chapter 4

HCN synthesis: Results

As indicated in Chapter 1.3, HCN is synthesized by Degussa (1500-1600 K, Pt catalyst) and Andrussow (1400-1500 K, PtRh catalyst, O_2) processes. Both are carried out at high temperatures with very short contact times, making the reaction on the surface extremely fast. That poses difficulties for the experimental determination of the reaction mechanism. Then, a theoretical study is the best option to unravel the mechanism reaction. In Figure 4 we can see the intricacies of the reaction network, and how many possible intermediates can be formed. If we consider CH_x and NH_y (x,y=0,1,2) species, we obtain nine possible coupling products, as well as four isomerizations and sixteen H_xCNH_y dehydrogenations. Besides this, O_2 presence (Andrussow conditions) can further modify how the reaction works. These considerations give us an idea of the complexity of the system.

The Chapter is divided into two main sections. The first section study in deep the process on Pt under both oxidative and non-oxidative conditions. In the second section, the most important reactions involved in Andrussow process (oxidative conditions) process (C+N, C+NH, H+CN and HC+N couplings) on the surface of several transition metals (Au, Cu, Ir, Pd, Pt and Rh) are presented. Finally, the conclusions are stated.

UNIVERSITAT ROVIRA I VIRGILI
FIRST-PRINCIPLES MECHANISTIC STUDIES OF AMMONIA-RELATED INDUSTRIAL PROCESSES
Jaime Gómez Díaz
ISBN:978-84-694-1247-3/T-317-2011

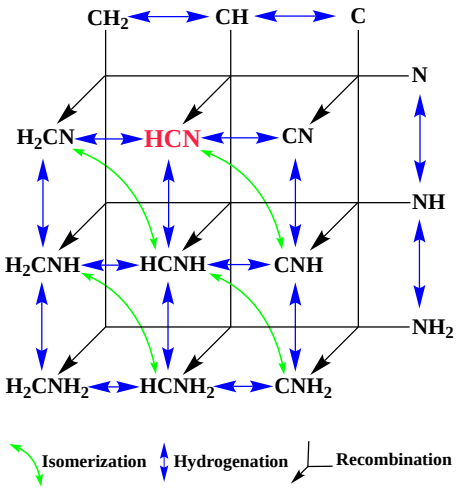

Figure 4.1: Reaction network to produce HCN from methane and ammonia. All possible reactions between NH_3- and CH_4-derived intermediates are shown, as well as isomerizations and de/hydrogenations.

4.1 Previous works

The determination of this complex reaction path has been addressed by many groups during decades. Prof. Schmidt and co-workers have widely worked in this field, starting these studies with their first article in 1985 [138] with a Temperature Programmed Desorption (TPD) experiment under Ultra High Vacuum (UHV) supported by Auger Electron Spectroscopy (AES) on a clean Rh surface precovered with CH_4 and NH_3 under anaerobic conditions. They indicated the need for the presence of C atoms on the surface, and proposed **C+NH** coupling as the most likely way to form C-N bonds due to the small quantities of C_2N_2, CH_3NH_2, CH_3CN, N and H observed. One year later [139], they carried out the experiment under similar conditions on polycrystalline Pt. Again, C atoms covering the surface were shown as necessary, and both, **C+N** or **C+NH**, couplings were then mentioned as possible. After these studies, many other articles were published by Schmidt's group [12, 140, 141, 142, 143, 144, 145, 146], all of them under aerobic conditions. No new mechanisms were suggested in these papers, but H_2 addition was described as a way to increase selec-

UNIVERSITAT ROVIRA I VIRGILI
FIRST-PRINCIPLES MECHANISTIC STUDIES OF AMMONIA-RELATED INDUSTRIAL PROCESSES
Jaime Gómez Díaz
ISBN:978-84-694-1247-3/T-317-2011

tivity [145]. As well, in 2006, Schuurman and Delagrange [13] performed Temporal Analysis of Products (TAP) experiments over platinum black catalyst under anaerobic conditions, proposing **CH+N** or **CN+H** coupling as HCN formation mechanism.

The group of Prof. Trenary has also studied these reactions. Early in 1998, they performed a Temperature Programmed Reaction Spectroscopy (TPRS) supported with Reflection Absorption Infra-Red Spectroscopy (RAIRS) experiment on Pt(111) and Cu(100) [147] where they pointed out the presence of adsorbed $\mathbf{CNH_2}$, and proposed **H+CN** as the most likely coupling. A later TPD experiment [148] on Pt(111) covered with an initial layer of CH_3I and NH_3 pointed to **C+N** as the likely path, since no hydrogenated species were detected. A later study in the same surface [149], supported with RAIRS and X-ray Photoelectron Spectroscopy (XPS) likewise indicate **C+N** as the coupling mechanism and estimate the reaction barrier for this reaction around 120 kJ/mol. A similar work that includes DFT calculations for a Pt_7 cluster [150], bears out $\mathbf{NH_3}$+$\mathbf{C_2}$ as C-N bond formation mechanism. In 1999, Prof. Schwarz and co-workers carried out gas phase Pt^+ ion experiments plus DFT calculations [151]. They proposed a mechanism involving $\mathbf{CH_2NH_3}$ species. Very recent TAP experiments on the industrial alloy catalyst [152, 153], suggest the participation of absorbed oxygen species, and they propose as more likely CH_x+N or CH_x+NO reactions as main C-N formation steps. They determined, as well, that the presence of other possible minority products as CO or NO_x may decrease the selectivity of the process.

Some theoretical studies have also been carried out. Ammonia [90, 104] and methane [104, 154, 155] dehydrogenations have been studied for several metals. The adsorption energy of the different fragments has been found to correlate with the adsorption energy of the central atom [64]. As well, oxygen and hydroxyl are known to ease some dehydrogenation processes involving ammonia, see Chapter 3 [80]. **C+N** and C+H coupling were studied by Michaelides and Hu.[156] **C+N** direct coupling has been studied by Crawford and Hu [157] over the 4d metals from Zr to Pd. Also the trends in the activation energy and the chemisorption for these metals were analyzed in a later paper [158]. The electronic structure of CN adsorbed on Pt(111) surface, modeled on a cluster, has been studied by Ample and co. [159]. As well, HCN formation on Rh(111) has been

UNIVERSITAT ROVIRA I VIRGILI
FIRST-PRINCIPLES MECHANISTIC STUDIES OF AMMONIA-RELATED INDUSTRIAL PROCESSES
Jaime Gómez Díaz
ISBN:978-84-694-1247-3/T-317-2011

studied by Ricart *et al.* [160], only through the **CH+N** reaction or by **C+N** coupling and later hydrogenation. They conclude that **CH+N** is the favored path. Other works, focusing on the analysis of the metal-cyanide bond have been presented [161, 162], but no comprehensive studies on the whole mechanism have been presented. No other steps than **C+N** and **CH+N** have been theoretically addressed, even when experimental works point out to the presence of other H-containing intermediates.

In sumary, after many studies no consensus has been reached about the mechanisms that govern the processes. The key, unanswered, question is, how is the C-N bond formed, through atomic species, **C+N**, or through partially hydrogenated intermediates, $\mathbf{H}_x\mathbf{C}+\mathbf{NH}_y$.

4.2 Computational details.

All the calculations were performed with DFT solved with VASP package [32, 45, 47, 69, 70, 71, 72] applied to slabs representing the different metal (111) surfaces. The exchange-correlation functional used is RPBE [33], and the core electrons have been described with PAW pseudopotentials [36]. The plane waves used to describe valence electrons have a cut-off energy of 400 eV. The employed supercell is p(3x3), giving a coverage of 0.11 monolayers when only one species is adsorbed. The slab contains 4 metal layers, and the two uppermost and the adsorbate have been allowed to relax. Vacuum space has been added, equivalent to 8 metal layers, and the dipole generated due to the asymmetry of the system has been removed. The *k-points* sampling is Monkhorst-Pack type [41] and as dense as 5x5x1. The transition state (TS) search has been performed by means of CI-NEB [58], and they show a single imaginary frequency.

4.3 Degussa and Andrussow processes on Pt(111)

In this section, the reactions that lead to HCN under presence or absence of oxygen over Pt are studied comprehensively. Adsorption of the different species involved has been studied, as well as the vibrational modes frequencies of the most representative H_xCNH_y species. Both, NH_3 and CH_4, dehydrogenations to atomic species N and C are explained in this section. Recombinations (H_xC+NH_y couplings) and isomerizations are

UNIVERSITAT ROVIRA I VIRGILI
FIRST-PRINCIPLES MECHANISTIC STUDIES OF AMMONIA-RELATED INDUSTRIAL PROCESSES
Jaime Gómez Díaz
ISBN:978-84-694-1247-3/T-317-2011

also shown. The relevant structures (initial, transition and final states) for all the reactions are represented (Figs. 4.2-4.7) and the most important distances between atoms for the transition states are presented. If not expressly indicated, all the adsorption energies presented are calculated with respect to the corresponding gas phase fragment.

4.3.1 Adsorption of species.

The adsorption of the species involved in this process is shown in this section. Ammonia molecule adsorbs preferably on *top* position. The coverage used for all the calculations is 1/9 ML. The adsorption energy for this species is -0.57 eV. NH_2 adsorption takes place at a *bridge* site, and adsorbs exothermically, E_{ads}=-1.90 eV. The last hydrogenated species of the set, NH, shows preference for *fcc* site, with a binding energy of -3.37 eV. Methane does not adsorb on Pt. CH_3 adsorbs on *top* position, and the adsorption energy is -1.67 eV. CH_2 adsorption shows preference for *bridge* site, and adsorbs exothermically, E_a=-1.90 eV. CH adsorption takes place on *fcc* site, with a binding energy of -3.37 eV. All these adsorptions follow the Bond-Order conservation rule: adsorbing on the sites where more of the bonds that are missing can be satisfied. Atomic species N and C show adsorption energies of 2.14 and 0.76 eV with respect to N_2 and CH_4 respectively. Molecules produced by C-N couplings, H_xCNH_y, have more complex adsorption sites. HCN adsorbs on *tbt* position and its adsorption energy is small, -0.46 eV. Its isomer, CNH, adsorbs through C atom, the C-N bond is almost perpendicular to the surface and C-N-H angle is 122.9°. Its desorption is hindered by a large barrier of 1.60 eV. HCNH adsorbs on a position almost identical to that for HCN with and extra H atom, and its adsorption energy is -2.27 eV. CNH_2 adsorption, instead, is perpendicular to the surface, and the adsorption energy is -3.98 eV.

All those structures are shown in Figure 4.3, page 95. Normal vibrational modes frequencies have been determined for H_xCNH_y species. Table 4.1 shows the calculated frequencies, ν in cm^{-1}, as well as experimental values. The determination of frequencies by DFT calculations is not always accurate. For example, the calculated C-N stretching frequency on Pt(111) *fcc* site is 1870 cm^{-1}, but the experimental value is 2132 cm^{-1} [163]. On the other hand, the calculated stretching frequency when C-N is adsorbed on *top* position is 2155 cm^{-1}, in better agreement with the

UNIVERSITAT ROVIRA I VIRGILI
FIRST-PRINCIPLES MECHANISTIC STUDIES OF AMMONIA-RELATED INDUSTRIAL PROCESSES
Jaime Gómez Díaz
ISBN:978-84-694-1247-3/T-317-2011

experimental value. This problem with the accurate determination of the adsorption site has been reported as well for CO [164]. Nevertheless, the agreement of calculated frequencies shown in Table 4.1 is in reasonably agreement with the experimentally determined.

Table 4.1: Vibrational frequencies, ν in cm^{-1}, for adsorbed H_xCNH_y species. Experimental (exp.) values for active vibrations are given into brackets.

Species	Site	ν cm^{-1}					
HCN	tbt	3045	1583	931			
	exp [147]	3298	1325				
CNH	fcc	3506	1653	721			
CNH_2	fcc	3611	3487	1551	1301	1060	497
	exp [148]		3369	1566	1328		
CN	top	2155					
	exp [147]	2132					

4.3.2 CH_4 and NH_3 dehydrogenations.

Structures are shown in Fig. 4.2, and energies in Table 4.2. On Pt(111) surface, CH_4 does not adsorb. This kind of mechanisms in which one of the reactants reacts directly from the gas phase, without being adsorbed at the surface, Eley-Rideal mechanisms, are much less probable than Langmuir-Hinselwood ones. First proton abstraction is hindered by 0.73 eV, and dissociation leads to a methyl group adsorbed on *top* a Pt center and a H atom sitting on a *fcc* site. The reaction is almost thermoneutral, 0.04 eV. Due to the Eley-Rideal character of this reaction, this process is one of the responsible for the high temperature required in the Degussa process. Successive CH_3 dissociation, has a barrier of 0.89 eV and is endothermic by 0.30 eV. Next proton abstraction, CH_2 on *bridge* position, shows a barrier of 0.38 eV and ΔE=-0.43 eV. This is the smallest barrier for dehydrogenation of CH_x species and the only exothermic. CH (on *fcc* site) dissociation shows a 1.51 eV barrier and it is endothermic by 0.94 eV. This reaction shows the highest barrier and it is the most endothermic reaction of all the dehydrogenations.

Ammonia is adsorbed on *top* position, with a binding energy of 0.6

UNIVERSITAT ROVIRA I VIRGILI
FIRST-PRINCIPLES MECHANISTIC STUDIES OF AMMONIA-RELATED INDUSTRIAL PROCESSES
Jaime Gómez Díaz
ISBN:978-84-694-1247-3/T-317-2011

Table 4.2: Reaction energy, ΔE, and activation energies for direct reaction, E_a, and inverse reaction, E_a^{inv}. All energies in eV.

Dehydrogenations	ΔE	E_a	E_a^{inv}
$CH_4 \rightarrow CH_3 + H$	0.04	0.73	0.68
$CH_3 \rightarrow CH_2 + H$	0.30	0.89	0.59
$CH_2 \rightarrow CH + H$	-0.43	0.38	0.81
$CH \rightarrow C + H$	0.94	1.51	0.57
$NH_3 \rightarrow NH_2 + H$	0.45	1.39	0.94
$NH_2 \rightarrow NH + H$	0.19	1.30	1.11
$NH \rightarrow N + H$	0.54	1.32	0.78

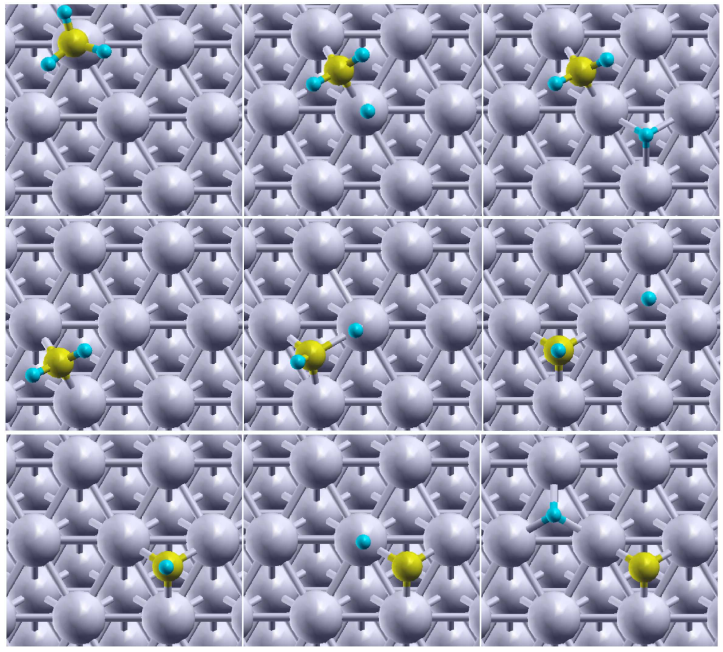

Figure 4.2: Schematic representations for dehydrogenation reactions. Initial (left), transition (center) and final (right) states for CH_3 (top), CH_2 (centre) and CH (bottom) proton abstractions. Grey spheres represent Pt, yellow ones C and turquoise small ones H, atoms. Structures for N (blue spheres in next figures) hydrogenation, omitted, are formally identical.

UNIVERSITAT ROVIRA I VIRGILI
FIRST-PRINCIPLES MECHANISTIC STUDIES OF AMMONIA-RELATED INDUSTRIAL PROCESSES
Jaime Gómez Díaz
ISBN:978-84-694-1247-3/T-317-2011

eV. This value is larger than others reported in literature [104], due to the lower coverage employed in the present calculations, 0.11 *vs* 0.25 ML, that minimizes lateral repulsion. First ammonia hydrogen abstraction is hindered by a 1.39 eV barrier, the largest for ammonia-related species dehydrogenation, and the reaction is endothermic by 0.45 eV. NH_2, on *bridge* site, dehydrogenation is hindered by 1.30 eV, the smallest barrier and the less endothermic reaction in this group, 0.19 eV. NH, on *fcc* hollow, dissociation has a barrier of 1.32 eV, the smallest in this group, and is the most endothermic endothermic reaction, ΔE=0.54 eV.

4.3.3 $CH_x + NH_x$ couplings

Structures are shown in Figures 4.3-4.5, and energies in Table 4.3. As previously mentioned, in general CH_4, CH_3 and NH_3 species are excluded to easily react on the surface. On the other hand, CH_3 and NH_3 are discarded by experimental reasons [148]. This can be explained in therms of Bond-Order conservation, as the formation of Y-XH_3 bond would imply loss of bonds with the surface.

Table 4.3: Reaction energy, ΔE, activation energies for direct reaction, E_a, from infinitely separated fragments, E_a^∞, and inverse reaction, E_a^{inv}, in eV.

$CH_x + NH_y$ coupling	ΔE	E_a	E_a^∞	E_a^{inv}
$C + N \rightarrow CN$	-0.97	1.79	2.25	2.76
$C + NH \rightarrow CNH$	-1.33	2.05	1.98	3.38
$C + NH_2 \rightarrow CNH_2$	-1.22	1.03	1.07	3.25
$HC + N \rightarrow HCN$	-0.26	1.97	2.29	2.23
$HC + NH \rightarrow HCNH$	-0.81	1.65	1.99	2.46
$HC + NH_2 \rightarrow HCNH_2$	0.07	0.70	1.24	0.63
$H_2C + N \rightarrow H_2CN$	0.50	1.82	1.96	1.32
$H_2C + NH \rightarrow H_2CNH$	-0.56	1.66	1.76	2.22
$H_2C + NH_2 \rightarrow H_2CNH_2$	-1.18	1.37	1.36	2.55

The first set of couplings, C+NH_x (x=0,1,2), see Fig. 4.3, starts with the most simple reaction, C+N. This reaction takes place by N activation and has a barrier of 1.79 eV and it is exothermic by -0.97 eV. Resulting CN is placed on a *hollow* site C-down. For C+NH reaction the barrier is large,

UNIVERSITAT ROVIRA I VIRGILI
FIRST-PRINCIPLES MECHANISTIC STUDIES OF AMMONIA-RELATED INDUSTRIAL PROCESSES
Jaime Gómez Díaz
ISBN:978-84-694-1247-3/T-317-2011

2.08 eV, and resulting CNH is placed on *fcc* site C-down, but is the most exothermic of this set. The distance between C and N at the transition state is 2.050 Å. The smallest barrier in this group is for C+NH_2 coupling, 1.03 eV and exothermic by -1.22 eV, being the C-N distance 2.554 Å at the transition state. The produced CNH_2 is placed on a *bridge* site. This *tbt* CNH_2 can rotate its molecular axis to a position perpendicular to the surface without any considerable barrier. This position is equivalent to that for CNH with an extra H atom. This structure leads this fragment less reactive, as H and N atoms are far away from the surface.

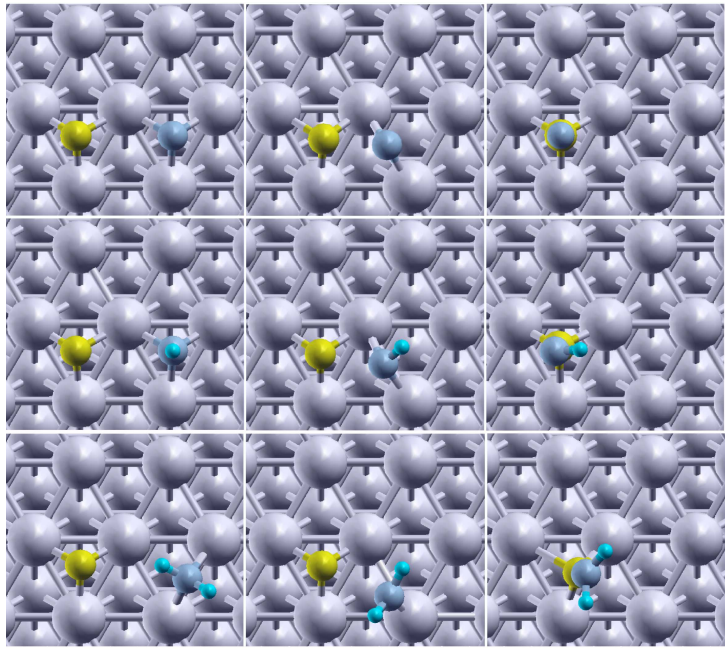

Figure 4.3: Schematic representations for C+NH_x (x=0,1,2) coupling reactions. Initial (left), transition (center) and final (right) states for C+N (top), C+NH (centre) and C+NH_2 (bottom). Same color code as in Figure 4.2.

Next set, HC+NH_x reactions (Fig. 4.4), starts with HC+N reaction, is hindered by a large barrier of 1.97 eV, and results in HCN on *tbt* position. The C-N distance at the transition state is 1.956 Å. The reaction is exothermic, ΔE=-0.26 eV. HC+NH reaction has an activation barrier

UNIVERSITAT ROVIRA I VIRGILI
FIRST-PRINCIPLES MECHANISTIC STUDIES OF AMMONIA-RELATED INDUSTRIAL PROCESSES
Jaime Gómez Díaz
ISBN:978-84-694-1247-3/T-317-2011

of 1.65 eV, and leads to HCNH on tbt position, being ΔE=-0.81. At the transition state, the distance C-N is 1.938 Å. The last reaction of this group, HC+NH_2, shows a small barrier of 0.70 eV and it is almost thermoneutral. This barrier is the smallest one for C-N bond formation, and the product, $HCNH_2$, is placed bonded by the C atom and with the molecular axis tilted to the surface. At the transition state C and N are separated by 2.240 Å.

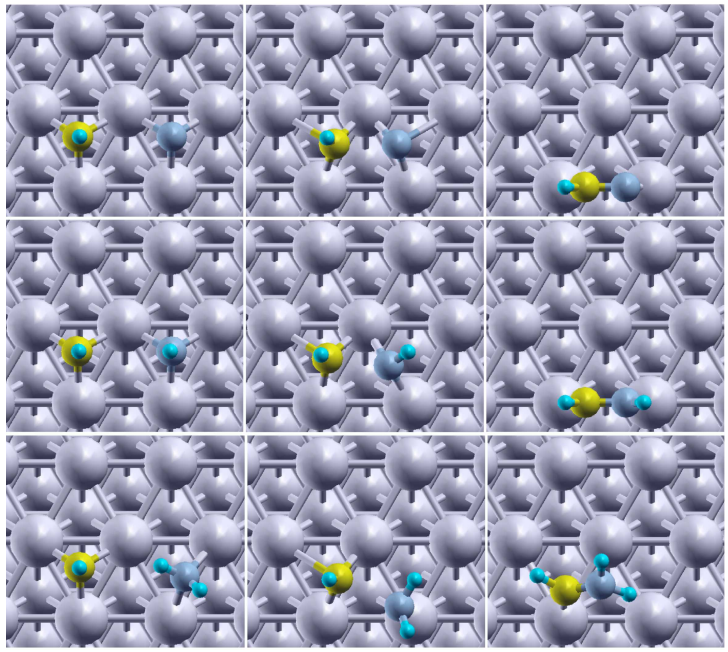

Figure 4.4: Schematic representations for HC+NH_x (x=0,1,2) coupling reactions. Initial (left), transition (center) and final (right) states for HC+N (top), HC+NH (centre) and HC+NH_2 (bottom). Same color code as in Figure 4.2.

Last set, H_2C+NH_x (Figure 4.5), starts by H_2C+N reaction, hindered by a barrier of 1.82 eV, and with ΔE=0.50 eV. The C-N distance is 2.421 Å at the transition state. H_2C+NH coupling has a activation energy of 1.66 eV and is exothermic by -0.56 eV. The product, H_2CNH, is adsorbed on a *tbt* site. The last coupling is H_2C+NH_2, and shows the smallest barrier for this group, 1.37 eV, and it is very exothermic, ΔE=-1.18 eV.

UNIVERSITAT ROVIRA I VIRGILI
FIRST-PRINCIPLES MECHANISTIC STUDIES OF AMMONIA-RELATED INDUSTRIAL PROCESSES
Jaime Gómez Díaz
ISBN:978-84-694-1247-3/T-317-2011

At the transition state for this reaction, the C-N distance is 3.209 Å.

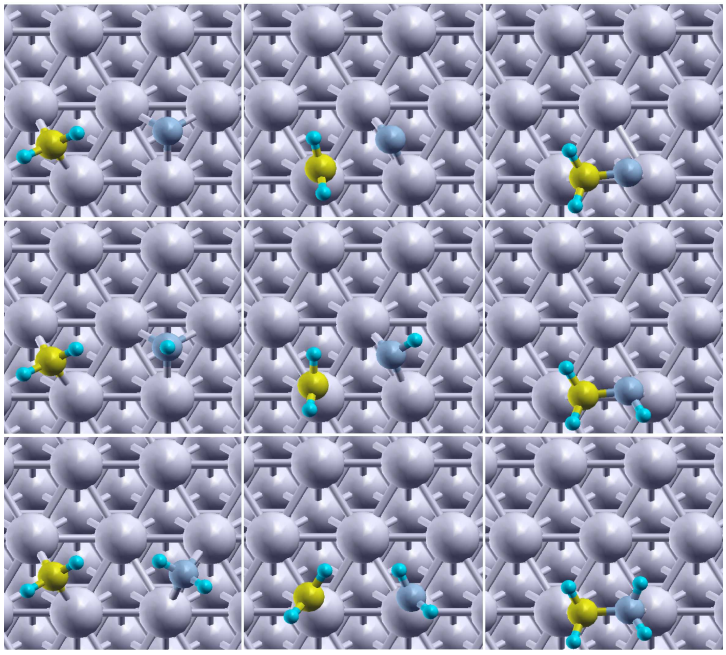

Figure 4.5: Schematic representations for H_2C+NH_x (x=0,1,2) coupling reactions. Initial (left), transition (center) and final (right) states for H_2C+N (top), H_2C+NH (centre) and H_2C+NH_2 (bottom). Same color code as in Figure 4.2.

4.3.4 H_xCNH_y dehydrogenation

Once C-N bond is formed, hydrogenations or dehydrogenations are necessary to obtain the desired HCN, see Fig. 4. CN protonation has a small barrier of 0.81 eV, and is exothermic by -0.33 eV. As well, HCNH deprotonation resulting in HCN, is hindered by a large barrier of 1.44 eV, being the reaction endothermic by 0.55 eV. The other possible HCNH deprotonation, that one that gives CNH, has the largest activation energy of the group, 1.54 eV, and is close to thermoneutral, ΔE=0.10 eV. Finally, the two possible dehydrogenations of $HCNH_2$ are hindered by, 0.89 eV to HCNH, and 1.24 eV to CNH_2, barriers. Both are endothermic, by 0.09

UNIVERSITAT ROVIRA I VIRGILI
FIRST-PRINCIPLES MECHANISTIC STUDIES OF AMMONIA-RELATED INDUSTRIAL PROCESSES
Jaime Gómez Díaz
ISBN:978-84-694-1247-3/T-317-2011

and 0.36 eV respectively.

Table 4.4: Reaction energy, ΔE, activation energy for direct reaction, E_a and inverse reaction, E_a^{inv}. All energies in eV.

H_xCNH_y Dehydrogenation	ΔE	E_a	E_a^{inv}
HCN $\rightarrow$ H + CN	0.26	2.22	1.97
HCNH $\rightarrow$ HCN + H	0.55	1.44	0.89
HCNH $\rightarrow$ H + CNH	0.10	1.54	1.44
$HCNH_2$ $\rightarrow$ HCNH + H	0.09	0.89	0.80
$HCNH_2$ $\rightarrow$ H + CNH_2	0.36	1.24	0.88

4.3.5 Isomerizations

Several of the H_xCNH_y species can undergo isomerizations as indicated in Figure 4. In the present study, we have investigated two of these processes: CNH $\rightarrow$ HCN and HCNH $\rightarrow$ CNH_2.

CNH and HCN are known to interconvert in gas phase. Under this conditions the reaction is exothermic by -0.64 eV, and the barrier starting from CNH is 1.40 eV. When they are adsorbed on the surface, CNH is more stable than its isomer by 1.14 eV. Interconversion of the two isomers on the surface resembles that of the gas phase, see Figure 4.7, and the barrier in this case is 2.41 eV. That means that once CNH is formed, isomerization is not likely and thus interconversion to HCN through hydrogenation/dehydrogenation steps is favored. Similar effects have been described by Andersin *et al.* [67] for the conversion of ethylene derivatives on Pd.

HCNH can also undergo interconversion to CNH_2. This species has been described by Trenary and coworkers as a common intermediate under UHV conditions [148]. The barrier for this process is 0.92 eV, and the reaction is endothermic by 0.71 eV. When looking at the transition state for this conversion, Fig. 4.7, the structure resembles that of a dehydrogenation plus a rotation to the CNH_2 structure. Therefore, as in the previous case and for other chemical transformations, there is an active role of the surface as hydrogen acceptor and donor in the isomerization steps.

UNIVERSITAT ROVIRA I VIRGILI
FIRST-PRINCIPLES MECHANISTIC STUDIES OF AMMONIA-RELATED INDUSTRIAL PROCESSES
Jaime Gómez Díaz
ISBN:978-84-694-1247-3/T-317-2011

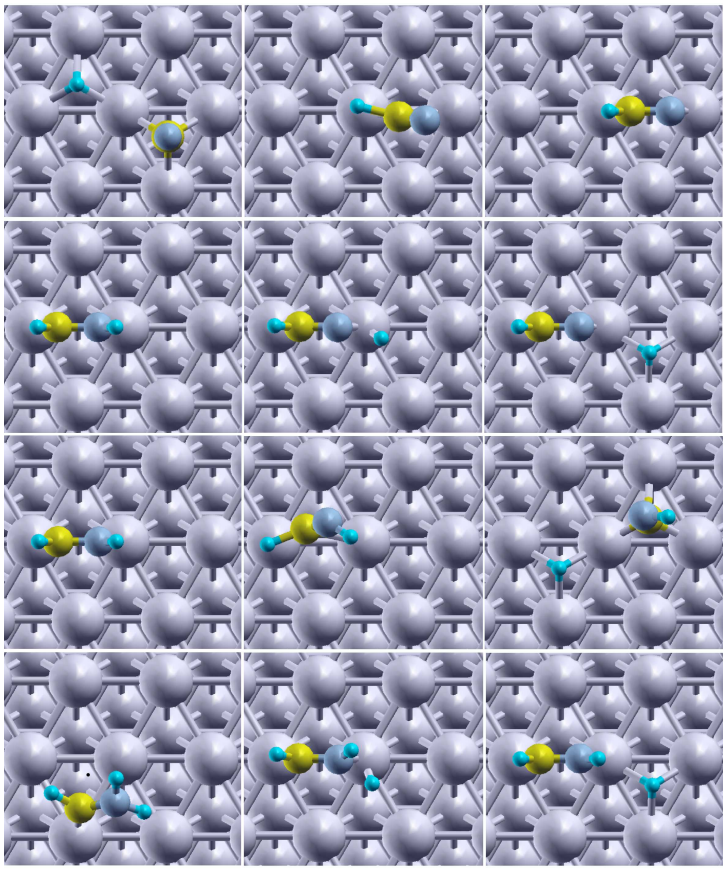

Figure 4.6: Schematic representations for dehydrogenation reactions. Initial (left), transition (center) and final (right) states for CNH → CN+H (top), HCNH (top-centre) and HCNH (top-bottom) and $HCNH_2$ (bottom). Same color code as in Figure 4.2.

Table 4.5: Reaction energy, ΔE, activation energy for direct reaction, E_a, and inverse reaction, E_a^{inv}, in eV.

Isomerizations	ΔE	E_a	E_a^{inv}
CNH → HCN	0.50	2.41	1.91
HCNH → CNH_2	0.71	0.92	0.21

UNIVERSITAT ROVIRA I VIRGILI
FIRST-PRINCIPLES MECHANISTIC STUDIES OF AMMONIA-RELATED INDUSTRIAL PROCESSES
Jaime Gómez Díaz
ISBN:978-84-694-1247-3/T-317-2011

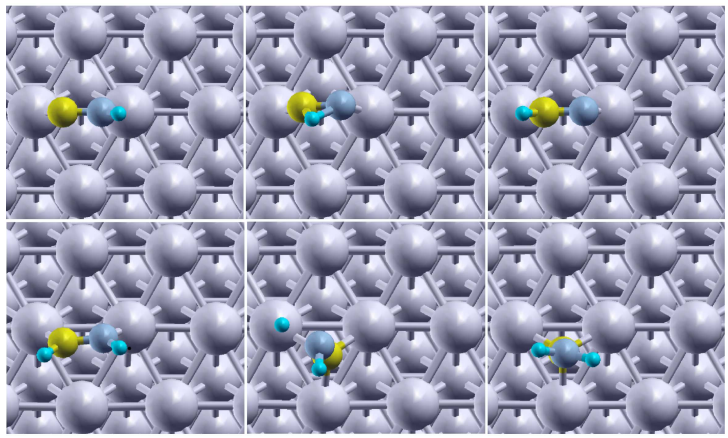

Figure 4.7: Schematic representations for isomerization reactions. Initial (left), transition (center) and final (right) states for CNH → HCN (top) and HCNH → CNH_2 (bottom). Same color code as in Figure 4.2.

4.3.6 Aerobic conditions

For Andrussow process (oxygen presence), the stability of the adsorbed species changes due to the presence of O atoms and OH groups adsorbed on the surface. Under these oxidative conditions, the relative contributions from different paths leading to HCN differ significantly from the non-oxidative conditions. To start with, the relative balance between different intermediates on the surface is perturbed by the presence of oxygen. We can see the relative stability for NH_3 related species in Figure 4.8 in presence of O atoms, OH groups and anaerobic conditions.

As we can see in Figure 4.8, adsorbed NH_3 is the most stable species for the anaerobic system. Under O presence, both NH_3 and NH are equally stable. Instead of this, at OH presence conditions, the most stable species is N coadsorbed with the hydroxyl group. The energy difference between NH_2+H and N+3H is 0.84 eV more favorable to NH_2 on anaerobic conditions, while N is 0.73 eV more stable in than NH_2 he presence of OH. Moreover, oxygen or hydroxyl-assisted dehydrogenations have much lower barriers and are more exothermic [87]. For NH_2 decomposition, O atoms lower the barrier from 1.30 to 0.55, see Table 4.6, and OH groups lower it

UNIVERSITAT ROVIRA I VIRGILI
FIRST-PRINCIPLES MECHANISTIC STUDIES OF AMMONIA-RELATED INDUSTRIAL PROCESSES
Jaime Gómez Díaz
ISBN:978-84-694-1247-3/T-317-2011

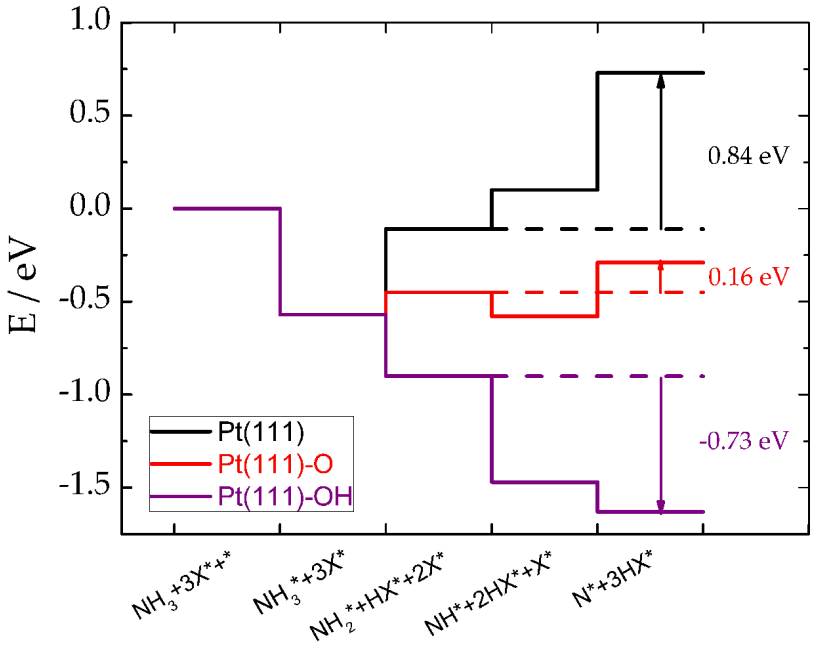

Figure 4.8: NH_3, NH_2, NH and N fragments stability on the clean and O or OH covered surfaces.

UNIVERSITAT ROVIRA I VIRGILI
FIRST-PRINCIPLES MECHANISTIC STUDIES OF AMMONIA-RELATED INDUSTRIAL PROCESSES
Jaime Gómez Díaz
ISBN:978-84-694-1247-3/T-317-2011

until 0.36 eV.

Table 4.6: Thermochemistry, ΔE, activation energies for: direct reaction, E_a and inverse reaction, E_a^{inv}, in eV, for the reactions described in Fig. 4. Non-assisted dehydrogenation included for comparison.

Dehydrogenations	ΔE	E_a	E_a^{inv}
$NH_2 \rightarrow NH + H$	0.19	1.30	1.11
$NH_2 + O \rightarrow NH + OH$	-0.03	0.55	1.53
$NH_2 + OH \rightarrow NH + H_2O$	-0.20	0.36	0.56

The influence of oxygen in methane fragments is shown in Fig. 4.9. For the clean and oxygen covered surfaces, the most stable species is CH. For the OH covered one, CH and C are almost equally stable. Furthermore, methane dehydrogenations are energetically much more favorable when oxygen is present on the surface.

Another very important effect produced by the presence of these groups is the reduction of H coverage, because the majority of dehydrogenations have been assisted by O or OH, resulting in OH or H_2O respectively. As well, hypothetical H atoms on the surface can react with H, O or OH.

4.3.7 Discussion

Once the elementary steps and the stability of fragments have been analyzed we consider the full reaction mechanism under anaerobic or aerobic conditions. We have summarized all the barriers all the C-N formation steps together with the C and N hydrogenation steps barriers, Fig. **??**. The figure shows a three-dimensional representation of Fig. 4, where *z axis* (columns height) is the activation energy for each coupling between species. We can see that the lowest barrier for coupling between CH_x and NH_x species is that for HC+NH_2. With these data and the analysis of the intermediates in Figs. 4.8-4.9 it is possible to analyze the reaction mechanisms under aerobic and anaerobic conditions and clarify some of the previous experiments reported in the literature.

For the BMA-Degussa (no oxygen) process, CH dehydrogenation leading to atomic C is the one with the largest barrier, followed by NH_x ones (all NH_3 dehydrogenations show very similar barriers). HC and NH_2 are

UNIVERSITAT ROVIRA I VIRGILI
FIRST-PRINCIPLES MECHANISTIC STUDIES OF AMMONIA-RELATED INDUSTRIAL PROCESSES
Jaime Gómez Díaz
ISBN:978-84-694-1247-3/T-317-2011

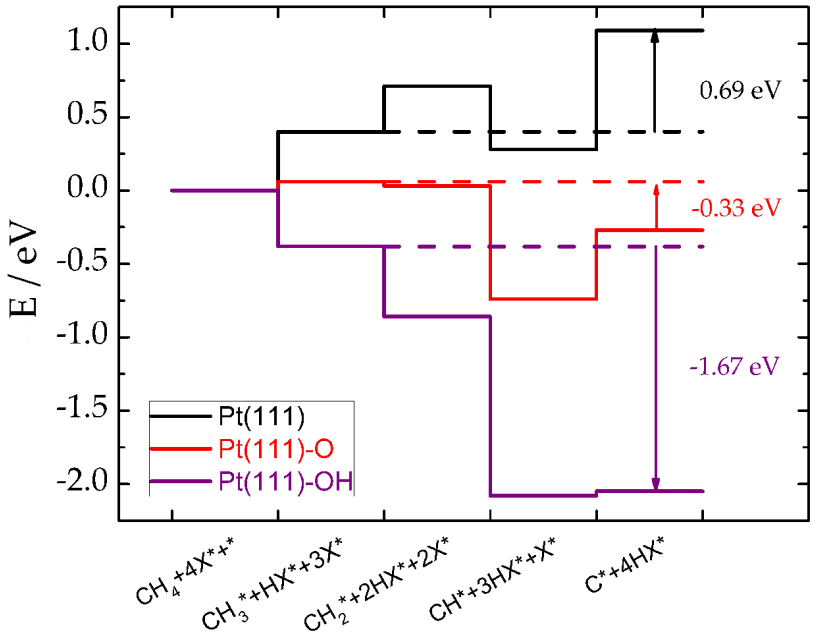

Figure 4.9: CH_3, CH_2, CH and C fragments stability on the clean and O or OH covered surfaces.

UNIVERSITAT ROVIRA I VIRGILI
FIRST-PRINCIPLES MECHANISTIC STUDIES OF AMMONIA-RELATED INDUSTRIAL PROCESSES
Jaime Gómez Díaz
ISBN:978-84-694-1247-3/T-317-2011

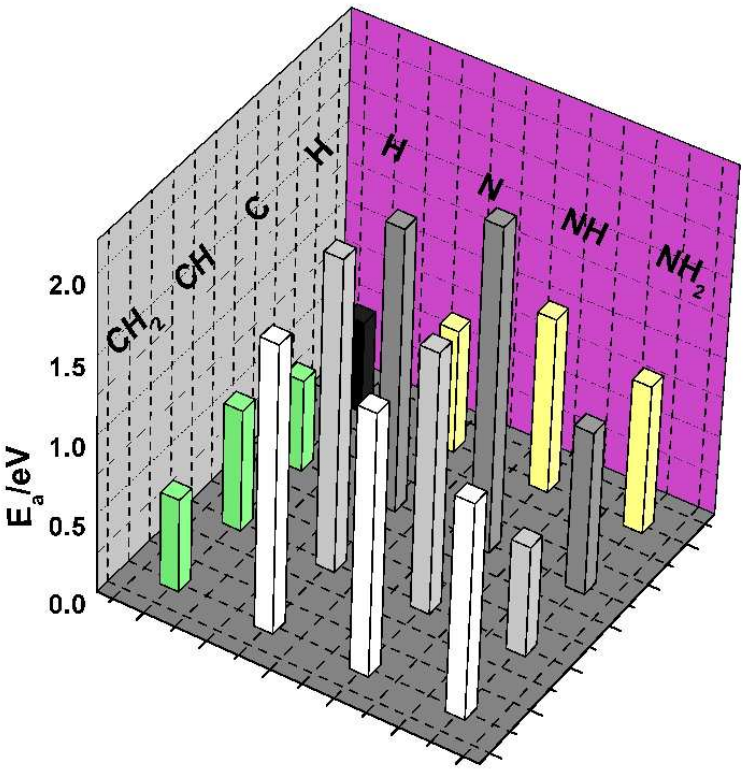

Figure 4.10: Three-dimensional representation of activation energies in the HCN formation path. The height of the column is the value for E_a for the reaction between the two species situated in both, CH_x and NH_x planes, crossing at this point of the graph.

UNIVERSITAT ROVIRA I VIRGILI
FIRST-PRINCIPLES MECHANISTIC STUDIES OF AMMONIA-RELATED INDUSTRIAL PROCESSES
Jaime Gómez Díaz
ISBN:978-84-694-1247-3/T-317-2011

the intermediates showing the largest total binding energies, see Figs. 4.8 and 4.9. The coupling of these species, HC+NH_2, is rather easy, the barrier is less than 1 eV, and thus is an effective way to generate the C-N bond under anaerobic conditions. From the resulting intermediate $HCNH_2$ dehydrogenation is likely, the first barrier being quite low, about 0.9 eV without considering the Zero-Point Energy vibrational contributions (that will reduce this value by about 0.2 eV). Therefore, the calculated barrier is very close to the experimentally determined, E_a=1.1-1.3 eV [148]. Thus, this set of reactions seems to be the leading route in the complex mechanism for HCN formation on Pt(111) under oxygen lean conditions. This is due both to the stability of HC and NH_2 fragments on the surface and the low barrier for C-N formation from these moieties. In the complete route, i.e. starting by methane and ammonia, the activation of methane is highly demanding due to the Eley-Rideal character of the process. It is very likely that this step is the responsible for the high temperatures required for the process.

Under aerobic (Andrussow) conditions, the abundance of the different species takes a relevant role. As a result of the already mentioned easy (low barriers) dehydrogenation of methane and ammonia, low presence of H and higher stability of dehydrogenated species are found. Thus, the most likely mechanism goes through low hydrogenated species coupling. The contribution from HC+N or direct C+N coupling to the formation of HCN should increase with respect to other parallel routes. Given that CN should need latter hydrogenation, HC+N coupling is revealed as the most likely. Therefore, under Andrussow conditions the recombination step to form the CN bond is likely the most energetically demanding in the process, as ammonia and methane decomposition are oxygen-assisted.

Experimental works

Regarding the previous experimental works, we can explain the different conclusions obtained with experiments at different conditions. These results showing different main C-N coupling steps depending on the reaction conditions conciliate previous experiments performed under very different environments.

In Schmidt group experiments, they proposed **C+N** and **HC+N**. The reactions were performed with [140, 144, 146] or without [138] O_2

UNIVERSITAT ROVIRA I VIRGILI
FIRST-PRINCIPLES MECHANISTIC STUDIES OF AMMONIA-RELATED INDUSTRIAL PROCESSES
Jaime Gómez Díaz
ISBN:978-84-694-1247-3/T-317-2011

and where compared to discuss the reaction mechanism. In view of the results presented in the present work, although the whole list of reactions included in the mechanisms is very similar their relative contributions to the rate are different. Experiments using gas-phase ions, as those performed by Schwarz's group [151], suffer from lack of the real ensembles that are present on the real catalyst. That makes difficult extrapolate these results to complex surfaces. Experiments performed by Trenary *et al.* with an high energy e^- beam might disturb the relative population of the different species, resulting in a starting point for the reaction different to that for the industrial process. As we have explained before, the relative weight of the different species is crucial to determine the path to generate the HCN.

In addition, we have seen how C+N coupling to generate CN is unlikely under Degussa conditions. However, when HCN is adsorbed at low temperatures and heated (TPD conditions [165]), H-C bond breaking is a possible process, and thus CN is a more common intermediate on the surface. The adsorption and formation of HCN shows hysteresis as the CN appears in HCN adsorption but it is unlikely in the HCN formation process. This complex behavior warns about the use of adsorption TPD studies of products when attempting to understand complex reaction networks as that described in the scheme shown in Fig. 4.

A final aspect that has been reported in the literature is the appearance of Brønsted-Evans-Polanyi relationships [60, 62] for the formation-dissociation of the CN group [158]. In Fig. 4.11 we present the correlations between the dissociation energy of all the intermediates containing CN groups and the corresponding reaction energies with respect to the final state position (i.e. dissociated moieties in neighboring sites). The figure clearly shows that H_xCNH_y dissociation follows two different regimes: the first corresponds to all the intermediates where y is either 0 or 1 and x=0,1 or 2; while the second groups all the barriers corresponding to y=2. The differences in this behavior can be assigned to the different structure of the H_xCNH_2 intermediates where the NH_2 fragments are not bound to the surface.

UNIVERSITAT ROVIRA I VIRGILI
FIRST-PRINCIPLES MECHANISTIC STUDIES OF AMMONIA-RELATED INDUSTRIAL PROCESSES
Jaime Gómez Díaz
ISBN:978-84-694-1247-3/T-317-2011

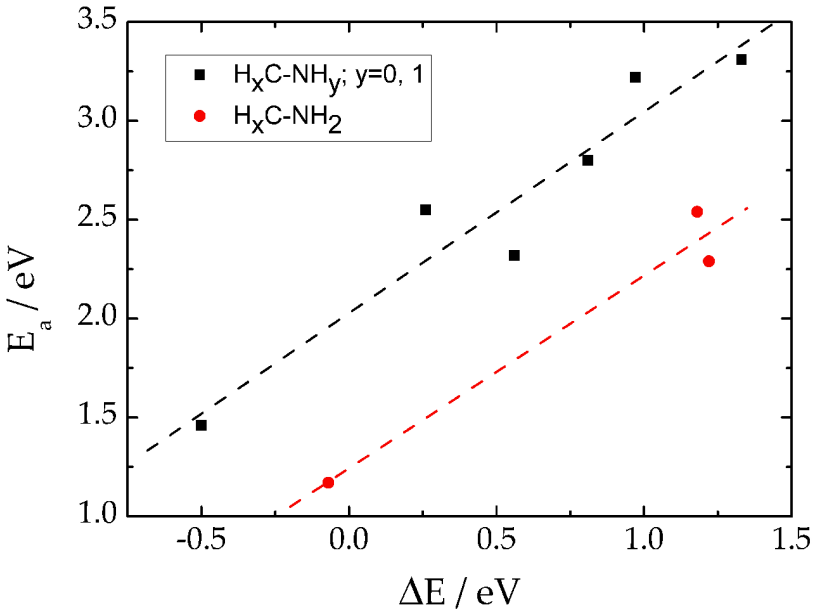

Figure 4.11: Brønsted-Evans-Polanyi relationships for the dissociation energy of $H_xC\text{-}NH_y$ intermediates, E_a *versus* energy reaction, ΔE. The corresponding linear fittings are:

UNIVERSITAT ROVIRA I VIRGILI
FIRST-PRINCIPLES MECHANISTIC STUDIES OF AMMONIA-RELATED INDUSTRIAL PROCESSES
Jaime Gómez Díaz
ISBN:978-84-694-1247-3/T-317-2011

4.4 Platinum conclusions

Under Degussa conditions, where the reactor is feed with ammonia and methane, we find the highest barriers in the dehydrogenation reactions. These reactions are necessary, because as we mention in Section 4.3.2, CH_4, CH_3 or NH_3 do not react easily. As well, CH + NH_2 coupling is the most favorable of all the C-N bond formation reactions. Product, $HCNH_2$, deprotonation is hindered by a low barrier and resulting HCNH has to lose one proton to obtain the final product HCN. The barrier for this latter step is the rate limiting step taken into account just the activation energies. The high working temperature of this process is mainly due to the endothermicity of the reaction and the difficulty to activate the reactants.

Working under Andrussow regime, the stability of the adsorbed fragments dramatically changes. As well, assisted dehydrogenations are favored. Hydrogenation reaction are then not likely, due to the small amount of H atoms, and CH+N appears as the most important path for HCN production. In this case, the large energy demand of the recombination step is the main reason for the high work temperature.

This computational study shows how the complex nature of reaction networks like the one presented here might be too difficult to tackle experimentally both by their nature and by the high temperatures and short times needed can benefit from detailed calculations. The deep analysis of the full reaction network can shed light on the different experimental results obtained under a wide variety of reaction conditions.

4.5 C-N coupling on transition metals

4.5.1 Species adsorption

In this section the adsorption of CN, HCN and CNH on the metal surfaces is going to be studied. CN shows small preference for adsorption on *fcc* sites for all the metals studied. The difference in energy with other sites is very small ($\sim$0.01-0.05).

These small differences poses difficulties in the accurate determination of the site of adsorption.

UNIVERSITAT ROVIRA I VIRGILI
FIRST-PRINCIPLES MECHANISTIC STUDIES OF AMMONIA-RELATED INDUSTRIAL PROCESSES
Jaime Gómez Díaz
ISBN:978-84-694-1247-3/T-317-2011

The adsorption energy of CN with respect to the radical is between -2.39 eV for Au and -3.65 eV for Rh. The most relevant data for species adsorption are shown in Table 4.7.

Table 4.7: Adsorption energies of C, N, CN, HCN and CNH with respect to CH_4, NH_3 and H_2 , in eV on the different metals.

Species	Au	Cu	Ir	Pd	Pt	Rh
C	4.86	4.42	2.19	2.03	2.14	2.01
N	4.06	2.84	1.17	1.37	1.65	0.92
CN	3.88	3.13	3.14	2.89	3.33	2.85
HCN	3.61	3.66	2.85	2.81	2.71	2.61
CNH	3.66	3.25	2.36	2.05	2.29	2.17

4.5.2 C+N coupling

Crawford and Hu determined [158] that the coupling of two species takes place through activation from the lowest free valences fragment towards the highest coordinated one (valence rule). In this case C has 4 free formal valences and N has 3 of them. Thus, the reaction takes place through N atom activation. At the initial configuration, both atoms are in neighbouring *fcc* positions, see Fig. 4.12. N is activated towards the *bridge* position and a subsequent rotation towards the perpendicular C-down CN configuration. The C-N distance at the transition state, as well as the most important kinetic data and the imaginary frequency associated to the transition state are shown in Table 4.8. The coupling is highly exothermic (<-4 eV) for Au and Cu, the metals where the lowest activation energies are found (0.99 and 0.39 eV respectively). The least exothermic couplings are found for Ir and Rh (ΔE$\approx$0.5 eV) and the largest barriers are those for Pt (1.79 eV) and Pd (1.64 eV). The rest of the metals have barriers around 1.5 eV. As shown by the C-N distances, Au and Cu have transition states geometrically "initial-like" and the other metals more "final-like".

4.5.3 H+CN coupling

The hydrogenation of CN generates the desired HCN product. The coupling starts with both H and CN on *fcc* sites. Hydrogen atom is activated

UNIVERSITAT ROVIRA I VIRGILI
FIRST-PRINCIPLES MECHANISTIC STUDIES OF AMMONIA-RELATED INDUSTRIAL PROCESSES
Jaime Gómez Díaz
ISBN:978-84-694-1247-3/T-317-2011

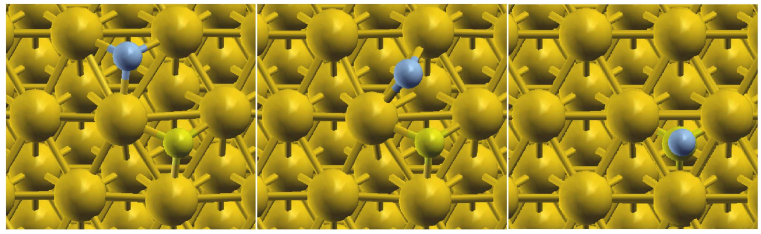

Figure 4.12: Schematic representations for C+N reaction on Au(111) surface. Initial (left), transition (centre) and final (right) states. Golden spheres represent Au, yellow ones C and blue ones N, atoms. The reaction on the rest of the metals proceeds similarly.

Table 4.8: Reaction energy, ΔE, and activation energy, E_a, in eV. C-N distance, d_{C-N} in Å, at the transition state and its associated imaginary frequency, ν in cm^{-1}, for C+N coupling in the different metals

Metal	ΔE	E_a	d_{C-N}	ν
Au	-4.39	0.99	2.343	310
Cu	-4.03	0.39	2.241	289
Ir	-0.45	1.51	1.990	452
Pd	-1.27	1.64	2.047	431
Pt	-0.97	1.79	2.005	449
Rh	-0.52	1.52	1.979	386

UNIVERSITAT ROVIRA I VIRGILI
FIRST-PRINCIPLES MECHANISTIC STUDIES OF AMMONIA-RELATED INDUSTRIAL PROCESSES
Jaime Gómez Díaz
ISBN:978-84-694-1247-3/T-317-2011

towards the *top* position, see Fig. 4.13, while CN starts tilting, and at the transition states the H-C distances range from 1.198 (Ir) to 1.802 (Au) Å. The reaction energy, the barriers, the H-CN distance and the transition state imaginary frequency for the set of metals is shown in Table 4.9. The formation of HCN through CN hydrogenation is exothermic in Au (0.6 eV) and Pt (0.3 eV), it is almost thermoneutral for Ir and Rh (-0.09 and 0.08 eV respectively) and it is endothermic for Pd (0.3 eV) and Cu (0.6 eV). The highest barrier is found in Cu (1.32 eV) and the lowest in Au (0.72 eV). All the other metals show barriers between 0.8-1.2 eV.

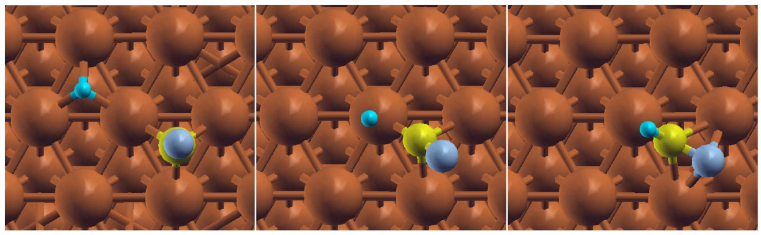

Figure 4.13: Schematic representations for H+CN reaction on Cu(111) surface. Initial (left), transition (centre) and final (right) states. Coppery spheres represent Cu, yellow ones C, blue ones N, and small turquoise ones H atoms. The reaction on the rest of the metals proceeds similarly.

Table 4.9: Reaction energy, ΔE, and activation energy, E_a, in eV. H-CN distance, d_{H-CN} in Å, at the transition state and its associated imaginary frequency, ν in cm^{-1}, for H+CN coupling in the different metals

Metal	ΔE	E_a	d_{H-C}	ν
Au	-0.59	0.72	1.802	728
Cu	0.59	1.32	1.553	1007
Ir	-0.09	0.95	1.198	524
Pd	0.28	1.15	1.534	773
Pt	-0.33	0.81	1.334	572
Rh	0.08	0.77	1.349	359

UNIVERSITAT ROVIRA I VIRGILI
FIRST-PRINCIPLES MECHANISTIC STUDIES OF AMMONIA-RELATED INDUSTRIAL PROCESSES
Jaime Gómez Díaz
ISBN:978-84-694-1247-3/T-317-2011

4.5.4 HC+N coupling

The coupling starts from both species on neighbouring *fcc* positions, see Fig. 4.14 showing reaction on Ir. In this reaction, both HC and N have the same number of free formal valences, three. Thus, both species are activated in accord with the previously mentioned rule. CH is activated towards a *top-bridge* and N to a *bridge*-like configuration. The resulting C-N distances at the transition state are between 1.877 (Rh) and 2.190 Å (Au). This coupling shows the smallest barrier for Cu (0.44 eV), followed by Au (1.11 eV). The barrier in Pd, Ir and Rh is very similar, between 1.5-1.6 eV, and Pt shows the largest barrier, 1.97 eV. The reaction is highly exothermic (ΔE=-2.4 eV) for Cu and Au, slightly exothermic (ΔE$\approx$-0.2) for Pt and Pd, sligthly endothermic for Rh (0.2 eV) and mildly endothermic for Ir (0.5 eV).

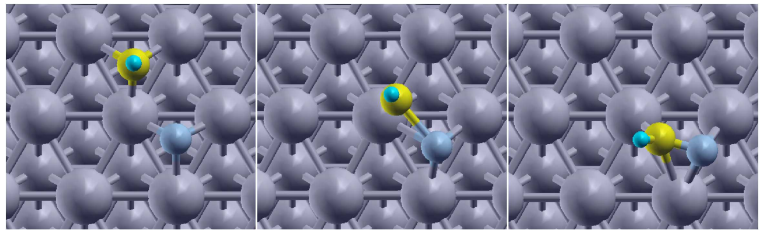

Figure 4.14: Schematic representations for HC+N reaction on Ir(111) surface. Initial (left), transition (centre) and final (right) states. Grey spheres represent Ir, yellow ones C, blue ones N and small turquoise H, atoms. The reaction on the rest of the metals proceeds equivalently.

4.5.5 C+NH coupling

The coupling starts from C and NH species on neighbouring *fcc* positions, see Fig. 4.15, Pt example. As predicted by the mentioned model, NH is activated towards the *bridge* position, and the final state corresponds to a CNH intermediate adsorbed with the CN almost perpendicular to the surface and where the H atom is tilted with respect to the CN axis. The reaction is hindered by a low barrier in Cu (0.5 eV). Au shows the following lowest barrier, 1.1 eV. All the other metals present much higher

UNIVERSITAT ROVIRA I VIRGILI
FIRST-PRINCIPLES MECHANISTIC STUDIES OF AMMONIA-RELATED INDUSTRIAL PROCESSES
Jaime Gómez Díaz
ISBN:978-84-694-1247-3/T-317-2011

Table 4.10: Reaction energy, ΔE, and activation energy, E_a, in eV. HC-N distance, d_{HC-N} in Å, at the transition state and its associated imaginary frequency, ν in cm^{-1} for HC+N coupling in the different metals

Metal	ΔE	E_a	d_{HC-N}	ν
Au	-3.07	1.11	2.190	454
Cu	-2.43	0.44	2.155	329
Ir	0.49	1.50	1.873	538
Pd	-0.23	1.46	1.925	620
Pt	-0.26	1.97	1.956	661
Rh	0.20	1.59	1.877	596

barriers, between 1.6-2.1 eV. The formation of CNH is exothermic for all the metals: highly (ΔE<-2.4 eV) in Cu and Au cases, mildly (1.3-1.4 eV) for Pd and Pt and weakly ($\sim$0.5 eV) for Ir and Rh. At the transition state, the distances between C and NH fragments are in the range of 2.026 (Ir) to 2.214 (Au). The final structure can be desorbed from the surface in the form of the CNH (hydrogen isocyanide) compound, however its desorption is in general quite energetically demanding, from 1.53 (Ir) to 1.84 (Pd) eV, except for Au and Cu (0.23 and 0.64 eV respectively). This is remarkable since the binding energy of the fragment to the surface makes it a more stable intermediate than the corresponding HCN structure, thus while HCN is the lowest isomer in the gas-phase when surfaces are present CNH is way more stable.

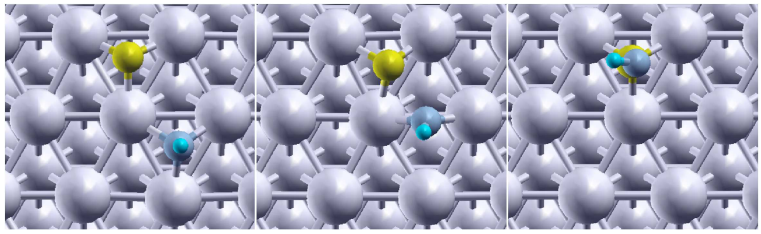

Figure 4.15: Schematic representations for C+NH reaction on Pd(111) surface. Initial (left), transition (centre) and final (right) states. Grey spheres represent Pd, yellow ones C, blue ones N and small turquoise ones H atoms. The reaction on the rest of the metals proceeds equivalently.

UNIVERSITAT ROVIRA I VIRGILI
FIRST-PRINCIPLES MECHANISTIC STUDIES OF AMMONIA-RELATED INDUSTRIAL PROCESSES
Jaime Gómez Díaz
ISBN:978-84-694-1247-3/T-317-2011

Table 4.11: Reaction energy, ΔE, and activation energy, E_a, in eV. C-NH distance, d_{C-NH} in Å, at the transition state and its associated imaginary frequency, ν in cm^{-1}, for C+NH coupling in the different metals

Metal	ΔE	E_a	d	ν
Au	-3.16	1.05	2.214	366
Cu	-2.49	0.45	2.179	356
Ir	-0.49	1.65	2.026	457
Pd	-1.39	1.61	2.101	492
Pt	-1.33	2.05	2.050	568
Rh	-0.50	1.65	2.078	493

4.5.6 CNH-HCN isomerization

The initial, transition and final states for the isomerization path are described in Fig. 4.16 for Rh. Starting by CNH, the isomerization implies a H shift from N to C plus a rotation to reach the most stable adsorption site of HCN on the surface. Isomerizations of this kind have been found to be difficult for ethylene derived moieties on Pd [67], even in several cases a sequential mechanism involving the loss of a H atom and the recombination have been proposed as more likely paths to obtain isomers. The reaction present barriers >2.0 eV for all metals except Cu (E_a ~1.8 eV). The reaction is exothermic in Au (1.2 eV) and Pt (0.3 eV), but endothermic for the other metals (0.2-0.8 eV).

Table 4.12: Reaction energy, ΔE, and activation energy, E_a, in eV. CNH angle, α_{CNH} in degrees, at the transition state and its associated imaginary frequency, ν in cm^{-1} for CNH-HCN isomerization on the different metals.

Metal	ΔE	E_a	d_{C-N}	α_{CNH}
Au	-1.21	2.05	128	1332
Cu	0.40	1.82	127	1342
Ir	0.49	2.25	121	1244
Pd	0.75	2.19	135	1158
Pt	-0.26	2.41	123	1449
Rh	0.20	2.25	126	363

UNIVERSITAT ROVIRA I VIRGILI
FIRST-PRINCIPLES MECHANISTIC STUDIES OF AMMONIA-RELATED INDUSTRIAL PROCESSES
Jaime Gómez Díaz
ISBN:978-84-694-1247-3/T-317-2011

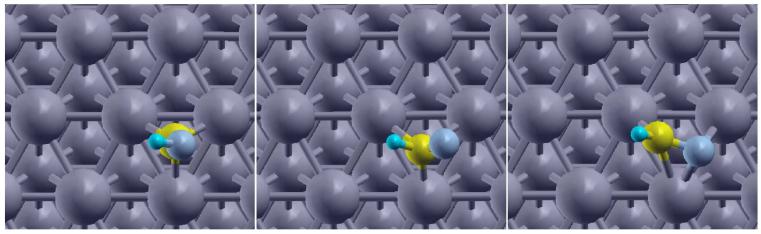

Figure 4.16: Schematic representations for CNH-HCN isomerization on Rh(111) surface. Initial (left), transition (centre) and final (right) states. Dark grey spheres represent Rh, yellow ones C, blue ones N and small turquoise H atoms. The reaction on the rest of the metals proceeds equivalently.

4.5.7 Linear scaling relationships

In this section, dissociation and adsorption energies have been correlated with respect to C and N atoms adsorption energy for all the relevant structures.

H_xCN_y adsorption-C adsorption energy relationship

Let us start with the correlation of the adsorption energy of the different adsorbates. As mentioned in Section 2.11, dependence of the adsorption energy of CH_x and NH_y fragments on the adsorption energy of the central (C or N) atom have been observed previously [64]. Moreover, we show a similar correlation for CN, CNH and HCN adsorption ($E_{H_xCNH_y}$), which correlates with C atom adsorption (E_C), see Fig. 4.17.

The equations that represent the linear regressions are the following:

$$\begin{aligned} E_{CN} &= 0.21 \pm 0.10 E_C + 2.59 \pm 0.31;\ r = 0.73 \\ E_{CNH} &= 0.49 \pm 0.04 E_C + 1.18 \pm 0.12;\ r = 0.99 \\ E_{HCN} &= 0.35 \pm 0.04 E_C + 2.03 \pm 0.12;\ r = 0.98 \end{aligned}$$

where we can observe that the worst correlation is found in CN adsorption. This is mainly due to the different behavior of Cu and Au, the most noble of the set of metals, with respect to the resting metals. We are going to analyse now the slopes of the equations in connection with

UNIVERSITAT ROVIRA I VIRGILI
FIRST-PRINCIPLES MECHANISTIC STUDIES OF AMMONIA-RELATED INDUSTRIAL PROCESSES
Jaime Gómez Díaz
ISBN:978-84-694-1247-3/T-317-2011

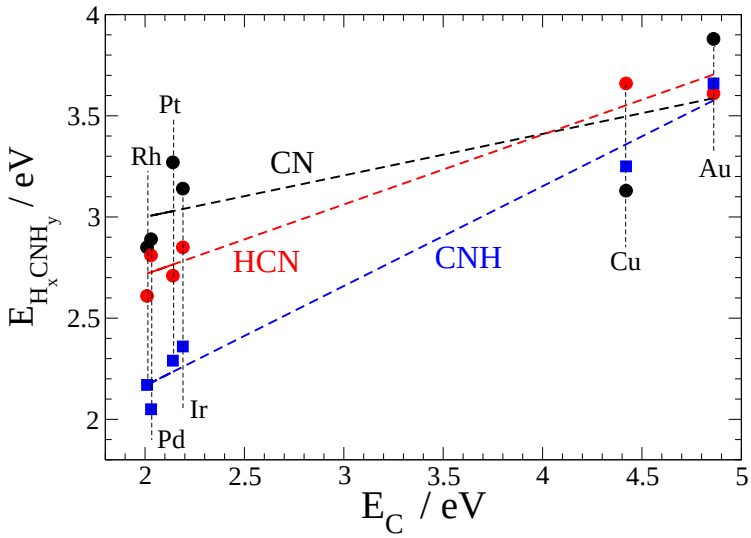

Figure 4.17: Linear scaling relationship for CN, CNH and HCN adsorption energy, $E_{H_xCNH_y}$, as a function of C adsorption energy, E_C on the different metals. All energies in eV.

UNIVERSITAT ROVIRA I VIRGILI
FIRST-PRINCIPLES MECHANISTIC STUDIES OF AMMONIA-RELATED INDUSTRIAL PROCESSES
Jaime Gómez Díaz
ISBN:978-84-694-1247-3/T-317-2011

the number of electrons bonding with the surface. CNH has a slope close to 0.5, and according to its Lewis structure it has the $2e^-$ corresponding to its lone pair available for bonding. When moving to CN radical we find $1e^-$ directly available for the bond in its Lewis structure. This would corresponds with a slope around 0.25 if the dependence is similar to that for CNH. The slope found, 0.21, agrees well with that. For HCN is more difficult as both C and N are bonded to the surface. The 0.35 slope found indicates that the number of e^- that are bonding is between that for CNH ($2e^-$) and that for CN ($1e^-$). This bond is made at expenses of weakening the C≡N bond, as reflect the lengthening of the bond from 1.16 Å in gas phase HCN to 1.20 (Au) to 1.32 (Ir) Å in adsorbed ones.

Dissociation energy-N adsorption energy relationship

The dissociation energy of C-N, HC-N and C-NH reactions ($E_{a,\,diss}$) have been correlated with the adsorption energy of N atom (E_N), see Fig. 4.18. The choice of dissociation energies produces better correlations than coupling ones due to the generally "final-like" character of the coupling reactions. The dissociation energy of H-CN reaction has been as well included for comparison.

The equations that describe the linear regressions are the following:

$$\begin{aligned} E_a^{C-N} &= 1.11 \pm 0.11 E_N + 1.02 \pm 0.25;\ r = 0.98 \\ E_a^{HC-N} &= 0.93 \pm 0.11 E_N + 0.37 \pm 0.25;\ r = 0.97 \\ E_a^{C-NH} &= 0.54 \pm 0.18 E_N + 1.89 \pm 0.41;\ r = 0.83 \end{aligned}$$

Following the reasoning in Ref. [63], the correlation should correspond with the adsorption energy of the activated fragment. This is indeed the case for C-N reaction, where N is the activated species, and for C-NH and CH-N, where both species are activated. For H-CN reaction we find and almost constant dissociation energy, not depending on N adsorption energy. The main factor here is the strength of the H-CN bond.

Besides this, the slope of the equations S seems to correlate with the free formal valences of the NH_x species involved in the reaction V_X:

UNIVERSITAT ROVIRA I VIRGILI
FIRST-PRINCIPLES MECHANISTIC STUDIES OF AMMONIA-RELATED INDUSTRIAL PROCESSES
Jaime Gómez Díaz
ISBN:978-84-694-1247-3/T-317-2011

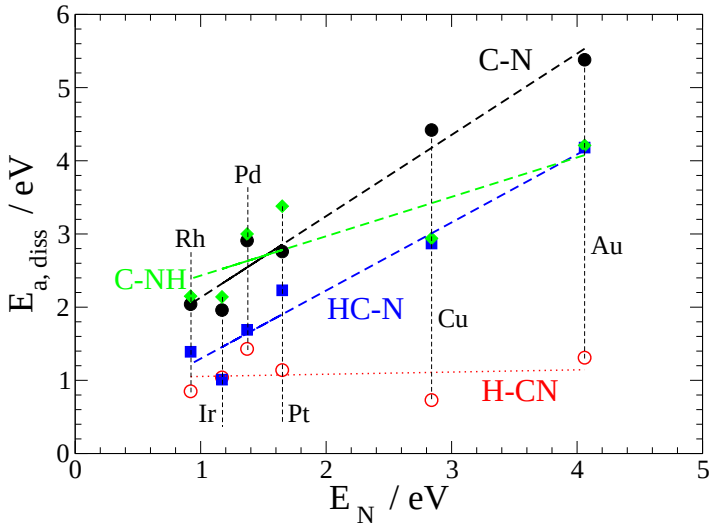

Figure 4.18: Linear scaling relationship for C-N, C-NH and HC-N dissociation barriers, $E_{a,\,diss}$ in eV, as a function of N adsorption energy, E_N on the different metals. H-CN deprotonation is as well included.

$$\begin{aligned} \text{C-N coupling:} \quad & V_N = 3;\ S/V_N = 1.11/3 = 0.37 \\ \text{HC-N coupling:} \quad & V_N = 3;\ S/V_N = 0.930/3 = 0.31 \\ \text{C-NH coupling:} \quad & V_N = 2;\ S/V_N = 0.538/2 = 0.27 \end{aligned}$$

Thus, the slope of linear regression that fits $E_{a,\,diss}$ with E_N for the different metals can be estimated as $S = 0.32 \cdot V_N$. That means that the more valences does the NH_x activated fragment has, the more dependent with the adsorption energy of N is the dissociation energy. This can be understood in terms of the numbers of bonds that link the fragment to the surface.

4.5.8 Conclusions

DFT models have been employed to study Andrussow and Degussa processes, HCN formation, under oxidative and non-oxidative conditions, re-

UNIVERSITAT ROVIRA I VIRGILI
FIRST-PRINCIPLES MECHANISTIC STUDIES OF AMMONIA-RELATED INDUSTRIAL PROCESSES
Jaime Gómez Díaz
ISBN:978-84-694-1247-3/T-317-2011

spectively.

Platinum surface

-In the Degussa (non-oxidative) process HCN formation mainly comes from the coupling of the most likely methane and ammonia intermediates, CH + NH_2 coupling, with the subsequent elimination of H atoms. HCNH deprotonation shows the largest barrier in this recombination channel, our estimate for the activation energy of this step agrees with the experimental value determined in the group of Prof. Trenary. The high energy demand of the Degussa process comes from reactant activation: Eley-Rideal methane activation and also ammonia dehydrogenation on the surface.

-Under Andrussow (oxidative) conditions: the presence of oxygen changes the stability of the adsorbed fragments, and thus their populations. CH+N and C+N appear as the most important paths for C-N bond production. The high energy requirements needed for these recombination processes are the responsible for the high temperatures needed for the process in this case.

Transition metals

-Low barriers are found for couplings on Au and Cu due to their weak adsorption energy. C+N reaction is the less energetically demanding way to form C-N bond on Au, Cu, Pt and Rh; and CN hydrogenation does not show high barriers. On Ir and Pd, C-N bond is more likely formed via HC+N recombination.

-Linear-scaling relationships are found for the adsorption energy of CN, HCN and CNH species with respect to the atomic C adsorption energy for all the metals considered.

-Linear-scaling relationships are found for dissociation energy of CN-containing compounds with respect to N atom adsorption energy. This paves the way for a rapid evaluation of these kinetic parameters for other materials.

UNIVERSITAT ROVIRA I VIRGILI
FIRST-PRINCIPLES MECHANISTIC STUDIES OF AMMONIA-RELATED INDUSTRIAL PROCESSES
Jaime Gómez Díaz
ISBN:978-84-694-1247-3/T-317-2011

UNIVERSITAT ROVIRA I VIRGILI
FIRST-PRINCIPLES MECHANISTIC STUDIES OF AMMONIA-RELATED INDUSTRIAL PROCESSES
Jaime Gómez Díaz
ISBN:978-84-694-1247-3/T-317-2011

Chapter 5

Gold ore cleaning

The present chapter tries to shed light into the fundamental mechanisms that control gold cyanidation. Density Functional Theory (DFT) has been applied to study the adsorption of CN, CN^-, KCN and multiple CN; on Au(111) and Au(211) surfaces and compare them to the well-understood Au-CO interaction. From this work, the aim is to understand the crucial steps in gold extraction and electrodeposition.

The chapter is organized as follows: first, previous works on the field are reviewed. Second, computational details are introduced, and after that, CO, CN, CN^-, KCN, and multiple CN adsorption on both surfaces are discussed. Next, the electronic structure by means of Local Density of States (LDOS) and Electron Localization Function (ELF) analysis for various systems are presented. Finally, the results are discussed and the conclusions are risen.

5.1 Previous works

Many experimental studies have been performed on gold extraction from ores *via* the MacArthur-Forrest process, mainly in the field of metallurgy [166, 167, 168]. Otherwise, several alternatives to this process have been proposed, as those using thiourea, thiosulphate or thiocyanate [169]. Even processes involving biological systems, as bacteria, have been developed [170].

The mechanism that drives gold cyanidation has been studied by means

UNIVERSITAT ROVIRA I VIRGILI
FIRST-PRINCIPLES MECHANISTIC STUDIES OF AMMONIA-RELATED INDUSTRIAL PROCESSES
Jaime Gómez Díaz
ISBN:978-84-694-1247-3/T-317-2011

of different techniques.

-Dissolution experiments: Recent experiments under corrosion conditions with Sum Frequency Generation (SFG) techniques [171, 172] conclude that a single adsorption site for CN^- is found on different orientation electrodes. In a similar experiment, Cimatu and Baldelli were able to identify several $Au(CN)_n$ (n=1,2,4) compounds depending both on the concentration of the cyanide solution and the position of gold atoms (surface or edge sites) [173]. An electrochemical quartz crystal microbalance experiment, shows that pure gold and ultrapure cyanide solution do not imply metal dilution [174]. They proposed that a film of AuCN is covering the surface, avoiding dissolution. In a experiment of the same kind, the same group found that Au/Ag alloy shows a leach rate substantially higher than that of pure gold [175].

-Electrodeposition experiments: Several detailed Scanning Tunneling Microscopy (STM) experiments on the electrochemical deposition of gold cyanides exist in the literature [176, 177]. In these experiments, ordered gold cyanide adlayers were investigated and, for instance, the higher mobility of Au atoms in the presence of cyanide solutions was reported [176]. Surface Enhanced Raman Spectroscopy (SERS) [178], SERS combined with SFG [171] and SFG combined with Difference Frequency Generation, DFG, [172] experiments, were carried out by Bozzini and co-workers, concluding that several mechanism can yield to gold deposition. A SERS (combined with DFT) work [179], studied the Au-CN interaction and the consequences of the electric field in the vibrational frequency. They assign the 2100 cm^{-1} mode to the stretch vibration on *top* position on Au(100) and Au(110) surfaces.

-Theoretical studies: In spite of the relevance of this process and both, practical and scientific interest, not many theoretical studies on the cyano group interaction with Au surfaces have been presented. Tadjeddine and Flament, through multiconfigurational self-consistent field (MCSCF) and DFT cluster calculations [180], tried to reproduce IR and Raman Au-CN^- properties. They found the bond as covalent and pointed out the dramatic effect of the level of calculation in the results. A previously mentioned SERS and DFT work [179] is focused on the analysis of the Au-CN bond, that they claimed to be ionic based on the dipole moments and charges found. Due to the low binding energy found on Au(111)

UNIVERSITAT ROVIRA I VIRGILI
FIRST-PRINCIPLES MECHANISTIC STUDIES OF AMMONIA-RELATED INDUSTRIAL PROCESSES
Jaime Gómez Díaz
ISBN:978-84-694-1247-3/T-317-2011

Table 5.1: Comparison between electrodeposition and dissolution processes for gold.

	Electrodeposition	**Dissolution**
Species	Gold in solution	Metallic Gold
Reaction	Au(I) reduction	Au(0) oxidation
Redox pair	Current	Oxygen reduction

surface, they exclude this surface to react. Whereas, several studies can be found for other metals, in particular Pt [161, 179, 181, 182]. CN^- is isoelectronic with CO, and the interaction of the latter with Au surfaces has been extensively studied in literature [97, 98].

The widely accepted diffusion-adsorption-oxidation model takes place through the following reactions:

- CN^- diffusion from the solution to the gold interface:

$$CN^-(sol) \rightarrow CN^-(int) \tag{5.1}$$

- CN^- adsorption on the gold surface:

$$CN^-(int) \rightarrow AuCN^-(ads) \tag{5.2}$$

- Electron transfer:

$$AuCN^-(ads) \rightarrow AuCN(ads) + e^- \tag{5.3}$$

- Second CN^- adsorption on gold:

$$AuCN(ads) + CN^- \rightarrow [Au(CN)_2]^-(ads) \tag{5.4}$$

- Elimination of the soluble compound:

$$[Au(CN)_2]^-(ads) \rightarrow [Au(CN)_2]^-(sol) \tag{5.5}$$

UNIVERSITAT ROVIRA I VIRGILI
FIRST-PRINCIPLES MECHANISTIC STUDIES OF AMMONIA-RELATED INDUSTRIAL PROCESSES
Jaime Gómez Díaz
ISBN:978-84-694-1247-3/T-317-2011

This first set of reactions corresponds to the anodic reactions. In addition, the reactions inverse to those in Eqs. 5.1-5.5 were proposed by Harrison and Thompson [183] to describe Au electrodeposition from $[Au(CN)_2]^-$ solutions, and employed by Eisenmann [184] in the kinetic analysis of the deposition process. The reduction reactions take place on the gold surface (in solution processes) or on the cathode (in electrodeposition processes). This oxygen reduction can be expressed in two equations (not elementary steps) involving $2e^-$ transfer each one.

- First (two-electron) oxygen reduction:

$$O_2 + H_2O + 2e^- \rightarrow HO_2^- + OH^- \tag{5.6}$$

- Second (two-electron) oxygen reduction:

$$HO_2^- + H_2O + 2e^- \rightarrow 3OH^- \tag{5.7}$$

All those equations can be summarized in the following global reaction:

$$4Au + 8CN^- + O_2 + 2H_2O \leftrightarrow 4[Au(CN)_2]^- + 4OH^- \tag{5.8}$$

Refractory ores (those containing interfering elements or minerals) result in a reduction of the metal recovery. For such ores, direct cyanidation cannot be used. As well, sulfide ores must be converted into oxidized form, typically by roasting under pressure oxidation, before gold can be efficiently extracted by conventional methods. Also it is well known that extraction is favored for small grains. Recovery techniques are designed to meet the specific extraction requirements for the ore [14]. This chapter focuses on the anodic reactions, present in both solution and electrodeposition processes. The cathodic reactions will not be considered, due to the complexity of including oxygen and water species.

5.2 Computational details

All the calculations were performed with DFT solved with GPAW package [39, 40] applied to slabs representing Au(111) and Au(211) surfaces. The exchange-correlation functional used is RPBE [33], and the core electrons

UNIVERSITAT ROVIRA I VIRGILI
FIRST-PRINCIPLES MECHANISTIC STUDIES OF AMMONIA-RELATED INDUSTRIAL PROCESSES
Jaime Gómez Díaz
ISBN:978-84-694-1247-3/T-317-2011

have been described with PAW pseudopotentials [36]. The grid spacing was set to 0.2 Å in all surface calculations and the Brillouin zone was sampled with (3x3x1) Monkhorst-Pack k-points [41].

For neutral systems periodic boundary conditions were applied only in the xy plane, whereas for systems with added charge the periodic boundary conditions were applied in all directions. A vacuum space of 13 Å was set. In the non-periodic cases, 5 Å of were below and 8 Å above the slab. The experimental lattice constant, 4.080 Å, was applied throughout the calculations. The regular Au(111) surface was modeled by a three-layer slab and a p(3x4) orthorhombic supercell. The atoms in the bottom layer were fixed to their bulk positions while all the other atoms were relaxed (until the residual force was below 0.05 eV/Å). The Au(211) slab has twelve layers, where the lowest six were fixed to the ideal positions. Fragments were adsorbed only on one side of the slab. Molecules were calculated in a non cubic cell at Γ-point with 0.1 Å grid spacing, and spin unrestricted when necessary.

Since the amount of charge at the interface might be crucial to the formation of $[Au(CN)_2]^-$, several calculations involving one of the possible salts (KCN) in the cyanidation process or calculations with a charged system where an artificial charge was added to obtain CN^- as the interacting fragment, were conducted. In the latter case, a compensating background was introduced, to obtain a system where the total charge in the supercell is zero [185, 186].

The charge analysis of adsorbates and Au atoms with the Bader approach [50] were carried out. Finally, the projected Local Density Of States (LDOS) and Electron Localization Function (ELF) [54] analysis to describe the bond type between the ligand and the surface were employed.

5.3 Results

In this section the interaction of CO and CN species, on Au(111) and Au(211) surfaces, are compared. In order to make this comparison, the adsorption of: CO molecule, radical CN, KCN coadsorption, ionic CN^- and coadsorption of two cyano groups are studied. The most important of these structures are shown in Fig. 5.1. The adsorption energies and the most important geometrical aspects, are summarized in Table 5.2.

UNIVERSITAT ROVIRA I VIRGILI
FIRST-PRINCIPLES MECHANISTIC STUDIES OF AMMONIA-RELATED INDUSTRIAL PROCESSES
Jaime Gómez Díaz
ISBN:978-84-694-1247-3/T-317-2011

Bader analysis charges are shown in Table 5.3 and electronic properties are compiled in Table 5.4.

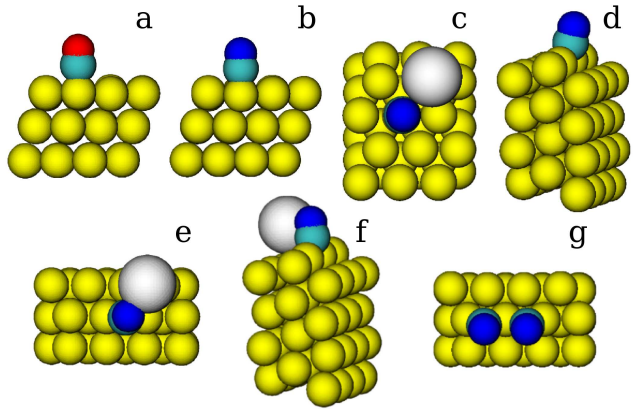

Figure 5.1: Schematic representation of adsorption: (a) CO adsorbed *on-top* Au(111) position, (b) CN *on-top* Au(111), (c) KCN on Au(111), (d) CN on *bridge* position on Au(211) (a) and (b) KCN on Au(211) and (b) multiple adsorption at the step Au(211)-2(CN) structure. Yellow spheres represent Au atoms, white K, turquoise C, blue N and red O.

5.3.1 CO Adsorption

CO adsorption on Au(111) is found to be very weak, as previously reported [82, 97, 98]. Our calculations retrieve a slightly endothermic value for *on-top* adsorption on the flat surface, ΔE=0.11 eV. The Bader analysis for adsorbed CO shows neutral charge (0.0 $|e^-|$), and the gold atom bonded to it, a positive charge of 0.1 $|e^-|$.

If we separate the charges of C and O atoms, we find charges of 1.0 and -1.0 $|e^-|$ respectively, values quite similar to those found for gas phase CO, 1.1 and -1.1 $|e^-|$. Thus, according to this, the bond seems to be strongly ionic. On the other hand, experimental CO molecular dipole is quite small, 0.112 D [187]. If we compare it with KBr, a true ionic species, that has a molecular dipole moment p=10.63 D [188] we find a clear disagreement. This problem was noticed previously [189]. It is known that, although the total electron density is a quantum-mechanical observable, atomic charges

UNIVERSITAT ROVIRA I VIRGILI
FIRST-PRINCIPLES MECHANISTIC STUDIES OF AMMONIA-RELATED INDUSTRIAL PROCESSES
Jaime Gómez Díaz
ISBN:978-84-694-1247-3/T-317-2011

Table 5.2: Adsorption *site* (t≡*top*, f≡*fcc*, b≡*bridge*, h≡*four fold hollow*), adsorption energy, E_{ads}, in eV, on Au(111) and Au(211) surfaces, relaxation of bonded gold atom from its original position, δdAu, and Au-heteroatom distance, d_{Au-X} , in Å. E_{ads} have been obtained as E_{ads}=E_{Au-X}-$N_X E_X$-E_{Au} for X=CO and CN and N_X the number of adsorbed X species. For CN^- adsorption a Born-Haber cycle was employed, see text for details.

	site	E^X_{ads}	δd_{Au}	d_{Au-X}
Au(111)				
CO	t	0.11	0.022	2.118
CN	t	-2.46	-0.161	2.045
CN^-	t	-4.18	-0.154	2.050
K	f	-2.48	-0.181	3.388
2K	f+t	-4.44	-0.199	3.080
3K	f+t+t	-5.80	-0.203	3.090
KCN	t[1]	-1.44	0.087	2.072
Au(211)				
CO	b	-0.37	0.195	2.160
CO	t	-0.33	0.260	2.040
CN	b	-2.93	0.201	2.181
CN	t	-2.87	0.178	2.023
CN^-	t	-4.36	0.172	2.035
CN^-	b	-4.31	0.197	2.189
K	h[2]	-2.58	0.197	3.611
KCN	b[3]	-1.76	0.324	2.160
KCN	b[4]	-1.81	0.194	2.208
2(CN)	b+b	-5.44	0.320	2.111
2(CN)	b+h	-4.72	0.370	2.036, 2.159
CN+$(CN)^-$	b+b	-6.94	0.301	2.118, 2.307
CN+$(CN)^-$	b+h	-6.24	0.369	2.047, 2.158
$[Au(CN)_2]^-$ (gp)	–	–	–	2.030

[1,3]K on upper terrace
[2,4]K on *four fold hollow*

UNIVERSITAT ROVIRA I VIRGILI
FIRST-PRINCIPLES MECHANISTIC STUDIES OF AMMONIA-RELATED INDUSTRIAL PROCESSES
Jaime Gómez Díaz
ISBN:978-84-694-1247-3/T-317-2011

Table 5.3: Bader charges for C, N, O, K and Au atoms for the most relevant structures on Au(111) and Au(211) surfaces in $|e^-|$. Au atoms are those bonded to the fragment.

	q(C or K)	q(N or O)	q_{total}(CN)	q(Au)
CN (gp)	+1.0	-1.0	0.0	–
Au111-CN	+0.7	-0.9	-0.2	+0.1(6)
Au211-CN (top)	+0.6	-0.9	-0.3	+0.1(3)
CN^- (gp)	+0.5	-1.5	-1.0	–
Au111-CN^-	+0.7	-1.2	-0.5	+0.1(3)
Au211-CN^- (top)	+0.7	-1.2	-0.5	+0.1(4)
CO (gp)	+1.1	-1.1	0.0	–
Au111-CO	+1.0	-1.0	0.0	+0.1(3)
Au211-CO (top)	+1.0	-1.0	0.0	+0.1(2)
Au111-K	+0.9	–	–	-0.1(4)
Au111-2K	+0.8	–	–	-0.1(5)
Au111-3K	+0.8	–	–	-0.2(6)
Au211-K	+0.9	–	–	-0.2(0)
Au111-KCN	+0.7	-1.2	-0.5	+0.1(3)
Au111-KCN-	+0.7	-1.3	-0.5	+0.1(2)
Au211-KCN (brid)	+0.6	-1.2	-0.6	+0.1(0)
Au211-$(CN)_2{}^-$	+0.7	-1.1	-0.4	+0.2(1)
$[Au(CN)_2]^-$ (gp)	+0.7	-1.3	-0.5	+0.2(1)

UNIVERSITAT ROVIRA I VIRGILI
FIRST-PRINCIPLES MECHANISTIC STUDIES OF AMMONIA-RELATED INDUSTRIAL PROCESSES
Jaime Gómez Díaz
ISBN:978-84-694-1247-3/T-317-2011

are not, as how the electron density is apportioned to atoms is arbitrary [190], in this case, through zero-flux surfaces.

On the stepped Au(211) surface, the adsorption is slightly more exothermic, E_{ads}=-0.33 eV, and the preferential site is *on-top* of the edge. The charge distribution is almost the same than in the flat surface, even for Au, in agreement with previous studies that have shown the large effect of Au coordination on the chemistry of gold [82, 98].

5.3.2 CN Adsorption

The CN radical adsorbs in an *on-top* position on the Au(111) surface. Adsorption energies have been calculated with respect to several references. Adsorption is clearly exothermic with respect to the radical, but it is endothermic with respect to both HCN (E_{ads}=0.74 eV) and C_2N_2 (E_{ads}=0.54 eV). In any case, adsorption is strongly reinforced by the presence of steps, similarly to what happens for CO. At steps, CN adsorption is endothermic with respect to HCN (E_{ads}=0.27 eV) and almost thermoneutral with respect to C_2N_2, but clearly exothermic with respect to the radical, E_{ads}= -2.93 eV. Regarding the electronic distribution, upon CN adsorption on Au(111) the fragment is polarized, with an excess negative charge of 0.2 e^-. Koper and coworkers [179] identified a total charge of 0.31 e^- for the adsorbed CN radical, employing a cluster model containing ten atoms using B3LYP functional and the Mulliken partition analysis for charge transfer.

5.3.3 CN^- Adsorption

Next, I consider adsorption of CN^- anion, which is isoelectronic to the already discussed CO molecule. First of all, the electronic properties of the Au surface (Table 5.4) and CN radical are calculated. The calculated electron affinity of a CN radical is 3.63 eV, which compares well with the experimental value: 3.82±0.02 eV [191]. The experimental value for Au work function is 5.2 eV [192], that is only slightly larger than our calculated value 5.14 eV for the Au(111) slab. Thus, the electron affinity of CN radical is smaller than the work function of the surface, see Fig. 5.2. Therefore, when the cyanide is adsorbed on the surface, the extra electron of the cyanide is mostly transferred to the metal. That is:

UNIVERSITAT ROVIRA I VIRGILI
FIRST-PRINCIPLES MECHANISTIC STUDIES OF AMMONIA-RELATED INDUSTRIAL PROCESSES
Jaime Gómez Díaz
ISBN:978-84-694-1247-3/T-317-2011

$$Au + CN^{-}(g.p.) \rightarrow Au^{-} + CN(g.p.)\ ;\ \Delta E = -1.51\ eV \tag{5.9}$$

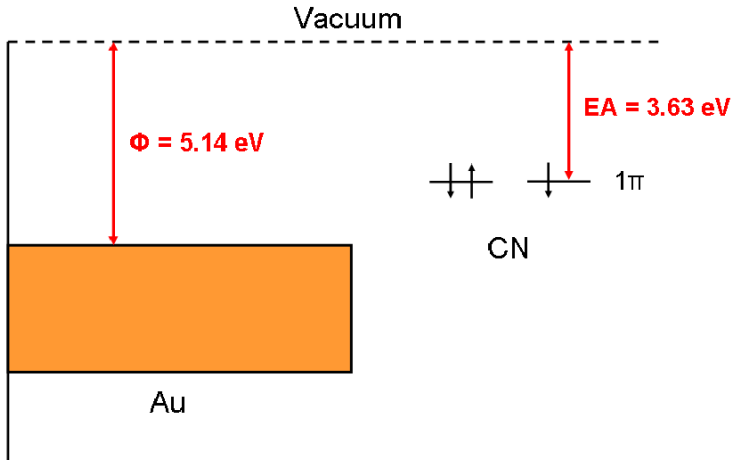

Figure 5.2: Diagram showing gold work-function, ϕ, and CN electron affinity, EA, in eV.

In order to add a negative extra charge to the supercell it is necessary to include a compensating homogeneous charged background to make the whole system neutral. Otherwise, the replication of the cell would imply repulsion between them, disturbing the calculation. This background results in an error that scales as $V^{-1/3}$, where V is the volume of the unit cell, and can be partially removed by adjusting the average potential [193]. Even when adding this later correction, the error is remarkable in metal charged slabs. For example, the value for including an extra negative charge in the slab severely differs from the work-function value. This is due to this compensating background introduced in the calculations, but also because of the number of atoms and size of the cell (that is no infinite). This makes the total energy values for charged systems not directly comparable with neutral ones.

To avoid this problem, the adsorption energies for charged species have been obtained by a Born-Haber cycle as follows:

UNIVERSITAT ROVIRA I VIRGILI
FIRST-PRINCIPLES MECHANISTIC STUDIES OF AMMONIA-RELATED INDUSTRIAL PROCESSES
Jaime Gómez Díaz
ISBN:978-84-694-1247-3/T-317-2011

$$E_{ads} = -\phi_{Au} + EA_{CN} + E_{Au^- - CN} \tag{5.10}$$

where ϕ_{Au} corresponds to the Au work function, EA_{CN} is the electron affinity of the CN radical and $E_{Au^- - CN}$ corresponds to the energy for the adsorption of neutral CN (i.e. the radical) to the charged slab, see Fig. 5.3.

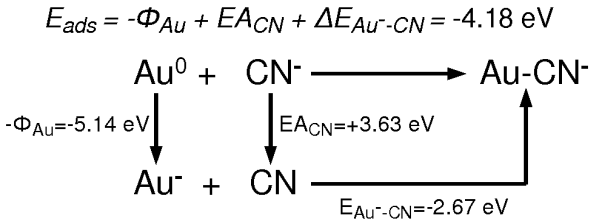

Figure 5.3: Born-Haber cycle for the adsorption of CN^- on the Au(111) surface.

This procedure avoids these internal inconsistencies of the calculations. However, the values obtained using this reference provide the largest possible adsorption energies at infinite CN^- dilution (i.e. no repulsion between charges).

With this set up, the CN^- adsorption energy is -4.18 eV. The charge distribution for this adsorption leads to a larger charge on the CN moiety with respect to the neutral radical, 0.2 vs. 0.5 $|e^-|$. Therefore, the binding mechanism of the CN^- is radically different from that of CO, for which a large HOMO-LUMO gap exists and the HOMO orbital is far to low in energy to assist electron transfer to the metal.

Surface coordination affects only little CN^- adsorption, and the adsorption energy on Au(211) differs by 0.08 eV from that on the Au(111) surface. This may point out that the main contribution to the adsorption energy in this case is due to the electron transfer. In addition, very similar Au-C distances for the CN and the CN^- moieties on both surfaces are found, and Bader charges on the stepped surface are similar to those on the Au(111) surface.

UNIVERSITAT ROVIRA I VIRGILI
FIRST-PRINCIPLES MECHANISTIC STUDIES OF AMMONIA-RELATED INDUSTRIAL PROCESSES
Jaime Gómez Díaz
ISBN:978-84-694-1247-3/T-317-2011

5.3.4 K adsorption

The adsorption energy of K with respect to the atom is highly exothermic, E_{ads}=-2.47 eV. On Au(111), potassium shows small preference for adsorption on a *fcc* site, 0.04 eV more stable than that for *on-top*, the least favorable. However, as the potential energy surface is so flat, sites are not well-defined. Potassium on the surface has a positive charge of 0.9 $|e^-|$, thus almost the whole electron is transfered to the surface. This negative charge on the surface is well distributed among the surface: the gold atoms bonded to the potassium have a negative charge around -0.1 $|e^-|$, and for the rest of the surface atoms it is around 0.0-0.1 $|e^-|$. An increase in the concentration of K on the surface leads to lower average adsorption energies per atom (-1.93 eV/atom for 3 K atoms). The charge, as well, is somehow quenched (0.8 $|e^-|$/atom for three K atoms on the surface) due to both, electronic saturation of the surface and to minimize the electrostatic repulsion between cations. On the stepped Au(211) surface the preferential site is the *four fold hollow* at the step, where adsorption is slightly more exothermic than for the flat surface, E_{ads}=-2.58. This position is 0.16 eV more stable than the corresponding *hollow* site on the upper terrace.

The largest effect of K adsorption on the surface is the strong reduction that it induces on the work function of gold, see Table 5.4. The work-function decrease from 5.14 eV to 4.09 eV upon a single K atom adsorption. At higher K coverage the reduction is even larger, and the work-functions are 3.37 (2 K) and 3.06 eV (3 K), respectively. Notice that the work function depends sensitively on the structure apart from the presence of electropositive adsorbates, see Table 5.4.

5.3.5 K and CN coadsorption

For K and CN coadsorption on the same unit cell, CN sits on the top position and K is on the bridge site, see Fig. 5.1. At this configuration the distance between K and C atoms is 3.76 Å and, with respect to gas-phase KCN, adsorption is exothermic E_{ads}=-1.44 eV. Bring together these two fragments from infinite to the same cell is exothermic by 0.71 eV. For the coadsorbed system the Bader charges on Au and CN are identical to those retrieved by CN^- adsorption.

UNIVERSITAT ROVIRA I VIRGILI
FIRST-PRINCIPLES MECHANISTIC STUDIES OF AMMONIA-RELATED INDUSTRIAL PROCESSES
Jaime Gómez Díaz
ISBN:978-84-694-1247-3/T-317-2011

Table 5.4: Work function, ϕ, average *d*-band center of the entire slab, $\epsilon_{d\ total}$, and average *d*-band center of the top layer or step edge atoms, $\epsilon_{d\ surf/edge}$. All energies in eV.

Surface	Adsorbate	ϕ	$\epsilon_{d\ total}$	$\epsilon_{d\ surf/edge}$
Au(111)	–	5.14	-3.34	-3.26
Au(111)	K	4.09	-3.38	-3.33
Au(111)	2K	3.37	-3.38	-3.37
Au(111)	3K	3.06	-3.39	-3.41
Au(211)	–	4.87	-3.65	-3.22
Au(211)	K	4.12	-3.74	-3.28

On Au(211) surface, K and CN coadsorption is studied for the following configuration: CN sitting at the step edge and the K atom residing in the vicinity, see Fig. 5.1. Two different potassium positions have been investigated: a *fcc* site at the upper terrace and near the *four-fold hollow* site under the step. The second configuration is found to be slightly more stable. The KCN adsorption energy in that case is -1.81 eV (with respect to gas-phase KCN), thus about 0.4 eV larger than the corresponding value for the terrace. This increase is equal to the one found for a CN radical adsorbed on these surfaces. In the case of the Au(211)-KCN structure the Bader charge is almost zero for Au and close to -0.5 $|e^-|$ for CN.

5.3.6 Multiple CN Adsorption

Gold solubilization occurs due to the formation of the $[Au(CN)_2]^-$ molecule. The chemical nature of this molecule is going to be analyzed. The gas-phase $[Au(CN)_2]^-$ structure has been explored recently [194], and they found the covalency of the Au-C bond to be larger than for other molecular counterparts of the same family (Cu, Ag). Our calculated structure shows $D_{\infty h}$ symmetry, and the Au-C and C-N distances are 2.030 and 1.171 Å respectively. The obtained Bader charges are +0.2 for Au and -0.6 $|e^-|$ for CN. Our data are in reasonable agreement with those molecular calculations, that provide a somewhat shorter Au-C distance 1.99 Å and gold charges are in the range of 0.31, by means of NPA method, to 0.04 $|e^-|$, by using Hirsfield partition. According to this explanation the

UNIVERSITAT ROVIRA I VIRGILI
FIRST-PRINCIPLES MECHANISTIC STUDIES OF AMMONIA-RELATED INDUSTRIAL PROCESSES
Jaime Gómez Díaz
ISBN:978-84-694-1247-3/T-317-2011

relatively short Au-C distance is a good indicator of the bond strength.

Next, I focus on adsorption structures that could lead to the formation of $[Au(CN)_2]^-$ species. Firstly, the coadsorption of two neutral CN species on the most open surface, Au(211) has been studied and two configurations are analyzed in the following. One possible structure is shown in Fig. 5.1 (d). This is the minimum energy structure found and adsorption is exothermic by -5.44 eV (-2.72 eV/CN group). Thus, CN-CN repulsion is about 0.4 eV. Then, the Au in contact with both CN groups relaxes outwards by 0.32 Å while the NC-Au-CN angle is 95.7°. A second configuration, where one CN is at the step edge and the second one resides at the hollow site right behind the step has also been explored (not shown in the figure). Adsorption is exothermic by -4.72 eV with respect to gas-phase radicals, i.e. -2.36 eV/CN group. Then, the Au atom in contact with both CN groups is extracted from the step by about 0.37 Å and the NC-Au-CN angle is 99.0°. The CN Bader charges are similar in both cases but slightly smaller in the bridge-bridge configuration.

The coadsorption of one neutral and one charged CN leads to an adsorption geometry as in Fig. 5.1 (d). Then the NC-Au-CN angle is 94.8°, and the Au extraction is 0.30 Å. In this configuration, adsorption of the second CN^- to the already existent Au(211)-CN structure is exothermic by 2.77 eV, thus indicating that multiple adsorption favorable. The total adsorption for both CN and CN^- is -6.94 eV (CN and CN^- as references and calculated through a Born-Haber cycle). For the second structure, with a *bridge-hollow* configuration, the total adsorption energy is -6.24 eV (Born-Haber cycle). Starting by the Au(211)-CN structure, CN^- adsorption scheme provides and adsorption energy of -2.07 eV (Born-Haber cycle). This $[Au(CN)_2]^-$ structure also resembles its neutral counterpart: equal Au extraction (about 0.37 Å) and a similar NC-Au-CN angle, 98.1°. The Bader charges are very similar for multiple CN adsorption at the step edge both in presence and absence of extra charges.

5.4 Electronic structure

Figures 5.4, 5.5 and 5.6 present the projected density of states for the most relevant structures described above. Figure 5.4 (a) and (b) shows the clean Au(111) and Au(211) surfaces.

UNIVERSITAT ROVIRA I VIRGILI
FIRST-PRINCIPLES MECHANISTIC STUDIES OF AMMONIA-RELATED INDUSTRIAL PROCESSES
Jaime Gómez Díaz
ISBN:978-84-694-1247-3/T-317-2011

Adsorbed CO

I start by describing CO moiety on the Au(111) surface. CO interacts weakly with the Au surface, and indeed, only minor band overlaps are observed in the LDOS, see Fig. 5.4 (c). The empty $2\pi^*$ CO levels, peak centered around 2.5 eV, are far away from the Au *d*-band and thus, the interaction is very small. The peak corresponding to the CO HOMO level, 5σ, is far too low in energy, around -7.5 eV, to allow charge transfer from the adsorbate to the metal *d*-band, in any case, a small interaction is observed. When going to the Au(211) surface, several differences can be observed. The interaction between CO and the Au(211) surface involves a larger overlap between the *d*-band of the edge atoms and CO orbitals than in the corresponding case on the Au(111) surface. The overlap with the CO 5σ orbital is not present now because the most preferential site on Au(211) surface is *bridge*. Thus, this interaction is geometrically unfavorable.

Adsorbed CN

Overlap between metal *d*-band and CN radical orbitals is larger than for CO, see Fig. 5.5 (c). However, electron sharing is small. The CN band close to the Fermi level is shallow and the resonance with Au is minor. The small peak due to CN 5σ overlap is again present. On Au(211) surface, CN radical shows much larger overlap. As in the case of CO, CN 5σ orbital overlap disappears due to geometrical aspects when CN is adsorbed on Au(211) on a *bridge* position. The Au(211)-CN interaction resembles the Au(111)-CN^- or Au(111)-KCN systems, see Fig. 5.5 (b), more than the Au(111)-CN system. This is due to the fact that the states of Au edge atoms are closer to the Fermi level, and thus more prone to interact with incoming molecules, like in the case of KCN adsorption on Au(111). Moreover, the overlap between the CN levels and the Au edge states is larger indicating a more covalent bond than for the Au(111) counterpart.

Adsorbed CN^- and KCN

CN^- electronic structure is almost equivalent to that for the CN fragment in KCN. Thus, the CN^- structure is not shown. Upon KCN adsorption, several modifications take place with respect to CN, as can be seen from Fig. 5.5 (d). In that case, the overlap between the Au *d*-band and the

UNIVERSITAT ROVIRA I VIRGILI
FIRST-PRINCIPLES MECHANISTIC STUDIES OF AMMONIA-RELATED INDUSTRIAL PROCESSES
Jaime Gómez Díaz
ISBN:978-84-694-1247-3/T-317-2011

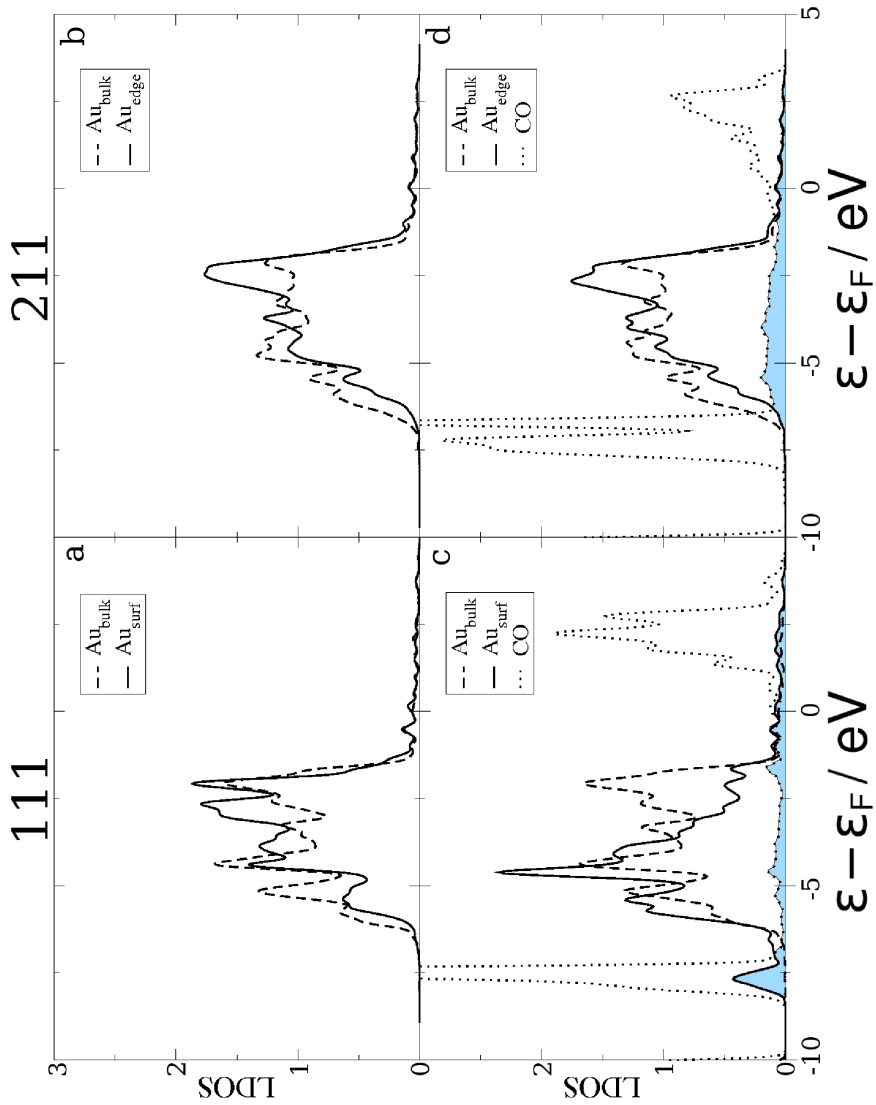

Figure 5.4: Projected Local Density Of States for clean Au(111) (a) and Au(211) (b) surface and CO adsorbed on Au(111) (c) and Au(211) (d) surfaces. Blue colored areas represent the overlap.

UNIVERSITAT ROVIRA I VIRGILI
FIRST-PRINCIPLES MECHANISTIC STUDIES OF AMMONIA-RELATED INDUSTRIAL PROCESSES
Jaime Gómez Díaz
ISBN:978-84-694-1247-3/T-317-2011

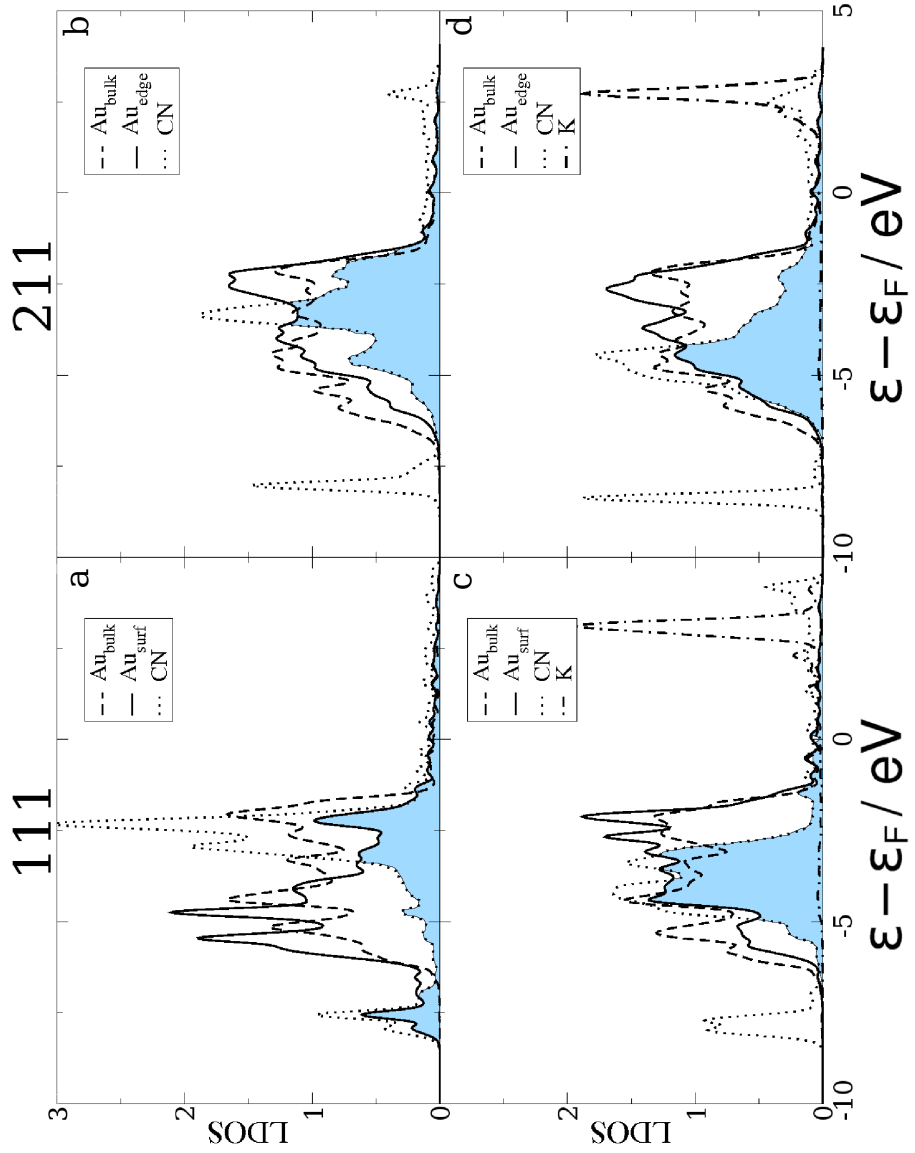

Figure 5.5: Projected Local Density Of States for CN adsorbed on Au(111) (a) and Au(211) (b) surface and KCN adsorbed on Au(111) (c) and Au(211) (b) surfaces.

UNIVERSITAT ROVIRA I VIRGILI
FIRST-PRINCIPLES MECHANISTIC STUDIES OF AMMONIA-RELATED INDUSTRIAL PROCESSES
Jaime Gómez Díaz
ISBN:978-84-694-1247-3/T-317-2011

CN orbitals is large and extends over several eV. In addition, the *d*-band center is closer to the Fermi level than in the previous case. Finally, the empty states of K appear at the high unoccupied values. For Au(211) surface, the CN levels drop to lower energy values, making the interaction stronger.

Multiple CN

The DOS analysis for multiple CN adsorption at the step edge on *bridge* positions is presented in Fig. 5.6 for the neutral (a) and charged (b) system. The plot shows that for the neutral and charged systems both CN groups behave equally, due to the fact that their local environments are alike. Charge is then equally distributed in the anionic case. Only minor differences are found between neutral and charged systems, pointing out that the charge is almost completely transferred and has a little effect on the electronic structure. In any case, overlap is slightly more intense and lowest in energy for the negatively charged system.

Comparison between single, Fig. 5.5 (b), and multiple, Fig. 5.6 (a), CN adsorption on bridge sites shows that for multiple adsorption the CN band closer to the Fermi energy is larger than that for the isolated CN. Yet, the center of the band is located about 2.5 eV below the Fermi energy. The CN bands close to the Fermi level, are slightly shifted down in energy.

5.5 ELF analysis

Electron Localization Function analysis have been carried out for several significant structures: $[Au(CN)_2]^-$ molecule, Au(111)-CN and Au(111)-CN^-. Figure 5.7 (a) presents the ELF analysis for the gas phase molecule $[Au(CN)_2]^-$, calculated by plane waves on periodic systems and a localized basis set on a single molecule. This plot resembles that from Wang *et al.* [194] generated by DFT PW91/TZ2P level calculation, Fig. 5.7 (b). From this plot and photoelectron spectroscopy (PES) these authors identified the Au-CN bond in $[Au(CN)_2]^-$ as covalent. They based their claim in the comparison with other molecules, $Cu(CN)_2^-$ and $Ag(CN)_2^-$, and in the observed vibrational progressions in the photodetachment transitions. They found lower positive charge of gold, larger Au-CN bond order and

UNIVERSITAT ROVIRA I VIRGILI
FIRST-PRINCIPLES MECHANISTIC STUDIES OF AMMONIA-RELATED INDUSTRIAL PROCESSES
Jaime Gómez Díaz
ISBN:978-84-694-1247-3/T-317-2011

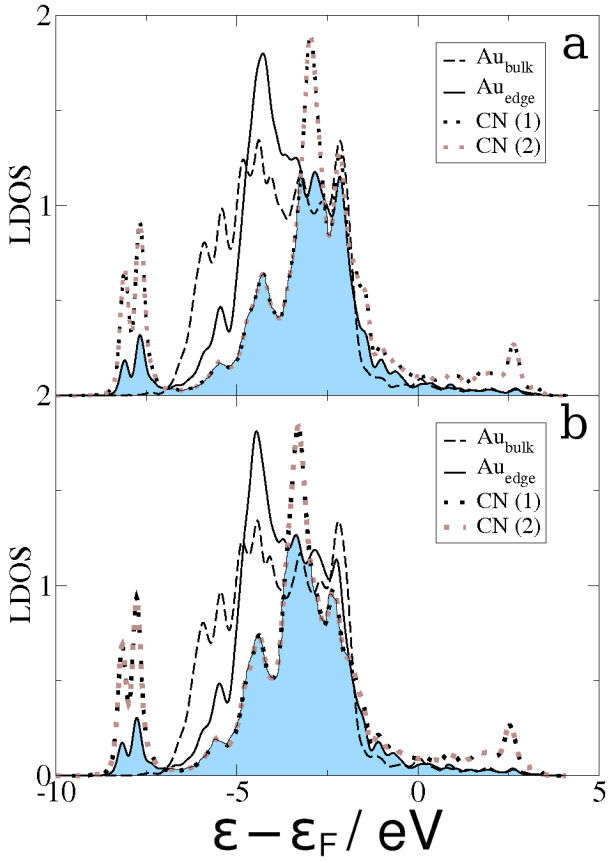

Figure 5.6: Projected Local Density Of States for (a) Au(211)-$(CN)_2$ and (b) Au(211)-$(CN)_2^-$. Blue colored areas represent the overlap.

UNIVERSITAT ROVIRA I VIRGILI
FIRST-PRINCIPLES MECHANISTIC STUDIES OF AMMONIA-RELATED INDUSTRIAL PROCESSES
Jaime Gómez Díaz
ISBN:978-84-694-1247-3/T-317-2011

shorter bond distance. All these aspects point at the presence of covalent bond.

Comparing both plots, we observe differences around the nuclei, that are due to the use of pseudopotentials in our calculations. The probability around oxygen in the direction opposite to gold looks slightly smaller in our periodic calculations. Despite these points, the plots are qualitatively similar, pointing out that our approach is valid for this gas phase molecule.

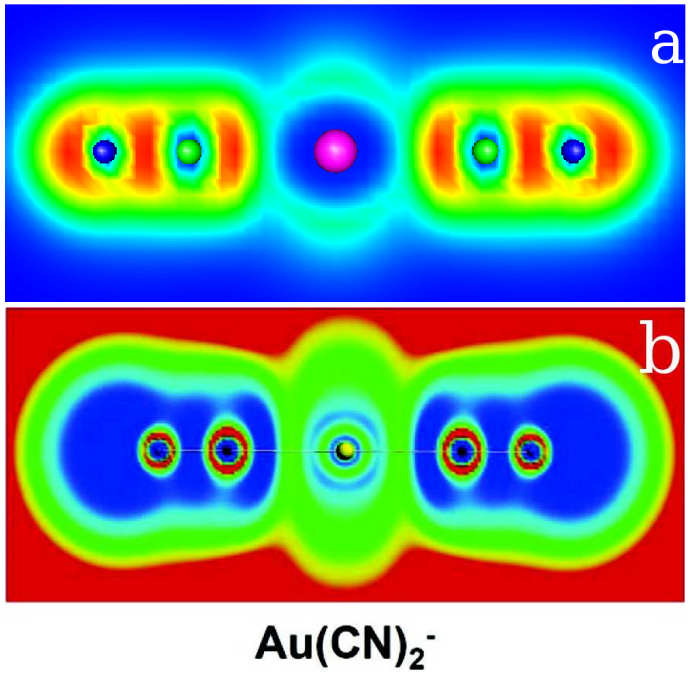

Figure 5.7: ELF plots for: (a) $[Au(CN)_2]^-$ calculated with periodic conditions. Low ELF values (close to 0) are indicated in blue colors while high ELF values (close to 1) are shown in red. (b) $[Au(CN)_2]^-$ calculated by DFT PW91/TZ2P. Notice that now, low ELF values (close to 0) are indicated in red colors while high ELF values (close to 1) are shown in blue. Graph taken from reference [194].

The ELF plots of surface systems, Fig. 5.8, are very similar to the ELF plot for gas-phase $[Au(CN)_2]^-$, which indicates that the bonding between CN and a Au surface is very similar than that for the molecule. This, as

UNIVERSITAT ROVIRA I VIRGILI
FIRST-PRINCIPLES MECHANISTIC STUDIES OF AMMONIA-RELATED INDUSTRIAL PROCESSES
Jaime Gómez Díaz
ISBN:978-84-694-1247-3/T-317-2011

well as the similar Bader charges and bond distances, support that the bond is as well mainly covalent and our understanding that the charge of CN^- moiety is not localized at CN not even at the Au-C bond but mostly transferred to the metal.

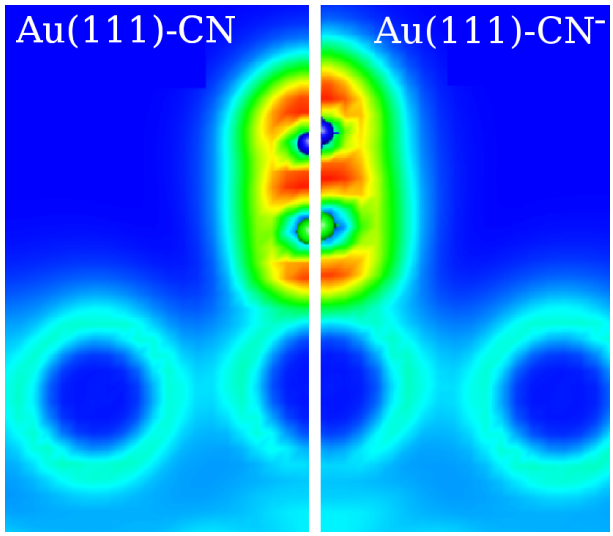

Figure 5.8: ELF plots for (a) Au(111)-CN and (b) Au(111)-CN^-. Low ELF values (close to 0) are indicated in blue colors while high ELF values (close to 1) is shown in red.

5.6 Discussion

All the calculations above support the reaction mechanism for the solubilization and deposition presented in Eqs. 5.1-5.5. According to our results, the first CN^- adsorption is accompanied by electron transfer to the metal. Thus, the steps reported in Eqs. 5.2 and 5.3 would be better described as a single elementary step.

Koper and coworkers [179] claimed that the Au-CN bond is ionic for all the low-index surfaces of gold. They base this statement on the dipole moments found in their calculations for the Au-CN bond and on the negative charges observed in the CN fragment. They also state that the more

UNIVERSITAT ROVIRA I VIRGILI
FIRST-PRINCIPLES MECHANISTIC STUDIES OF AMMONIA-RELATED INDUSTRIAL PROCESSES
Jaime Gómez Díaz
ISBN:978-84-694-1247-3/T-317-2011

ionic is the interaction the stronger is the bond. The electronic structure analysis presented in this chapter shows a significant overlap that indicates the covalent contribution to the bond.

From our data, CN^- adsorption would require an electron sink in order for the reaction to take place. Au could then work as an electron acceptor and further transfer the electron to incoming oxygenated species to complete the redox couple. This support the well-known requirement of O_2 [168] to perform gold extraction from the ore. Second CN^- addition is still exothermic on Au(211) surface, making the solubilization trough $[Au(CN)_2]^-$ possible. However, the calculations indicate a possible qualitative scenario for the previously reported experiments.

5.7 Conclusions

-CO and CN adsorptions on Au(111) are endothermic with respect to CO and C_2N_2 respectively, but almost thermoneutral (CN) and exothermic (CO) on Au(211) surface. The shift in adsorption energy induced by the change in the surface is similar in these adsorbates.

-Present results explain why a positive effect of small size particles is observed in the extraction of ores [167] and why preferential multiadsorption is localized at edges and defects [173]. This is due to the dependence of the adsorption energy with the average coordination number for Au.

-Electronically, CN adsorption on gold surfaces is qualitatively different from that of CO. The covalency of the Au-CN bond is supported by Bader charges, bond distances and ELF analysis.

-CN adsorption depends strongly on the presence of extra charge or electropositive compounds. Extra charges also increase the amount of covalency of the Au-CN due to positive interaction with the Au bands that are pushed towards the Fermi level. These observations agree with recent reports on the large covalent contribution to the $[Au(CN)_2]^-$ gas-phase compounds.[194] In order to obtain $[Au(CN)_2]^-$ compounds increasing the electron density at the Au centers (either by electropositive compounds, by artificially including extra charges or by employing edge sites) increases the bond strength of Au-CN by covalent contributions and allows large outward relaxations, like in Au(211)-$(CN)_2^-$ precursors of the soluble molecule in gold-ore cleaning.

UNIVERSITAT ROVIRA I VIRGILI
FIRST-PRINCIPLES MECHANISTIC STUDIES OF AMMONIA-RELATED INDUSTRIAL PROCESSES
Jaime Gómez Díaz
ISBN:978-84-694-1247-3/T-317-2011

-Our calculations combined with the LDOS and ELF analysis support the mechanism presented by Harrison and Thompson [183] and Eisenmann [184] where the adsorption of the first CN introduces electron transfer towards the metal. In particular, CN^- adsorption is demonstrated to take place simultaneously with charge transfer, leading to a mostly delocalised negative charge, that can be employed in the reduction part of the redox reaction. Under these conditions, specially at under-coordinated sites second CN^- adsorption is still a favorable event and constitutes the seed for the formation of the soluble $[Au(CN)_2]^-$ species.

UNIVERSITAT ROVIRA I VIRGILI
FIRST-PRINCIPLES MECHANISTIC STUDIES OF AMMONIA-RELATED INDUSTRIAL PROCESSES
Jaime Gómez Díaz
ISBN:978-84-694-1247-3/T-317-2011

UNIVERSITAT ROVIRA I VIRGILI
FIRST-PRINCIPLES MECHANISTIC STUDIES OF AMMONIA-RELATED INDUSTRIAL PROCESSES
Jaime Gómez Díaz
ISBN:978-84-694-1247-3/T-317-2011

Part III

Conclusions

UNIVERSITAT ROVIRA I VIRGILI
FIRST-PRINCIPLES MECHANISTIC STUDIES OF AMMONIA-RELATED INDUSTRIAL PROCESSES
Jaime Gómez Díaz
ISBN:978-84-694-1247-3/T-317-2011

UNIVERSITAT ROVIRA I VIRGILI
FIRST-PRINCIPLES MECHANISTIC STUDIES OF AMMONIA-RELATED INDUSTRIAL PROCESSES
Jaime Gómez Díaz
ISBN:978-84-694-1247-3/T-317-2011

Conclusions

Ostwald Process

DFT models have been employed to study the selectivity of the first step of the process leading to HNO_3 synthesis, i.e. ammonia oxidation to NO, over a set of transition metals and a model of the industrially employed alloy. The following conclusions have been obtained:

Au(111)

- Oxygen and hydroxyl-assisted ammonia dehydrogenations show a much lower activation energies than Au(111) pure reactions. In addition, the barriers for N+N and N+O recombination are 0.95 eV and 1.03 eV.
- Thus, the Au(111) shows a intrinsic selectivity towards the formation of N_2.
- NO adsorbs only weakly on Au(111) and its readsorption or recombination with other atoms on the surface are unlikely events.
- The microkinetic model of the selectivity as a funcition of the DFT calculated energies taking into account the detailed balance of the species present in the surface can properly described the experimental observations in the group of Prof. Mullins.

Transition metals

The reaction profiles for the formation of N_2 and NO have been investigated for Au, Cu, Ir, Pd, Pt, and Rh for both (111) and (211) surfaces.

UNIVERSITAT ROVIRA I VIRGILI
FIRST-PRINCIPLES MECHANISTIC STUDIES OF AMMONIA-RELATED INDUSTRIAL PROCESSES
Jaime Gómez Díaz
ISBN:978-84-694-1247-3/T-317-2011

The conclusions are the following:

- The reaction profiles for the competing reactions on the surfaces can be summarized in three different categories: (i) NO is not readsorbed on the surface; (ii) NO is readsorbed but cannot dissociate due to a large barrier for the inverse step; (iii) NO readsorbs from the gas-phase and can dissociate. Depending on the behaviour of NO on the surface the model for the selectivity between NO and N_2 production needs to take into account different steps as rate-limiting ones in the formation of NO and thus in the selectivity.

- In the particular case of Pt, step sites produce a strong adsorption of NO that thus can dissociate on the surface. This agrees with the experimental results reported by the group of Prof. King.

PtRh activity and stability

I have analyzed the competitive N_2 and NO formation reactions on PtRh model systems and investigated the stability of different oxygen containing compounds. The following conclusions can be extracted:

- The use of PtRh alloys can not be assigned to the improvement of the activity or selectivity of the competing N_2 and NO formation reactions. The barriers at mixed sites are similar or slightly larger than the corresponding to the Pt pure system.

- Selectivity might be affected by the largest residence time of NO (stronger binding energy) to mixed sites on the surface.

- Rhodium oxides have been found more stable than platinum ones, in agreement with experimental phase diagrams.

- Instead, Rh atoms can be extracted from the bulk to the surface by adsorbed oxygen atoms. Rh atoms on the surface behave as sinks for adsorbed O atoms and thus reduce the effective pressure on the Pt atoms. This effect linked to the fact that Rh atoms are less proned to be eliminated as volatile compounds might explain the longer stability of the alloys at high oxygen pressures.

UNIVERSITAT ROVIRA I VIRGILI
FIRST-PRINCIPLES MECHANISTIC STUDIES OF AMMONIA-RELATED INDUSTRIAL PROCESSES
Jaime Gómez Díaz
ISBN:978-84-694-1247-3/T-317-2011

Andrussow and Degussa processes: HCN synthesis

DFT models have been employed to study Andrussow and Degussa processes: HCN formation under oxidative and non-oxidative conditions, respectively. The following conclusions have been obtained:

Platinum surface

- In the Degussa (non-oxidative) process, HCN formation mainly comes from the most likely coupling of methane and ammonia intermediates, CH + NH_2 reaction, with the subsequent elimination of H atoms. HCNH deprotonation shows the largest barrier in this recombination channel, our estimation for the activation energy of this step agrees with the experimental value determined in the group of Prof. Trenary. The high energy demand of the Degussa process comes from reactant activation: Eley-Rideal methane activation and also ammonia dehydrogenation on the surface.

- Under Andrussow (oxidative) conditions, the presence of oxygen changes the dehydrogenation barriers and the stability of the adsorbed fragments, and thus their populations. CH+N and C+N appear as the most important paths for C-N bond production. The high energy requirements needed for these recombination reactions are the responsible for the high temperatures needed for the process in this case.

Transition metals

- Low barriers are found for couplings on Au and Cu due to their weak adsorption energy. C+N reaction is the less energetically demanding way to form C-N bond on Au, Cu, Pt and Rh; and CN hydrogenation barriers are not high. On Ir and Pd, C-N bond is more likely formed via HC+N recombination.

- Linear-scaling relationships are found for the adsorption energy of CN, HCN and CNH species with respect to the atomic C adsorption energy for all the metals considered.

UNIVERSITAT ROVIRA I VIRGILI
FIRST-PRINCIPLES MECHANISTIC STUDIES OF AMMONIA-RELATED INDUSTRIAL PROCESSES
Jaime Gómez Díaz
ISBN:978-84-694-1247-3/T-317-2011

- Linear-scaling relationships are found for dissociation energy of CN-containing compounds with respect to N atom adsorption energy. This paves the way for a rapid evaluation of these kinetic parameters for other materials.

MacArthur-Forrest

I have described the interaction of CN-containing compounds with different gold models to understand the molecular origin of the process involved in gold ore purification. The following conclusions have been obtained.

- CN adsorption on gold surfaces is qualitatively different from that of CO. The covalent contributions for CN adsorption are much larger than for CO. When CN^- is considered, the extra electron is partially transferred to the surface, improving the adsorption.

- The calculations support the mechanism presented by Harrison and Thompson and Eisenmann where the adsorption of the first CN group introduces electron transfer towards the metal. This allows second CN^- adsorption, that is still a favorable event and constitutes the seed for the formation of the soluble $[Au(CN)_2]^-$ species responsible for the elimination of pure Au from the impure ore.

UNIVERSITAT ROVIRA I VIRGILI
FIRST-PRINCIPLES MECHANISTIC STUDIES OF AMMONIA-RELATED INDUSTRIAL PROCESSES
Jaime Gómez Díaz
ISBN:978-84-694-1247-3/T-317-2011

Part IV

List of publications

UNIVERSITAT ROVIRA I VIRGILI
FIRST-PRINCIPLES MECHANISTIC STUDIES OF AMMONIA-RELATED INDUSTRIAL PROCESSES
Jaime Gómez Díaz
ISBN:978-84-694-1247-3/T-317-2011

UNIVERSITAT ROVIRA I VIRGILI
FIRST-PRINCIPLES MECHANISTIC STUDIES OF AMMONIA-RELATED INDUSTRIAL PROCESSES
Jaime Gómez Díaz
ISBN:978-84-694-1247-3/T-317-2011

List of publications

1. NH_3 Oxidation on Oxygen-Precovered Au(111): A Density Functional Theory Study on Selectivity. Núria López, Mónica García-Mota and Jaime Gómez-Díaz. *J. Phys. Chem. C* **2008**, *112*, 247-252.

2. Mónica García-Mota, Jaime Gómez-Díaz, Javier Pérez-Ramírez and Núria López. *"In Quantum Chemical Calculations of Surfaces and Interfaces of Materials". Catalysis by gold containing systems: selectivity is the key*, 55-63 , **2009** American Scientific Publishers, EEUU.

3. A Density Functional Theory study on gold cyanide interactions: The fundamentals of ore cleaning. Jaime Gómez-Díaz, Karoliina Honkala and Núria López. *Surf. Sci.* **2010**, *604*, 1552-1557.

4. A density functional theory study of the mythic Lindlar hydrogenation catalyst. Mónica García-Mota, Jaime Gómez-Díaz, G. Novell-Leruth, Crisa Vargas-Fuentes, Luca Bellarosa, Blaise Bridier, Javier Pérez-Ramírez, Núria López. *Theor. Chem. Acc.* DOI: 10.1007/s00214-010-0800-0

5. Mechanistic switch between aerobic (Andrussow) and anaerobic (Degussa) formation of HCN on Pt(111) by Density Functional Theory. *Under revision.*

6. C-N coupling on transition metal surfaces: a Density Functional Theory study. *Submitted*

The author has performed the majority of the numerical work in the publications 3, 5 and 6; and part of the calculations in the publications 1,

UNIVERSITAT ROVIRA I VIRGILI
FIRST-PRINCIPLES MECHANISTIC STUDIES OF AMMONIA-RELATED INDUSTRIAL PROCESSES
Jaime Gómez Díaz
ISBN:978-84-694-1247-3/T-317-2011

2 and 4 by using the Density Functional Theory codes VASP and GPAW. He has participated actively in the writing of all the publications.

UNIVERSITAT ROVIRA I VIRGILI
FIRST-PRINCIPLES MECHANISTIC STUDIES OF AMMONIA-RELATED INDUSTRIAL PROCESSES
Jaime Gómez Díaz
ISBN:978-84-694-1247-3/T-317-2011

Part V

Appendix

UNIVERSITAT ROVIRA I VIRGILI
FIRST-PRINCIPLES MECHANISTIC STUDIES OF AMMONIA-RELATED INDUSTRIAL PROCESSES
Jaime Gómez Díaz
ISBN:978-84-694-1247-3/T-317-2011

UNIVERSITAT ROVIRA I VIRGILI
FIRST-PRINCIPLES MECHANISTIC STUDIES OF AMMONIA-RELATED INDUSTRIAL PROCESSES
Jaime Gómez Díaz
ISBN:978-84-694-1247-3/T-317-2011

Appendix A

Bulks, surfaces and molecules construction

In this appendix, the characterization of all the metals (Au, Cu, Ir, Pd, Pt and Rh) and metal oxides used in the previous chapters is stated. As well, the gas phase molecules employed in the previous chapters are described.

A.1 Bulks

A.1.1 Metals

Calculations have been performed for Au, Cu, Ir, Pd, Pt and Rh in faced-centered cubic (*fcc*) structure, the most stable for all of them. For this structure, $a = b = c$, thus, there is only one lattice constant.

The metal bulks have been calculated performing a Brillouin-zone integration with grids of 11x11x11 Monkhorst-Pack k-points. In order to optimize the cell parameter a, a scan around the expected value (for example, the experimental one) is performed. That is, we select a set of values close to the experimental one, and calculate the energy for each one. Then, we represent the energy with respect to the selected values. After that, the values are approximated to a third degree polynomial equation and the minimum is located. In Figure A.1, Cu optimization by this method is shown.

The results for the set of metals are shown in Table A.1. All the cell

UNIVERSITAT ROVIRA I VIRGILI
FIRST-PRINCIPLES MECHANISTIC STUDIES OF AMMONIA-RELATED INDUSTRIAL PROCESSES
Jaime Gómez Díaz
ISBN:978-84-694-1247-3/T-317-2011

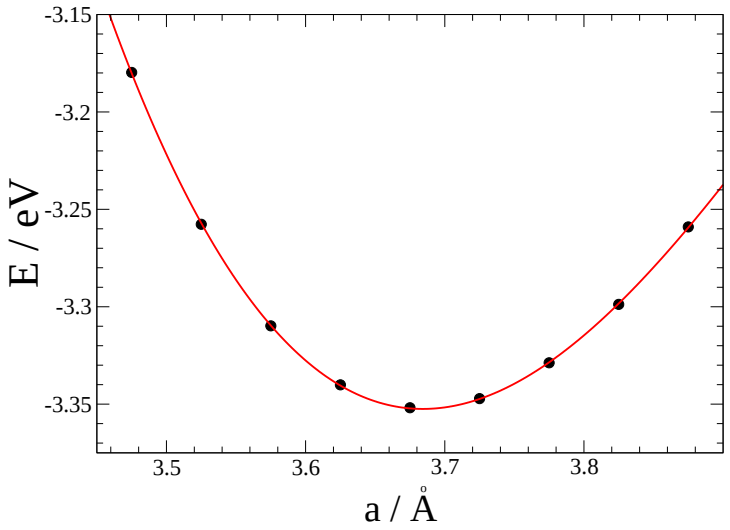

Figure A.1: Cu cell parameter a optimization. The black points represent the calculated values and the red curve the fitted polynomial.

parameters are larger than the experimental ones, as usual in calculations using RPBE functional [33]. The agreement with the experimental data [195] is good, being the errors 3% as maximum, for Ag and Au, and minimum 1% for Ir and Rh. These calculated parameters a have been used in the previous calculations. In Fig. A.2, the dependence of the error on the electronic configuration is shown.

Table A.1: Calculated cell parameter a, in Å versus experimental [195] ones

Metal	Calculated	Experimental	Error %
Ag	4.227	4.0853	3
Au	4.208	4.0782	3
Cu	3.676	3.6149	2
Ir	3.879	3.839	1
Pd	3.987	3.8907	2
Pt	3.990	3.9242	2
Rh	3.856	3.8034	1

In its standard mode, VASP performs a fully relativistic calculation

UNIVERSITAT ROVIRA I VIRGILI
FIRST-PRINCIPLES MECHANISTIC STUDIES OF AMMONIA-RELATED INDUSTRIAL PROCESSES
Jaime Gómez Díaz
ISBN:978-84-694-1247-3/T-317-2011

for the core-electrons, and treats valence electrons in a scalar relativistic approximation, but does not compute spin-orbit coupling of the valence electrons. This may be one of the most important sources of error in the determination of the cell parameters.

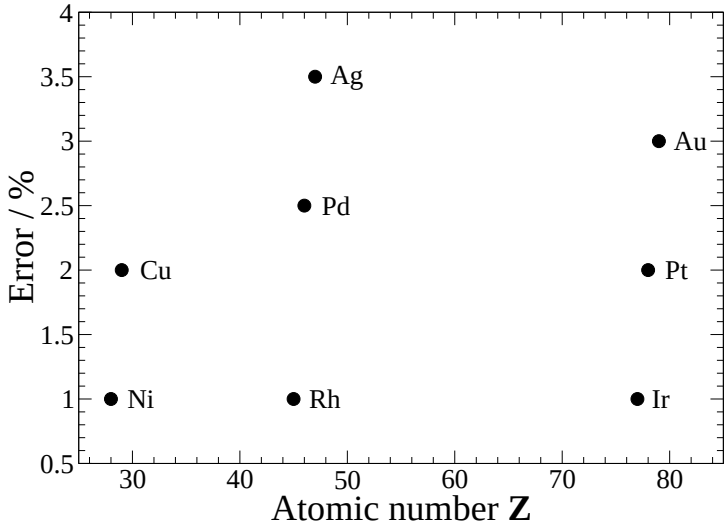

Figure A.2: Error in lattice constant a (with respect to the experimental one) dependence on the atomic number Z

A.1.2 Metal oxides

The studied metal oxides cells contains two different cell parameters, $a = b \neq c$. The convergence of these parameters have been carried out in two different ways. First, using and iterative method, where a is optimized in an equivalent way to that explained for metals, and the value obtained is used to optimize c and successively until convergence. The second method employed is the VASP tag "IBRION=3", where all the cell parameters are automatically optimized. Both results were very similar. To compare the obtained results with the experimental data check Table 3.9 in Chapter 3, page 78.

UNIVERSITAT ROVIRA I VIRGILI
FIRST-PRINCIPLES MECHANISTIC STUDIES OF AMMONIA-RELATED INDUSTRIAL PROCESSES
Jaime Gómez Díaz
ISBN:978-84-694-1247-3/T-317-2011

Cohesive energy.

The cohesive energy, E_{coh}, is the change in energy when a solid is formed from its isolated atomic species, that is:

$$E_{coh} = E_{solid} - \sum_{A} E_A^{isolated} \tag{A.1}$$

where E_{solid} is the energy of the solid and $E_A^{isolated}$ that of its atoms in gas-phase. The process of formation of the solid phase is exothermic for metals.

Table A.2: Cohesive energy in eV/atom.

Metal	Structure	Calculated	Experimental	Error Δ
Ag	fcc	-2.89	-2.95	+0.06
Au	fcc	-3.33	-3.81	+0.48
Cu	fcc	-3.90	-3.49	-0.41
Ir	fcc	-7.23	-6.94	-0.29
Pd	fcc	-3.72	-3.89	+0.17
Pt	fcc	-5.56	-5.84	+0.28
Rh	fcc	-5.33	-5.75	+0.42

Even when the trend is well reproduced, as expected, the agreement is not as good as, for example, the distances. The absolute error range goes from +0.48 eV for Au, to -0.41 eV for Cu. It is important to take into account that the pseudopotentials used are fitted to be reliable in metals in solid phase. The atoms behave in a different way in solid than in gas-phase state, and they can have different electronic configurations. That makes the results obtained for solids more reliable then those for isolated atoms.

A.2 Surface relaxation

Slabs have been built for all the metal surfaces. In adittion, a vacuum layer is included. The thickness of the vacuum layer is in general approximately twice that of the slab. For example, around 12 Å of vacuum are added for a four layers metal slab, see Fig. A.3. The vacuum separates the slabs enough to minimize the interaction between replicated slabs.

UNIVERSITAT ROVIRA I VIRGILI
FIRST-PRINCIPLES MECHANISTIC STUDIES OF AMMONIA-RELATED INDUSTRIAL PROCESSES
Jaime Gómez Díaz
ISBN:978-84-694-1247-3/T-317-2011

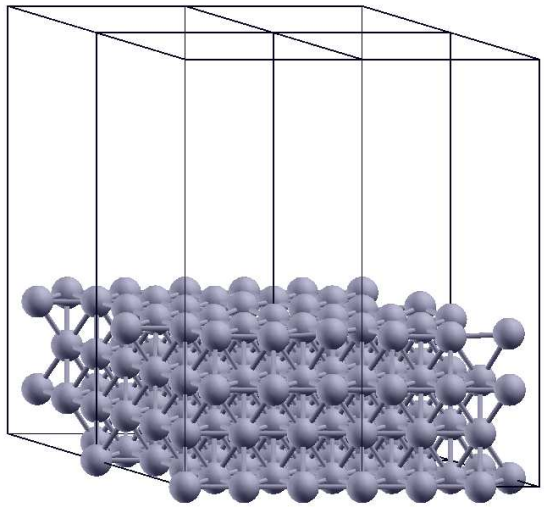

Figure A.3: Replicated four layers slab with 12 Å vacuum. Supercell in black lines.

Surface energy

The surface energy, γ, is the work required to increase the surface area of a substance by unit area. The surface energy γ gives us an estimation of the stability of this surface respect to the bulk or to any other surface. It can be obtained in the calculations as follows:

$$\gamma = \gamma^{unrel} + E^{rel} \tag{A.2}$$

where E^{rel} is the energy changes during relaxation, and γ^{unrel} is

$$\gamma^{unrel} = 1/2(E_{surf} - N_{atoms} \cdot E_{bulk}) \tag{A.3}$$

Where E_{surf} is the total energy of the unrelaxed surface, N_{atoms} is the total number of atoms in this slabs, and E_{bulk} is the energy of an bulk atom. Table A.3 shows the results for our set of metals. The agreement of these results with those from Ref. [196] is reasonable.

UNIVERSITAT ROVIRA I VIRGILI
FIRST-PRINCIPLES MECHANISTIC STUDIES OF AMMONIA-RELATED INDUSTRIAL PROCESSES
Jaime Gómez Díaz
ISBN:978-84-694-1247-3/T-317-2011

Table A.3: Surface energy in J/m^2

Metal	Structure	Relaxation	Surface free energy	Reference[196]
Ag	fcc	6.6%	0.74	0.76
Au	fcc	0.3%	0.63	
Cu	fcc	0.3%	1.06	
Ir	fcc	-1.2%	1.82	
Pd	fcc	0.0%	1.20	1.33
Pt	fcc	0.6%	1.19	
Rh	fcc	-2.1%	1.75	2.01

A.3 Isolated molecules

All the isolated molecules, except on those detailed in Chapter 3, Section 3.1, page 41; have been calculated with VASP in an asymmetric box of approximately 10 Å lenght, a Γ k-point, and, if neccesary, under a spin unrestricted calculation.

A.3.1 Diatomic molecules

Calculations for N_2, O_2 and NO have been carried out. In table A.4, we show the results for the diatomic molecules N_2, O_2. The dissociation energy (D_e) for a diatomic molecule XX′ has been calculated as:

$$D_e = E_X(gp) + E_{X'}(gp) - E_{molecule} \tag{A.4}$$

Where E_X(gp) is the energy of the X atom in gas phase and $E_{molecule}$ is the energy of the isolated molecule XX′. For O the ^3P ground state was employed and for N the ^4S one. There is a very good agreement between experiments and calculations for the geometries. Dissociation energy is not as good, but the absolute error is 0.37 eV as maximum.

Table A.4: Bond energies and distances for the diatomic molecules.

	D_e/eV				**Distance/Å**		
Molecule	Calc	Exp [197]	Error %	ΔE	Calc	Exp [197]	Error %
N_2	10.00	9.95	1	+0.05	1.098	1.117	2
O_2	5.72	5.35	6	+0.37	1.207	1.236	2
NO	6.92	6.66	4	+0.26	1.150	1.172	2

UNIVERSITAT ROVIRA I VIRGILI
FIRST-PRINCIPLES MECHANISTIC STUDIES OF AMMONIA-RELATED INDUSTRIAL PROCESSES
Jaime Gómez Díaz
ISBN:978-84-694-1247-3/T-317-2011

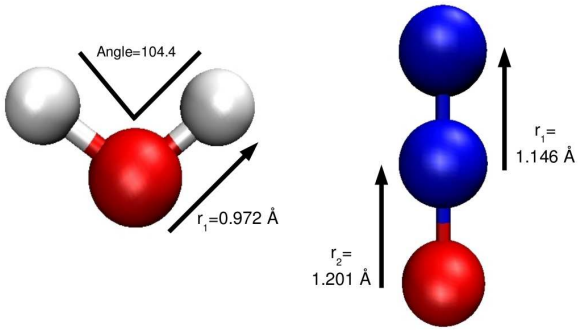

Figure A.4: H_2O and N_2O molecules. The relevant angles and distances are shown.

A.3.2 Triatomic molecules

The triatomic molecules we present there are N_2O, H_2O, PtO_2 and RhO_2. As in the previous case, the agreement with experiments is good (Table A.5). In this case, only geometries are reported.

Table A.5: Molecule geometries. Distances, r_1 and r_2 in Å, and angles, α in degrees.

		Calculated			**Experimental**		
Molecule	Sym. group	r_1	r_2	α	r_1	r_2	α
N_2O	$C_{\infty v}$	1.146	1.201	180.0	1.128 [1]	1.184	180.0
H_2O	C_{2v}	0.972	0.972	104.4	0.958 [1]	0.958	104.5
PtO_2	$C_{\infty v}$	1.723	1.723	180.0	1.728 [2]	1.728	180.0
RhO_2	C_{2v}	1.703	1.703	155.9	1.714 [3]	1.714	155.6

[1]Ref. [197].
[2]Ref. [198].
[3]Ref. [199].

UNIVERSITAT ROVIRA I VIRGILI
FIRST-PRINCIPLES MECHANISTIC STUDIES OF AMMONIA-RELATED INDUSTRIAL PROCESSES
Jaime Gómez Díaz
ISBN:978-84-694-1247-3/T-317-2011

UNIVERSITAT ROVIRA I VIRGILI
FIRST-PRINCIPLES MECHANISTIC STUDIES OF AMMONIA-RELATED INDUSTRIAL PROCESSES
Jaime Gómez Díaz
ISBN:978-84-694-1247-3/T-317-2011

Part VI

Bibliography

UNIVERSITAT ROVIRA I VIRGILI
FIRST-PRINCIPLES MECHANISTIC STUDIES OF AMMONIA-RELATED INDUSTRIAL PROCESSES
Jaime Gómez Díaz
ISBN:978-84-694-1247-3/T-317-2011

UNIVERSITAT ROVIRA I VIRGILI
FIRST-PRINCIPLES MECHANISTIC STUDIES OF AMMONIA-RELATED INDUSTRIAL PROCESSES
Jaime Gómez Díaz
ISBN:978-84-694-1247-3/T-317-2011

Bibliography

[1] Chorkendorff, I.; Niemantsverdriet, J. W. *Concepts of Modern Catalysis and Kinetics*; Wilei-VCH: Weinhem, 2003.

[2] Nørskov, J. K.; Christensen, C. H. *Science* **2006**, *312*, 5778.

[3] Greeley, J.; Jaramillo, T. F.; Bonde, J.; Chorkendorff, I.; Nørskov, J. K. *Nat. Mat.* **2006**, *5*, 909.

[4] Clarke, S. I.; Mazzafro, W. J. *Nitric Acid*; John Wiley & Sons, Inc., 2005; pp 1–27.

[5] Ostwald, W. *U.S. Pat. No. 858,904: Process of manufacturing nitric acid* **1902**.

[6] Novell-Leruth, G. *Phd Thesis: Catalytic Ammonia Oxidation on Noble Metal surfaces: A Theoretical Study*; Universidad Rovira i Virgili: Tarragona, 2008.

[7] Pesce, L. D. *Cyanides*; John Wiley Sons, Inc., 2000; pp 171–199.

[8] Potter, V. R. *J. Biol. Chem.* **1941**, *137*, 13–20.

[9] Araki, K.; Ozeki, T. *Amino acids*; John Wiley Sons, Inc., 2003; pp 554–618.

[10] Pritchard, J. D. *Health Protection Agency Comp. of Chem. Hazards* **2007**.

[11] Andrussow, L. *U.S. Pat. No. 1,934,838: Production of Hydrocyanic Acid* **1933**.

UNIVERSITAT ROVIRA I VIRGILI
FIRST-PRINCIPLES MECHANISTIC STUDIES OF AMMONIA-RELATED INDUSTRIAL PROCESSES
Jaime Gómez Díaz
ISBN:978-84-694-1247-3/T-317-2011

[12] Hickman, D. A.; Huff, M.; Schmidt, L. D. *Ind. Eng. Chem. Res.* **1993**, *32*, 809–817.

[13] Delagrange, S.; Schuurman, Y. *Catal. Today* **2007**, *121*, 204–209.

[14] Cohn, J. G.; Stern, E. W.; Etris, S. F. *Gold and gold compounds*; John Wiley Sons, Inc., 2001; pp 682–713.

[15] http://www.gold price.org/, **2010**.

[16] http://www.utilisegold.com/, **2010**.

[17] Haruta, M. *Catal. Today* **1997**, *36*, 153–166.

[18] Hashmi, A. S. K.; Hutchings, G. J. *Angew. Chem. Int.-Ed.* **2006**, *45*, 7896–7936.

[19] Frondelius, P.; Häkkinen, H.; Honkala, K. *Phys. Rev. B* **2007**, *76*, 073406.

[20] Jiménez-Nuñez, E.; Echavarren, A. M. *Chem. Commun.* **2007**, 333–346.

[21] García-Mota, M.; Cabello, N.; Maseras, F.; Echavarren, A. M.; Pérez-Ramírez, J.; López, N. *ChemPhysChem* **2008**, *9*, 1624–1629.

[22] Schwerdtfeger, P.; Dolg, M.; Schwarz, W. H. E.; Bowmaker, G. A.; Boyd, P. D. W. *J. Chem. Phys.* **1989**, *91*, 1762–1774.

[23] MacArtur, J. S.; Forrest, R. W.; Forrest, W. *British Pat. No. 14174: Process of obtaining gold and silver from ores* **1887**.

[24] Korte, F.; Spiteller, M.; Coulston, F. *Ecotox. Environ. Safe.* **2000**, *46*, 241–245.

[25] http://www.marthamine.co.nz, **2010**.

[26] Hohenberg, P.; Kohn, W. *Phys. Rev. B* **1964**, *136*, B864.

[27] Parr, R. G.; Yang, W. T. *Density Functional Theory of atoms and molecules*; Oxford University Press: New York, 1989.

UNIVERSITAT ROVIRA I VIRGILI
FIRST-PRINCIPLES MECHANISTIC STUDIES OF AMMONIA-RELATED INDUSTRIAL PROCESSES
Jaime Gómez Díaz
ISBN:978-84-694-1247-3/T-317-2011

[28] Kohn, W.; Sham, L. *Phys. Rev.* **1965**, *140*, 1133.

[29] Perdew, J. P.; Zunger, A. *Phys. Rev. B* **1981**, *23*, 5048–5079.

[30] Wang, Y.; Perdew, J. P. *Phys. Rev. B* **1991**, *43*, 8911–8916.

[31] Wang, Y.; Perdew, J. P. *Phys. Rev. B* **1991**, *44*, 13298–13307.

[32] Perdew, J. P.; Burke, K.; Ernzerhof, M. *Phys. Rev. Lett.* **1996**, *77*, 3865.

[33] Hammer, B.; Hansen, L. B.; Nørskov, J. K. *Phys. Rev. B* **1999**, *59*, 7413–7421.

[34] Payne, M. C.; Teter, M. P.; Allan, D. C.; Arias, T. A.; Joannopoulos, J. D. *Rev. Mod. Phys.* **1992**, *64*, 1045–1097.

[35] Vanderbilt, D. *Phys. Rev. B* **1990**, *41*, 7892–7895.

[36] Blöchl, P. E. *Phys. Rev. B* **1994**, *50*, 17953–17979.

[37] Johnson, B. G.; Gill, P. M. W.; Pople, J. A. *J. Chem. Phys.* **1992**, *98*, 5612–5626.

[38] Ashcroft, N. W.; Mermin, N. D. *Solid State Physics*; Saunders College Publishing: Philadelphia, 1976.

[39] Mortensen, J. J.; Hansen, L. B.; Jacobsen, K. W. *Phys. Rev. B* **2005**, *71*, 035109.

[40] Walter, M.; Häkkinen, H.; Lehtovaara, L.; Puska, M.; Enkovaara, J.; Rostgaard, C.; Mortensen, J. J. *J. Chem. Phys.* **2008**, *128*, 244101.

[41] Monkhorst, H. J.; Pack, J. D. *Phys. Rev. B* **1976**, *13*, 5188–5192.

[42] Wood, D.; Zunger, A. *J. Phys. A: Math. Gen.* **1985**, *18*, 1343–1359.

[43] Teter, M.; Payne, M.; Allan, D. *Phys. Rev. B* **1989**, *40*, 12255–12255.

[44] Pulay, P. *Chem. Phys. Lett.* **1980**, *73*, 393–398.

[45] Kresse, G.; Hafner, J. *Phys. Rev. B* **1994**, *49*, 14251–14269.

UNIVERSITAT ROVIRA I VIRGILI
FIRST-PRINCIPLES MECHANISTIC STUDIES OF AMMONIA-RELATED INDUSTRIAL PROCESSES
Jaime Gómez Díaz
ISBN:978-84-694-1247-3/T-317-2011

[46] Liu, B. *Report on Workshop, Lawrence Berkley Lab. Univ. of California* **1978**, 49.

[47] Kresse, G.; Furthmüller, J. *Phys. Rev. B* **1996**, *54*, 11169–11186.

[48] Press, W. H.; Flannery, B. P.; Teukolsky, S. A.; Vetterling, W. T. *Numerical Recipes*; Cambridge University Press: New York, 1986.

[49] Bader, R. F. W. *Atoms in Molecules- A Quantum Theory*; University of Oxford Press: Oxford, 1990.

[50] Bader, R. F. W. *Chem. Rev.* **1991**, *91*, 893–928.

[51] Schwinger, J. *Phys. Rev.* **1951**, *82*, 664–679.

[52] Dunitz, J.; Gavezzotti, A. *Angew. Chem.-Int. Ed.* **2005**, *44*, 1766–1787.

[53] Becke, A. D.; Edgecombe, K. E. *J. Chem. Phys.* **1990**, *92*, 5397–5403.

[54] Savin, A.; Becke, A. D.; Flad, J.; Nesper, R.; Preuss, H.; Vonschnering, H. G. *Angew. Chem. Int. Ed.* **1991**, *30*, 409–412.

[55] Jónsson, H.; Mills, G.; Jacobsen, K. W. *Classical and Quantum Dynamics in Condensed Phase Simulations*; Ed: B. J. Berne, G. Ciccotti and D. F. Coker, 1998; p 385.

[56] Jónsson, H.; Mills, G. *Phys. Rev. Lett.* **1995**, *72*, 1124.

[57] Jónsson, H.; Mills, G.; Schenter, G. *Surf. Sci.* **1995**, *324*, 305.

[58] Henkelman, G.; Uberuaga, B.; Jónsson, H. *J. Chem. Phys.* **2000**, *113*, 9901–9904.

[59] http://theory.cm.utexas.edu/vtsttools/neb/, **2010**.

[60] Brønsted, J. N. *Chem. Rev.* **1928**, *5*, 231–338.

[61] Eyring, H.; Polanyi, M. *Z. Phys. Chem. B-Chem. Elem. Aufbau. Mater.* **1931**, *12*, 279–311.

UNIVERSITAT ROVIRA I VIRGILI
FIRST-PRINCIPLES MECHANISTIC STUDIES OF AMMONIA-RELATED INDUSTRIAL PROCESSES
Jaime Gómez Díaz
ISBN:978-84-694-1247-3/T-317-2011

[62] Evans, M.; Polanyi, M. *Trans. Faraday Soc.* **1938**, *34*, 0011–0023.

[63] Fernandez, E. M.; Moses, P. G.; Toftelund, A.; Hansen, H. A.; Martínez, J. I.; Abild-Pedersen, F.; Kleis, J.; Hinnemann, B.; Rossmeisl, J.; Bligaard, T.; Nørskov, J. K. *Angew. Chem. Int. Ed.* **2008**, *47*, 4683–4686.

[64] Abild-Pedersen, F.; Greeley, J.; Studt, F.; Rossmeisl, J.; Munter, T. R.; Moses, P. G.; Skulason, E.; Bligaard, T.; Nørskov, J. K. *Phys. Rev. Lett.* **2007**, *99*, 016105.

[65] Logadottir, A.; Rod, T. H.; Nørskov, J. K.; Hammer, B.; Dahl, S.; Jacobsen, C. J. H. *J. Catal.* **2001**, *197*, 229–231.

[66] Nørskov, J. K.; Bligaard, T.; Logadottir, A.; Bahn, S.; Hansen, L. B.; Bollinger, M.; Bengaard, H.; Hammer, B.; Sljivancanin, Z.; Mavrikakis, M.; Xu, Y.; Dahl, S.; Jacobsen, C. J. H. *J. Catal* **2002**, *209*, 275–278.

[67] Andersin, J.; López, N.; Honkala, K. *J. Phys. Chem. B* **2009**, *113*, 8278–8286.

[68] Hammond, G. S. *J. Am. Chem. Soc.* **1955**, *77*, 334–338.

[69] Kresse, G.; Hafner, J. *Phys. Rev. B* **1993**, *47*, 558–561.

[70] Kresse, G.; Furthmüller, J. *Comput. Mat. Sci.* **1996**, *6*, 15–50.

[71] Kresse, G.; Joubert, D. *Phys. Rev. B* **1999**, *59*, 1758–1775.

[72] Perdew, J. P.; Burke, K.; Ernzerhof, M. *Phys. Rev. Lett.* **1997**, *78*, 1396.

[73] Frisch, M. J. et al. *Gaussian 09 Revision A.1*, Gaussian Inc. Wallingford CT 2009.

[74] Becke, A. D. *J. Chem. Phys.* **1993**, *98*, 5648–5652.

[75] Andrae, D.; Haussermann, U.; Dolg, M.; Stoll, H.; Preuss, H. *Theor. Chim. Acta* **1990**, *77*, 123–141.

UNIVERSITAT ROVIRA I VIRGILI
FIRST-PRINCIPLES MECHANISTIC STUDIES OF AMMONIA-RELATED INDUSTRIAL PROCESSES
Jaime Gómez Díaz
ISBN:978-84-694-1247-3/T-317-2011

[76] Wolfram Research, I. *Mathematica Edition: Version 5.2*, Wolfram Research, Inc. 2005.

[77] Chen, M. S.; Goodman, D. W. *Science* **2004**, *306*, 252–255.

[78] Remediakis, I. N.; López, N.; Nørskov, J. K. *Angew. Chem.-Int. Ed.* **2005**, *44*, 1824–1826.

[79] Matthey, D.; Wang, J. G.; Wendt, S.; Matthiesen, J.; Schaub, R.; Laegsgaard, E.; Hammer, B.; Besenbacher, F. *Science* **2007**, *315*, 1692–1696.

[80] López, N.; García-Mota, M.; Gómez-Díaz, J. *J. Phys. Chem. C* **2008**, *112*, 247–252.

[81] Vestergaard, E. K.; Vang, R. T.; Knudsen, J.; Pedersen, T. M.; An, T.; Lægsgaard, E.; Stensgaard, I.; Hammer, B.; Besenbacher, F. *Phys. Rev. Lett.* **2005**, *95*, 126101.

[82] Bahn, S. R.; López, N.; Nørskov, J. K.; Jacobsen, K. W. *Phys. Rev. B* **2002**, *66*, 081405.

[83] Deng, X. Y.; Friend, C. M. *J. Am. Chem. Soc.* **2005**, *127*, 17178–17179.

[84] Gong, J.; Ojifinni, R. A.; Kim, T. S.; White, J. M.; Mullins, C. B. *J, Am. Chem. Soc.* **2006**, *128*, 9012.

[85] Kim, T. S.; Gong, J.; Ojifinni, R. A.; White, J. M.; Mullins, C. B. *J. Am. Chem. Soc.* **2006**, *128*, 6282–6283.

[86] Honkala, K.; Hellman, A.; Remediakis, I. N.; Logadottir, A.; Carlsson, A.; Dahl, S.; Christensen, C. H.; Nørskov, J. K. *Science* **2005**, *307*, 555–558.

[87] Offermans, W. K.; Jansen, A. P. J.; van Santen, R. A. *Surf. Sci.* **2006**, *600*, 1714–1734.

[88] Popa, C.; Offermans, W. K.; van Santen, R. A.; Jansen, A. P. J. *Phys. Rev. B* **2006**, *74*, 155428.

UNIVERSITAT ROVIRA I VIRGILI
FIRST-PRINCIPLES MECHANISTIC STUDIES OF AMMONIA-RELATED INDUSTRIAL PROCESSES
Jaime Gómez Díaz
ISBN:978-84-694-1247-3/T-317-2011

[89] Novell-Leruth, G.; Valcárcel, A.; Clotet, A.; Ricart, J. M.; Pérez-Ramírez, J. *J. Phys. Chem. B* **2005**, *109*, 18061.

[90] Novell-Leruth, G.; Valcárcel, A.; Pérez-Ramírez, J.; Ricart, J. M. *J. Phys. Chem. C* **2007**, *111*, 860–868.

[91] Bradley, J. M.; Hopkinson, A.; King, D. A. *J. Phys. Chem.* **1995**, *99*, 17032.

[92] Kim, M.; Pratt, S. J.; King, D. A. *J. Am. Chem. Soc.* **2000**, *122*, 2409–2410.

[93] Weststrate, C.; Bakker, J.; Rienks, E.; Martinez, J.; Vinod, C.; Lizzit, S.; Petaccia, L.; Baraldi, A.; Nieuwenhuys, B. *J. Catal.* **2005**, *235*, 92–102.

[94] Lescop, B.; Galtayries, A.; Fanjoux, G. *J. Phys. Chem. B* **2004**, *108*, 13711–13718.

[95] Pérez-Ramírez, J.; Kondratenko, E. V.; Kondratenko, V. A.; Baerns, M. *J. Catal.* **2004**, *227*, 90–100.

[96] Pérez-Ramírez, J.; Kondratenko, E. V.; Kondratenko, V. A.; Baerns, M. *J. Catal.* **2005**, *229*, 303–313.

[97] Mavrikakis, M.; Stoltze, P.; Nørskov, J. K. *Catal. Lett.* **2000**, *64*, 101–106.

[98] López, N.; Janssens, T. V. W.; Clausen, B. S.; Xu, Y.; Mavrikakis, M.; Bligaard, T.; Nørskov, J. K. *J. Catal.* **2004**, *223*, 232–235.

[99] Hammer, B. *Phys. Rev. Lett.* **1999**, *83*, 3681–3684.

[100] Hermse, C. G. M.; van Bavel, A. P.; Nieuwenhuys, B. E.; Lukkien, J. J.; van Santen, R. A.; Jansen, A. P. J. *Langmuir* **2005**, *21*, 8302–8311.

[101] Hermse, C. G. M.; Frechard, F.; van Bavel, A. P.; Lukkien, J. J.; Niemantsverdriet, J. W.; van Santen, R. A.; Jansen, A. P. J. *J. Chem. Phys.* **2003**, *118*, 7081–7089.

UNIVERSITAT ROVIRA I VIRGILI
FIRST-PRINCIPLES MECHANISTIC STUDIES OF AMMONIA-RELATED INDUSTRIAL PROCESSES
Jaime Gómez Díaz
ISBN:978-84-694-1247-3/T-317-2011

[102] Henkelman, G.; Jonsson, H. *Phys. Rev. Lett.* **2001**, *86*, 664–667.

[103] Gong, J.; Ojifinni, R. A.; Kim, T. S.; White, J. M.; Mullins, C. B. *J. Am. Chem. Soc.* **2006**, *128*, 9012.

[104] Michaelides, A.; Hu, P. *J. Am. Chem. Soc.* **2000**, *122*, 9866–9867.

[105] Ostermai, J. J.; Katzer, J. R.; Manogue, W. H. *J. Catal.* **1974**, *33*, 457–473.

[106] Morrow, B. A.; Cody, I. A. *J. Catal.* **1976**, *45*, 151–162.

[107] Nutt, C. W.; Kapur, S. *Nature* **1968**, *220*, 697.

[108] Nutt, C. W.; Kapur, S. *Nature* **1969**, *224*, 169.

[109] Gland, J. L.; Korchak, V. N. *J. Catal.* **1978**, *53*, 9–23.

[110] Asscher, M.; Guthrie, W. L.; Lin, T. H.; Somorjai, G. A. *J. Phys. Chem.* **1984**, *88*, 3233–3238.

[111] Vantol, M. F. H.; Siera, J.; Cobden, P. D.; Nieuwenhuys, B. E. *Surf. Sci.* **1992**, *274*, 63–81.

[112] Lombardo, S. J.; Fink, T.; Imbihl, R. *J. Chem. Phys.* **1993**, *98*, 5526–5539.

[113] Lombardo, S. J.; Esch, F.; Imbihl, R. *Surf. Sci.* **1992**, *271*, L367–L372.

[114] Dahl, S.; Logadottir, A.; Egeberg, R. C.; Larsen, J. H.; Chorkendorff, I.; Törnqvist, E.; Nørskov, J. K. *Phys. Rev. Lett.* **1999**, *83*, 1814–1817.

[115] Hammer, B.; Nørskov, J. K. *Phys. Rev. Lett.* **1997**, *79*, 4441–4444.

[116] Ge, Q.; Neurock, M. *J. Am. Chem. Soc.* **2004**, *126*, 1551–1559.

[117] Mei, D.; Du, J.; Neurock, M. *Ind. Eng. Chem. Res.* **2010**, *49*, 10364–10373.

[118] Bogicevic, A.; Hass, K. C. *Surf. Sci.* **2002**, *506*, 237–242.

UNIVERSITAT ROVIRA I VIRGILI
FIRST-PRINCIPLES MECHANISTIC STUDIES OF AMMONIA-RELATED INDUSTRIAL PROCESSES
Jaime Gómez Díaz
ISBN:978-84-694-1247-3/T-317-2011

[119] Gajdos, M.; Hafner, J.; Eichler, A. *J. Phys. Cond. Matt.* **2006**, *18*, 13–40.

[120] Gajdos, M.; Hafner, J.; Eichler, A. *J. Phys. Cond. Matt.* **2006**, *18*, 41–54.

[121] Pérez-Ramírez, J.; Kondratenko, E. V.; Novell-Leruth, G.; Ricart, J. M. *J. Catal.* **2009**, *261*, 217–223.

[122] Gopinath, C.; Zaera, F. *J. Phys. Chem. B* **2000**, *104*, 3194–3203.

[123] Zaera, F.; Gopinath, C. *Chem. Phys. Chem.* **2000**, *332*, 209–214.

[124] Zaera, F.; Gopinath, C. *Phys. Chem. Chem. Phys.* **2003**, *5*, 646–654.

[125] Koci, P.; Plat, F.; Stepanek, J.; Kubicek, M.; Marek, M. *Catal. Today* **2008**, *137*, 253–260.

[126] Chatterjee, D.; Koci, P.; Schmeisser, V.; Marek, M.; Weibel, M.; Krutzsch, B. *Catal. Today* **2010**, *151*, 395–409.

[127] Hannevold, L.; Nilsen, O.; Kjekshus, A.; Fjellvag, H. *Appl. Catal. A-Gen.* **2005**, *284*, 163–176.

[128] Greeley, J.; Nørskov, J. K. *Surf. Sci.* **2005**, *592*, 104–111.

[129] Chaston, J. C. *Plat. Met. Rev.* **1969**, *13*, 28–29.

[130] Rubel, M.; Pszonicka, M.; Palczewska, W. *J. Mater. Sci.* **1985**, *20*, 3639–3648.

[131] Rdzawski, Z. M.; Stobrawa, J. P.; Szynowski, J. *J. Achiev. Mat. Man. Eng.* **2007**, *24*, 106–114.

[132] Bollinger, M. V.; Jacobsen, K.; Nørskov, J. K. *Phys. Rev. B* **2003**, *67*, 085410.

[133] Seriani, N.; Pompe, W.; Ciacchi, L. C. *J. Phys. Chem. B* **2006**, *110*, 14860–14869.

[134] Seriani, N.; Jin, Z.; Pompe, W.; Ciacchi, L. C. *Phys. Rev. B* **2007**, *76*, 155421.

UNIVERSITAT ROVIRA I VIRGILI
FIRST-PRINCIPLES MECHANISTIC STUDIES OF AMMONIA-RELATED INDUSTRIAL PROCESSES
Jaime Gómez Díaz
ISBN:978-84-694-1247-3/T-317-2011

[135] McBride, J. R.; Graham, G. W.; Peters, C. R.; Weber, W. H. *J. Appl. Phys.* **1991**, *69*, 1596–1604.

[136] Grillo, M. E. *Phys. Rev. B* **2004**, *70*, 184115.

[137] Muller, O.; Roy, R. *J. Less-Comm. Met.* **1968**, *16*, 129.

[138] Hasenberg, D.; Schmidt, L. D. *J. Catal.* **1985**, *91*, 116–131.

[139] Hasenberg, D.; Schmidt, L. D. *J. Catal.* **1986**, *97*, 156–168.

[140] Hasenberg, D.; Schmidt, L. D. *J. Catal.* **1987**, *104*, 441–453.

[141] Waletzko, N.; Schmidt, L. D. *AlChE J.* **1988**, *34*, 1146–1156.

[142] Hickman, D.; Schmidt, L. D. *Ind. Eng. Chem. Res.* **1991**, *30*, 50–55.

[143] Hickman, D.; Schmidt, L. D. *J. Catal.* **1992**, *138*, 267–282.

[144] Bharadwaj, S. S.; Schmidt, L. D. *Ind. Eng. Chem. Res.* **1996**, *35*, 1524–1533.

[145] Dietz, A.; Schmidt, L. D. *Appl. Catal., A* **1999**, *180*, 287–298.

[146] Bodke, A.; Olschki, D.; Schmidt, L. D. *Appl. Catal., A* **2000**, *201*, 13–22.

[147] Celio, H.; Mills, P.; Jentz, D.; Pae, Y.; Trenary, M. *Langmuir* **1998**, *14*, 1379–1383.

[148] Herceg, E.; Trenary, M. *J. Am. Chem. Soc.* **2003**, *125*, 15758–15759.

[149] Herceg, E.; Trenary, M. *J. Phys. Chem. B* **2005**, *109*, 17560–17566.

[150] Deng, R.; Trenary, M. *J. Phys. Chem. C* **2007**, *111*, 17088–17093.

[151] Diefenbach, M.; Brönstrup, M.; Aschi, M.; Schroder, D.; Schwarz, H. *J. Am. Chem. Soc.* **1999**, *121*, 10614–10625.

[152] Kondratenko, V. A. *Appl. Catal. A-Gen.* **2010**, *381*, 74–82.

[153] Kondratenko, V. A.; Weinberg, G.; Pohl, M. M.; Su, D. S. *Appl. Catal. A-Gen.* **2010**, *381*, 66–73.

UNIVERSITAT ROVIRA I VIRGILI
FIRST-PRINCIPLES MECHANISTIC STUDIES OF AMMONIA-RELATED INDUSTRIAL PROCESSES
Jaime Gómez Díaz
ISBN:978-84-694-1247-3/T-317-2011

[154] Michaelides, A.; Liu, Z. P.; Zhang, C. J.; Alavi, A.; King, D. A.; Hu, P. *J. Am. Chem. Soc.* **2003**, *125*, 3704–3705.

[155] Psofogiannakis, G.; St-Amant, A.; Ternan, M. *J. Phys. Chem. B* **2006**, *110*, 24593–24605.

[156] Michaelides, A.; Hu, P. *J. Chem. Phys.* **2001**, *114*, 5792–5795.

[157] Crawford, P.; Hu, P. *Surface Science* **2007**, *601*, 341–345.

[158] Crawford, P.; Hu, P. *J. Chem. Phys.* **2007**, *126*, 194706.

[159] Ample, F.; Clotet, A.; Ricart, J. M. *Surf. Sci.* **2004**, *558*, 111–121.

[160] Ricart, J. M.; Ample, F.; Clotet, A.; Curulla, D.; Niemantsverdriet, J. W.; Paul, J. F.; Pérez-Ramírez, J. *J. Catal.* **2005**, *232*, 179–185.

[161] Ample, F.; Curulla, D.; Fuster, F.; Clotet, A.; Ricart, J. M. *Surf. Sci.* **2002**, *497*, 139–154.

[162] Shuttleworth, I. G. *Surf. Sci.* **2008**, *602*, 3308–3315.

[163] Fan, J. F.; Trenary, M. *Langmuir* **1994**, *10*, 3649–3657.

[164] Feibelman, P. J.; Hammer, B.; Nørskov, J. K.; Wagner, F.; Scheffler, M.; Stumpf, R.; Watwe, R.; Dumesic, J. *J. of Phys. Chem. B* **2001**, *105*, 4018–4025.

[165] Smentkowski, V. S.; Hagans, P.; Yates, J. T. *J. of Phys. Chem.* **1988**, *92*, 6351–6357.

[166] Magnussen, O. M. *Chem. Rev.* **2002**, *102*, 679–725.

[167] Ellis, S.; Senanayake, G. *Hydrometallurgy* **2004**, *72*, 39–50.

[168] Senanayake, G. *Hydrometallurgy* **2005**, *80*, 1–12.

[169] Hilson, G.; Monhemius, A. J. *J. Cleaner Prod.* **2006**, *14*, 1158–1167.

[170] Rawlings, D.; Silver, S. *Bio-Technology* **1995**, *13*, 773–778.

UNIVERSITAT ROVIRA I VIRGILI
FIRST-PRINCIPLES MECHANISTIC STUDIES OF AMMONIA-RELATED INDUSTRIAL PROCESSES
Jaime Gómez Díaz
ISBN:978-84-694-1247-3/T-317-2011

[171] Bozzini, B.; Busson, B.; De Gaudenzi, G. P.; D'Urzo, L.; Mele, C.; Tadjeddine, A. *J. Electroanal. Chem.* **2007**, *602*, 61–69.

[172] Bozzini, B.; Busson, B.; Mele, C.; Tadjeddine, A. *J. Appl. Electrochem.* **2008**, *38*, 897–906.

[173] Cimatu, K.; Baldelli, S. *J. Am. Chem. Soc.* **2008**, *130*, 8030–8037.

[174] Jeffrey, M.; Ritchie, I. *J. Electrochem. Soc.* **2001**, *148*, 29–36.

[175] Jeffrey, M. I.; Breuer, P. L.; Choo, W. L. *Metall. Mater. Trans.* **2001**, *32*, 979–986.

[176] McCarley, R. L.; Bard, A. J. *J. Phys. Chem.* **1992**, *96*, 7410–7416.

[177] Sawaguchi, T.; Yamada, T.; Okinaka, Y.; Itaya, K. *J. Phys. Chem.* **1995**, *99*, 14149–14155.

[178] Bozzini, B.; Mele, C.; Romanello, V. *J. Electroanal. Chem.* **2006**, *592*, 25–30.

[179] Beltramo, G. L.; Shubina, T. E.; Mitchell, S. J.; Koper, M. T. M. *J. Electroanal. Chem.* **2004**, *563*, 111–120.

[180] Tadjeddine, M.; Flament, J. P. *Chem. Phys.* **1999**, *240*, 39–50.

[181] Crawford, P.; Hu, P. *Surf. Sci.* **2007**, *601*, 341–345.

[182] Ford, D. C.; Xu, Y.; Mavrikakis, M. *Surf. Sci.* **2005**, *587*, 159–174.

[183] Harrison, J. A.; Thompson, J. *J. Electroanal. Chem.* **1972**, *40*, 113.

[184] Eisenmann, E. T. *J. Electrochem. Soc.* **1978**, *125*, 717–723.

[185] Filhol, J.; Neurock, M. *Angew. Chem.-Int. Ed.* **2006**, *45*, 402–406.

[186] Hansen, N.; Wodtke, A. *J. Phys. Chem. A* **2003**, *107*, 10608–10614.

[187] Burrus, C. A. *J. Chem. Phys.* **1958**, *28*, 427–429.

[188] Vanwache, R.; Deleeuw, F. H.; Dymanus, A. *J. Chem. Phys.* **1967**, *47*, 2256–2258.

UNIVERSITAT ROVIRA I VIRGILI
FIRST-PRINCIPLES MECHANISTIC STUDIES OF AMMONIA-RELATED INDUSTRIAL PROCESSES
Jaime Gómez Díaz
ISBN:978-84-694-1247-3/T-317-2011

[189] B, C.; Sarasa, J. P.; Poblet, J. M. *J. Phys. Chem.* **1993**, *97*, 6362–6366.

[190] Perrin, C. L. *J. Am. Chem. Soc.* **1991**, *113*, 2865–2868.

[191] Berkowit, J.; Chupka, W. A.; Walter, T. A. *J. Chem. Phys.* **1969**, *50*, 1497–1500.

[192] Lawson, R. P. W.; Carter, G. *Appl. Phys. Lett.* **1966**, *9*, 85–87.

[193] Paier, J.; Hirschl, R.; Marsman, M.; Kresse, G. *J. Chem. Phys.* **2005**, *122*, 234102.

[194] Wang, X.-B.; Wang, Y.-L.; Yang, J.; Xing, X.-P.; Li, J.; Wang, L.-S. *J. Am. Chem. Soc.* **2009**, *131*, 16368–16370.

[195] http://www.webelements.com, **2010**.

[196] Kwon, S. K.; Nabi, Z.; Kadas, K.; Vitos, L.; Kollar, J.; Johansson, B.; Ahuja, R. *Phys. Rev. B* **2005**, *72*, 235423.

[197] http://webbook.nist.gov/chemistry/, **2010**.

[198] Wang, W.; Andrews, L. *J. Phys. Chem. A* **2001**, *105*, 5812–5822.

[199] Citra, A.; Andrews, L. *J. Phys. Chem. A* **1999**, *103*, 4845–4854.

UNIVERSITAT ROVIRA I VIRGILI
FIRST-PRINCIPLES MECHANISTIC STUDIES OF AMMONIA-RELATED INDUSTRIAL PROCESSES
Jaime Gómez Díaz
ISBN:978-84-694-1247-3/T-317-2011

UNIVERSITAT ROVIRA I VIRGILI
FIRST-PRINCIPLES MECHANISTIC STUDIES OF AMMONIA-RELATED INDUSTRIAL PROCESSES
Jaime Gómez Díaz
ISBN:978-84-694-1247-3/T-317-2011

UNIVERSITAT ROVIRA I VIRGILI
FIRST-PRINCIPLES MECHANISTIC STUDIES OF AMMONIA-RELATED INDUSTRIAL PROCESSES
Jaime Gómez Díaz
ISBN:978-84-694-1247-3/T-317-2011